THE UNIVERSITY *of* EDINBURGH

Quantifying stress-induced mutagenesis in bacteria exposed to low-dose antibiotics

Lucy Lansch-Justen

Doctor of Philosophy

THE UNIVERSITY OF EDINBURGH

March 2025

Abstract

Bacteria are frequently exposed to antibiotics, particularly at low doses, which induces stress responses in the cells. Some of these responses increase mutagenesis and thus potentially accelerate resistance evolution. Many studies report increased mutation rates under stress, often using the standard experimental approach of fluctuation assays.

In this thesis, I extend the mathematical model behind the fluctuation assay to include within-population heterogeneity in stress responses. Our model is inspired by the DNA-damage response in *Escherichia coli* (SOS response). It accounts for a subpopulation with high expression of the stress response, which increases the mutation rate and decreases the division rate of a cell.

In Chapter 2, I implement maximum likelihood estimation and stochastic simulations of fluctuation assays under existing and our new population dynamic model. Using the simulated data, I show that this new model, in principle, allows for estimating the increase in mutation rate specifically associated with the induction of the stress response. However, I also show that when heterogeneity is neglected, an accurate estimate of the increase in population-mean mutation rate is recovered. Moreover, in many cases, different models can explain the data equally well and, therefore, cannot be distinguished using fluctuation assay data alone.

In Chapter 3, I apply our estimation method, which I converted into a user-friendly R tool, to published experimental data. I show that not all experiments that report an increase in mutation rate significantly support the hypothesis of stress-induced mutagenesis. Moreover, I find that DNA-damaging antibiotics particularly increase mutation rates and identify several signals of heterogeneity in stress-induced mutagenesis.

In Chapter 4, I study how stress-induced mutagenesis depends on the antibiotic dose. By modelling different antibiotic modes of action, I determine under which conditions within-population heterogeneity can lead to a non-monotonic increase in mutation rate with antibiotic concentration. Such a maximum increase for intermediate concentrations has been previously observed empirically.

Overall, this thesis improves the estimation of mutation rates in bacteria under stress, which could contribute to better predictions of the evolution of antibiotic resistance.

Lay Summary

The first antibiotic was discovered almost 100 years ago, and antibiotics have saved millions of lives since then. Antibiotics kill bacteria directly or stop them from reproducing, for example, by destroying their cell membrane or damaging their DNA. However, bacteria can become *resistant* to antibiotics, meaning an antibiotic treatment no longer works on them. One way in which bacteria can become resistant to antibiotics is through *mutations*. In general, mutations are changes in the DNA of an organism. Bacteria are single-celled organisms that reproduce by dividing into a mother and a daughter cell. For that, the cell has to make a copy of its DNA. If a mistake happens in the copying process, the daughter cell will have a mutation. Sometimes, mutations can help cells survive antibiotic treatment; these are called *resistance mutations*. Therefore, it is essential to know how often (at which *rate*) mutations happen in bacteria.

Researchers have discovered that mutations occur more frequently in bacteria if they face stressors. Examples of stressful conditions for bacteria are starvation, heat, or toxins. Of course, antibiotics themselves are stressful for bacteria, too. Antibiotics, particularly at low doses, can be found in many places, such as the soil, sewage, or the bodies of humans/animals after antibiotic treatment. Bacteria have ways to cope with stressful conditions, called *stress responses*. For example, they can change their metabolism in an environment with low nutrients. Bacteria also have stress responses to deal with antibiotics that damage their DNA. In that case, the stress response involves repairing the DNA damage. However, this repair process is prone to mistakes, introducing mutations into the DNA of the stressed cell. This phenomenon - an increased rate of mutations under stress - is called *stressed-induced mutagenesis*. One implication of stress-induced mutagenesis could be that bacteria are more likely to get a resistance mutation if they encounter low-dose antibiotics. Therefore, it is essential to know how much the mutation rate increases under stress (to *quantify* the increase) because it can have implications for antibiotic regimens.

Through technological advances in recent years, researchers have been able to study stressed bacterial populations at the level of individual cells. They have found that individual cells can respond to stressors differently, even if they are genetically identical and share the same environment. If a bacterial infection is treated with a DNA-damaging

antibiotic, different cells within the same bacterial population might have different mutation rates (that is, there is *heterogeneity in mutation rates*). In particular, some scientists have found a small subpopulation of highly stressed cells with a much higher mutation rate than the rest of the population. Heterogeneity in mutation rates makes it difficult to measure mutation rates. That is because most methods scientists use to measure mutation rates of bacteria are meant to measure the mutation rate of a whole population, not individual cells or small subpopulations. Before this work, there was no technically simple method to estimate the mutation rates of bacteria when they face stressful conditions, to which different cells respond differently.

In this thesis, we developed such a method to *estimate mutation rates under heterogeneous stress responses*. In particular, we wrote a computational tool that allows researchers to re-interpret the results of an existing simple experiment (called the *fluctuation assay*). We used computer simulations to show that our method, in principle, allows us to measure the specific mutation rate of highly stressed cells, even if there are only a few of those cells in a population. It is essential to measure the *specific* mutation rate of highly stressed cells because they could be fundamental for the evolution of multi-drug resistance. However, we also showed that if researchers use standard methods and ignore any heterogeneity in mutation rates, they obtain a reasonable estimate of the *average* mutation rate of the total bacterial population. This is reassuring because it means that previous results can be trusted. Next, we used our estimation method to re-analyse published experimental data (of the fluctuation assay). In the experiments we re-analysed, researchers reported that bacteria have a higher mutation rate when treated with antibiotics than when they are not. We found that DNA-damaging antibiotics (for example, ciprofloxacin) increase bacteria's mutation rate more than other types of antibiotics. Moreover, we identified several experiments for which there are indications of heterogeneity in mutation rates, of which many used again DNA-damaging antibiotics. This hints that it could be explicitly DNA-damaging antibiotics that increase the risk of antibiotic resistance evolution and should be considered more cautiously. Finally, we used a mathematical model to study how the increase in mutation rate in bacteria depends on the dose of antibiotic treatment. We showed that the *mode of action* of the antibiotic, i.e. whether it kills the bacteria or stops them from reproducing, plays an important role. Still, more work is needed to connect these results with experimental observations.

Overall, this thesis improves the estimation of mutation rates under stress, important for predicting antibiotic resistance evolution.

Acknowledgements

Thank you for being so supportive, Julie, Koorosh, Pierre, Shravan, Vignesh, Helen, Meriem, Daniel, Gabriela, Grace, James, KK, Nico, Nina, Doro, Iratxe, Leo, Peter, and thank you for understanding that this ~~is not the final version of the acknowledgement yet.~~ended up being the final version of the acknowledgements after all.

Contents

Figures and Tables

Figures

Tables

Nomenclature

α	Switching rate
$\bar{M}$	Increase in population-wide mutation rate
δ	Death rate of non-mutant cells
ε	Extinction probability of mutant cells
γ	Division rate of non-mutant cells
λ	Population growth rate
λ_{max}	Maximal population growth rate (in the absence of stress)
$\ln \mathscr{L}$	Log-likelihood
μ	Per-division mutation rate
ν	Mutation rate per unit time
ρ	Differential mutant fitness
θ	Set of model parameters
$\tilde{\alpha}$	Relative switching rate
b	Birth rate of mutant cells
C	Antimicrobial concentration
c	Number of parallel cultures
d	Death rate of mutant cells
E	Plating efficiency
f_{on}	Fraction of response-*on* subpopulation
f_{on}^*	Stationary fraction of response-*on* subpopulation
$G(z)$	Probability generating function
h	Hill coefficient of the dose-response curve
k	Number of parameters
N	Population size
n	Subpopulation size
N_f	Final population size
N_i	Initial population size
p_i	Probability to observe i mutant colonies
R	Number of replicates
r_{on}	Relative fitness of response-*on* subpopulation
S	Mutation-supply ratio

s Scaling factor between switching and division rate

t Time

t_f Duration of the growth phase

x Mutant count distribution

$x(i)$ Number of plates with i mutant colonies

AIC Akaike information criterion

BIC Bayesian information criterion

CV Coefficient of variation across replicates

HET_0 Heterogeneous-response model with zero relative division rate of response-*on* cells

HET_1 Heterogeneous-response model with non-zero relative division rate and known fraction of response-*on* cells

HET_2 Heterogeneous-response model with non-zero relative division rate and unknown fraction of response-*on* cells

HOM_0 Homogeneous-response model without differential mutant fitness

HOM_1 Homogeneous-response model with constrained differential mutant fitness

HOM_2 Homogeneous-response model with unconstrained differential mutant fitess

IC50 Half-maximal inhibitory concentration

LRT Likelihood-ratio test

MAC Minimum antibiotic concentration

MIC Minimum inhibitory concentration

N_0 Null model (no SIM) without differential mutant fitness

N_1 Null model (no SIM) with constrained differential mutant fitness

RE Relative error across replicates

S Stressed condition (antimicrobial treatment)

SIM Stress-induced mutagenesis

Subscript $_{off}$ Response-*off* cells

Subscript $_{on}$ Response-*on* cells

Subscript $_0$ Control condition

Subscript $_p$ Permissive condition

Subscript $_s$ Stressful condition

UT Untreated control condition

Chapter 1

General introduction

My PhD was initially titled ‘Evolutionary consequences of mutation rate variation in bacteria’, but as usual for PhD projects, it changed course significantly along the way. The project was motivated by my supervisor’s previous work [1], who had studied how within-population variation in mutation rates impacts genetic diversity and evolutionary dynamics. They proved that when mutation rates are heterogeneous, there is an increased frequency of both non-mutants and ‘complex’ mutants (with multiple mutations). As a consequence, heterogeneous populations can adapt faster to new environments while maintaining a reduced mutation load. (Importantly, this was in comparison to populations with a uniform mutation rate of the same magnitude as the mean in the heterogeneous population.)

Mutation rate variation in bacteria Coming from a theoretical population genetics background, I knew about the importance of the mutation rate as a source of genetic variation that selection can act on. However, as it is common in the field, I had always assumed a uniform mutation rate for all individuals in a population. Therefore, as a first task in my PhD, I began to read about variation in mutation rates. And indeed, I learned that the mutation rate can vary greatly, for example, due to genetic, environmental, or stochastic factors. In bacteria, so-called mutators with a genetically elevated mutation rate are expected to arise in natural populations [18], and have been found in clinical isolates [56, 19, 6] and evolution experiments in the lab [66]. Environmental factors like nutrient availability and population density [46] have been shown to influence the mutation rate. Therefore, fluctuations in the microenvironment can also cause variability in mutation rates. However, my supervisors and I decided to focus on yet another source of variation in mutation rates: heterogeneity in bacterial stress responses and DNA repair.

Bacterial stress responses Bacteria are constantly exposed to 'stressful' conditions, i.e. conditions that require a response to prevent and repair damage that would, otherwise, result in cell death (this definition of stress might be a Zirkelschluss but it is, in fact, not easy to define stress). Stress responses are transient phenotypic changes in, for example, gene expression, protein activity or cellular metabolism. Extreme examples of stress responses are the persister state [5], in which cells stop dividing entirely until the stressful condition has passed, or the recently discovered 'doubling-while-shrinking' phenotype [11]. Other examples include upregulation of efflux pumps (to remove harmful components from within the cell), flagella synthesis (to move away from the stress) and quorum sensing (to communicate the stress to other cells). Especially when stress results in DNA damage, stress responses also involve the upregulation of mutagenic repair mechanisms, called stress-induced mutagenesis [26, 24, 9].

At the same time, many stress responses are expressed heterogeneously across bacterial populations, for example, due to stochasticity in the induction (also in the absence of stress) coupled with regulatory feedback loops [48], resulting in extensive heterogeneity in mutagenesis under stress [72]. The reason to focus on heterogeneity in stress responses was that my second supervisor's lab uses single-cell fluorescence microscopy and microfluidics experiments to study the DNA-damage response (called SOS response) in *Escherichia coli*. In my second supervisor's weekly group meetings, I learned about the induction dynamics and heterogeneous expression of the SOS response, mutagenicity of DNA-damage repair and the population dynamic consequences of cell division arrest caused by the SOS response.

The SOS response: Heterogeneity and mutagenicity In particular, I learned about the key proteins initiating the SOS response. One of these key proteins (RecBCD), responsible for recognising the damage, is present in the cell in small numbers and, therefore, subject to stochasticity. Once initiated, the SOS system activates a whole cassette of genes in a time-dependent manner, many of which are involved in DNA repair processes. Early genes of the SOS response primarily involve repair mechanisms with low error rates, such as excision repair and homologous recombination. If the damage is repaired successfully, the SOS response is repressed again. However, if damage persists, error-prone polymerases are induced as part of the late-SOS genes, leading to translesion synthesis (for more details see, for example, this recent review [55]). Due to stochasticity in SOS induction and the dynamic nature of the response,

individual cells exhibit varying levels and timings of SOS gene activation, leading to distinct phenotypes. In single-cell experiments, fluorescently labelling one of the late SOS genes (sulA, more below), my second supervisor's lab found that cells appear as having either a 'low' or 'high'-SOS expression level [38]. Low-SOS cells express only early-SOS genes, if any. On the contrary, high-SOS cells also induce late-SOS genes and, therefore, have an increased mutation rate compared to the low-SOS cells.

The SOS response: Inhibition of cell division Besides its mutagenic consequences, I also learned about the division arrest caused by the SOS response. Inhibition of cell division is part of the late-SOS genes (sulA), implying that it affects mainly high-SOS cells. Interestingly, elongation and DNA replication (not *cell* replication) continue, such that high-SOS cells grow into long filaments, allowing for continued DNA repair and survival. However, the division arrest also implies that high-SOS cells can get outcompeted by low-SOS cells in fast-growth conditions [38].

In general, the expression of mutagenic stress responses impacts not only the mutation rate but also other cellular functions, like the division rate in the case of the SOS response. Therefore, my PhD project aimed to extend my supervisor's work on within-population heterogeneity in mutation rates by coupling the increase in mutation rate with a decrease in division rate at a cellular level, and evaluating the evolutionary consequences. However, I never got as far as the consequences. Instead, I followed a side quest which ultimately became the large body of my PhD: *Quantifying* mutation rate variation in bacteria.

Antibiotic dose-dependent mutagenesis The decision to detour was strongly influenced by one particular publication [62]. The authors investigated how mutagenesis is induced in *E. coli* populations when exposed to the antibiotic ciprofloxacin and the specific cellular mechanisms involved. They found that ciprofloxacin indeed induces mutagenesis in *E. coli*, also at concentrations below the minimum inhibitory concentration (MIC). This effect was dose-dependent, with maximal mutagenesis observed at the minimum antibiotic concentration (MAC, defined as 90% growth rate reduction). I was intrigued by such a non-monotonic dependence of mutagenesis on the antibiotic concentration because of the potential consequences on antibiotic resistance evolution. The authors of [62] found that mutagenesis was driven by a subpopulation of cells, which they called 'gamblers'. These gamblers are characterised by high levels of reactive oxygen species (ROS) and the activation of the general stress response, also

called σ^s response. ROS production triggers the σ^s response, enabling mutagenic repair of DNA double-strand breaks (DSBs), primarily by error-prone DNA polymerases. Mutagenesis is concentrated in the small gambler subpopulation ($10-25\%$ of cells) that exhibits high σ^s activity and is responsible for generating the majority of antibiotic-resistant mutants. Inhibiting ROS production and the subsequent activation of the σ^s response with the drug edaravone effectively reduced mutagenesis without affecting the antibiotic's ability to kill bacteria. The authors suggested targeting the mutagenic response as a potential strategy to prevent antibiotic resistance.

Reading scientific papers requires critical evaluation. Scientists have different approaches, which can broadly be classified as narrative-centric or data-centric [36]. When I first read the above-summarised paper, I applied a narrative-centric approach, i.e. following the authors' depictions to guide my understanding. Then, in one of our meetings, my second supervisor expressed concerns with the methods used: How exactly were mutation rates measured? Which assumptions were made here? Were these assumptions valid? The discussion made me re-read the paper, this time using a data-centric approach: How did the authors of [62] measure 'mutagenesis'? They measured mutation rates in populations treated with ciprofloxacin at different concentrations and compared these rates with untreated control populations. But how are mutation rates measured in bacteria?

Mutation-rate estimation in bacteria Methods to estimate mutation rates in bacteria can generally be divided into sequencing-based methods and ones using phenotypic markers [75]. For example, in mutation accumulation experiments, genetically identical lines are propogated multiple generations under relaxed selection, allowing mutations (except lethal ones) to accumulate. Then, whole-genome sequencing is used to detect mutations and calculate the per-generation mutation rate. Mutation rates can also be estimated from substitution rates in selectively neutral regions which, based on Kimura's neutral theory, accumulate roughly at a rate equal to the underlying mutation rate. Moreover, recent advances in single-molecule live-cell imaging have allowed researchers to directly observe DNA mismatch repair and estimate the rate of unrepaired mismatches - likely proportional to the mutation rate [21, 27]. On the other hand, the method the authors of [62] estimated mutation rates with a method using phenotypic markers: the fluctuation assay.

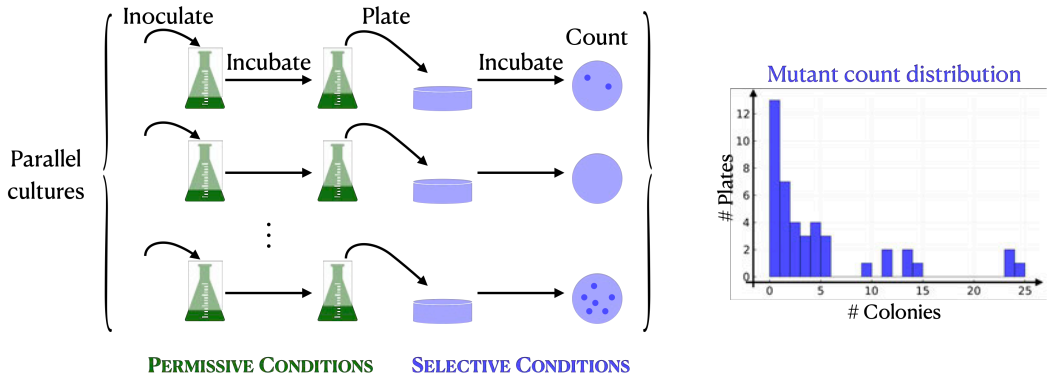

Figure 1.1: Schematic of the experimental setup of fluctuation assays.

The fluctuation assay: experimental setup The fluctuation assay or fluctuation test is a standard lab approach to measure microbial mutation rates. Originally, it was designed to test whether mutations arise spontaneously and are random, or whether they are actively induced by selection and directed [54]. The experimental setup of a fluctuation assay is comparably simple (see [47] for a protocol). A number of parallel cultures are inoculated at a small population size of around $10^4 - 10^5$ cells. The cultures are incubated under permissive conditions for several hours, typically overnight, called the *growth phase*. Then, each culture is plated onto a plate with strong selective media, which the cultures had initially been sensitive to, and such that only resistant mutant cells can grow. The number of mutant colonies per plate is counted, giving a so-called *mutant count distribution*. Fig 1.1 shows a schematic of the experimental setup of a fluctuation assay.

The fluctuation assay: mutant count distribution Now, the idea behind the fluctuation assay is that the shape of the mutant count distribution differs depending on whether mutations arise spontaneously during the growth phase or appear only on the plates as a consequence of the selection pressure. If the latter were true, with each cell having a small probability of obtaining a resistance mutation on the plate, the resulting mutant count distribution would be Possionian. On the other hand, if mutations arose spontaneously during the growth phase, the resulting number of mutant cells would show much greater fluctuation (hence the name of the experiment): most mutations would still arise at the end of the growth phase when the population size is large, but

in rare cases, a mutation arises early. This mutant cell then has many generations to proliferate, leading to a large mutant count on that plate, called a *jackpot event*. And sure enough, the first performed fluctuation assays supported the hypothesis of spontaneous mutations [54].

The fluctuation assay: mutation-rate estimation At the same time, the fluctuation assay allowed researchers to quantify bacterial mutation rates for the first time. The inventors of the fluctuation assays used the later-called p_0-method to calculate the mutation rate from the fraction of plates without any mutant colonies, which approximates the probability of no mutation occurring during the growth phase [54]. Other early methods to calculate the mutation rate in a fluctuation assay were based on the median (the mean cannot be used because of potential jackpot events) [23]. It took several more years after the invention of the fluctuation assay until an expression for the mutant count distribution was derived [52]. It was based on a simple population dynamic model: The non-mutant population grows exponentially and is modelled deterministically. *Mutations* arise randomly according to a time-inhomogeneous Poisson process (not to be confused with *mutants*), and each mutant lineage proliferates according to a pure birth process.

An analytical expression for the mutant count distribution paved the way for several computational mutation rate estimation tools. The most advanced methods use maximum-likelihood estimation and today there are several comparably easy to use tools available, see [51] for a recent review.

The authors of [62] also used an estimation tool [32] based on the above-described population dynamic model. But is this model applicable to treatment with ciprofloxacin? For one, the model does not account for cell death, which might lead to overestimating mutation rates [25]. Cell death could have also led to an overestimation of the increase in mutation rate in [62], but interestingly, it cannot explain its observed non-monotonic dependence on the antibiotic dose.

Mutation-rate estimation under heterogeneous stress responses Another assumption of the population dynamic model used in the estimation method used by [62] (and any other estimation method available at the time of the publication) is violated: the assumption that the mutation rate is constant across the bacterial population. One if not *the* key finding of [62] is that the mutation rate is increased only in a subpopulation of cells. However, within-population heterogeneity in stress responses is not captured by the population dynamic models used in mutation rate estimation tools. Of course, applying maximum-likelihood inference and inferring a uniform mutation rate for the overall population is possible. However, if the mutation rate is increased in only a subpopulation of cells, the estimated 'mutation rate' is rendered obsolete. This problem sparked a series of questions.

1. Does the estimated quantity (uniform mutation rate for a population with heterogeneous mutation rates) still have a biological interpretation?
2. What are general biases in mutation rate estimation introduced by neglecting heterogeneity in mutation rates?
3. Can we adapt the population dynamic model behind the fluctuation assay to capture heterogeneous stress responses and maybe even estimate the specific increase in mutation rate in the gambler subpopulation?
4. Are there other studies that have applied standard estimation methods and potentially overlooked heterogeneity in stress responses?
5. Can we identify heterogeneity in mutation rates from fluctuation assay data?
6. Can we explain the observed non-monotonic dose dependence of mutagenesis with heterogeneity in stress responses and mutation rates?

Answering these questions would take me the rest of my PhD.

To answer these questions, we developed an estimation method that accounts for heterogeneity in stress responses. Our model considers a highly mutating and slowly dividing subpopulation, inspired by the SOS response. First, we validated our estimation method using simulated fluctuation assay data; this work is published and directly follows as Chapter 2. In the Chapter 3, we then apply our estimation tool to published experimental fluctuation assay data. Finally, in Chapter 4, I mathematically model the dose dependence of stress-induced mutagenesis under heterogeneous stress responses.

Chapter 2

Estimating mutation rates under heterogeneous stress responses

To be able to estimate mutation rates under heterogeneous stress responses we had to take the following steps.

Develop a model of heterogeneous stress responses

First, we needed to develop a model that captures heterogeneity in bacterial stress responses. We based our model on previous work of my second supervisor Meriem El Karoui's lab, describing the heterogeneous expression of the SOS response in *E. coli* populations treated with low concentrations of ciprofloxacin [38]. In this model, cells can switch to a state of high SOS expression that leads to a reduction in growth rate. Together with my first supervisor Helen K. Alexander, I extended this model by the occurrence and dynamics of mutant lineages in the high- and low-SOS subpopulations. Here, we had to evaluate which of the standard (and less standard) assumptions that are made in fluctuation analysis we wanted to adopt.

- Typically, the growth of the wild-type cells is modelled as deterministic (exponential) growth, whereas mutant lineages are treated stochastically. An exception is the Bartlett formulation [7], in which wild-type and mutant cells are treated stochastically. Mutation rate estimation under this fully stochastic model version has been suggested [78] but, for sufficiently large wild-type population sizes, been shown to not significantly improve estimates while being computationally slow [80]. We wanted to adopt a deterministic treatment of wild-type cells for our

model. However, we worried that the size of the high-SOS subpopulation was too small. Therefore, together with Tibor Antal, we evaluated analytically and in stochastic simulations in which parameter regime the high-SOS subpopulation could be treated deterministically.

- Another standard assumption is that mutant cells grow at the same rate as non-mutant cells. This assumption has been relaxed in many existing mutation rate estimation tools [29, 58, 80] to account for mutant fitness costs or advantages due to cross resistance. We realised that we had to include such a differential mutant fitness for the high-SOS subpopulation because, in our model, expression of the stress response results in a reduction in growth rate. For simplicity, we decided to not consider differential fitness for the low-SOS subpopulation though.
- The dynamics of mutant lineages are classically described as pure birth processes with exponentially distributed division times. Arguably, such division times are not biologically realistic and mutation rate estimation under potentially more realsitic dynamics has been suggested and implemented: constant division times (Haldane model) [58, 80], lognormal- and gamma-distributed division times [58], and time-dependent division rates [57] but without significant impact on the resulting number of mutants. Together with my first and second supervisor we discussed at length about how to model the dynamics of the slowly dividing and filamenting high-SOS mutants. In the end, we decided to adopt exponentially distributed division times as a simplified first step.
- In a standard fluctuation assay, populations are grown under permissive conditions and cell death is ignored. Particularly under stress however, cell death might become substantial and, consequently, the standard model has been extended by cell death [41]. However, it proved not possible to infer rates of cell death together with mutation rates in fluctuation analysis and existing mutation rate estimation tools only allow to set the death rate as a fixed parameter in the inference, either only for mutant cells [58], as the same for wild-type and mutant cells [51], or as a stepwise constant parameter [25]. Even though there is evidence that neglecting cell death can lead to overestimation of mutation rates [25], we decided to ignore it in the estimation of the mutation rate but to evaluate any biases introduced by that.

- Further standard assumptions are a negligibly small initial population size (relaxed in [80, 51]), a constant final population size (relaxed in [58, 80, 51] and shown to be not significant as long as the coefficient of variation in the final population size is < 0.2), immediate exertion of mutations (phenotypic lag is considered in [67, 12, 51]), no post-plating mutations (relaxed in [51]) and perfect plating (imperfect plating implemented as binomial sampling in [58, 80, 51]). For simplicity, we decided to adopt those assumptions as a first step.

Decide on an inference method

Next, we needed to decide on a method to infer mutation rates from fluctuation assay data. In general, we wanted to use a method that uses information of the entire observed mutant count distribution. That meant that we had to, in some way or the other, evaluate the likelihood of observing a particular mutant count distribution given a model and model parameters. This is what is conceptualised in a *likelihood function*: the probability of seeing some data under different parameter values for a specific model. Examples of inference methods using the likelihood function are maximum-likelihood and Bayesian inference.

Briefly, in maximum-likelihood inference, the argument that maximises the likelihood function under a certain model is used as the point estimate for the respective model parameters. In Bayesian inference, on the other hand, the likelihood function is used to calculate the *posterior distribution*, which gives the probability of a hypothesis (a model with parameter values) given the data. This approach requires a *prior distribution*, i.e. information available beforehand. The prior distribution can be set to a non-informative (Normal) distribution or informative, for example gleaned from literature or previous experiments [22]. The required calculations in Bayesian inference often involve computationally expensive numerical approximations of solutions of integrals. Approximate Bayesian ('likelihood-free') computation can be a solution here [8]. Bayesian inference has the advantage of straightforward construction of confidence intervals.

Despite some advantages of Bayesian inference, we decided to use maximum-likelihood inference because it is by far most commonly used in fluctuation analysis (but see [2, 79]) and it matched my and my first supervisors expertise. Moreover, we decided to attempt to analytically derive and numerically implement the mutant count distribution for our new model of heterogeneous stress responses. This approach has the

advantage of being computationally faster than a simulation-based approach but can be impossible for complex models (as is the case, for example, in [25]). In fact, to be able to derive the mutant count distribution for our new model, we had to make a series of simplifying approximations. Together with my second supervisor Meriem El Karoui, we confirmed that these approximations were biologically appropriate. Making these approximations also implied that I could derive the mutant count distribution based on proofs that have appeared previously in [52, 42, 44].

Design and implement a simulation study

After developing the model and making necessary approximations, I implemented the numerical calculation of the (probability mass function of the) resulting mutant count distribution based on [41]. Next, I implemented the maximum-likelihood estimation approach we decided on. We wanted to use simulated fluctuation assay data to test our estimation method. Together with my first supervisor, we designed a (stochastic) simulation study, i.e. we chose a parameter regime and number of replicates to simulate and analyse, which I then implemented. After useful comments from a reviewer, I also implemented likelihood-ratio based confidence intervals and a bespoke model selection procedure.

Together with my first and second supervisor, we decided which figures best summarise the results of the simulation study. As a last step, I wrote the manuscript, with editing suggestions from my first and second supervisors, and made the accompanying figures.

PLOS COMPUTATIONAL BIOLOGY

RESEARCH ARTICLE

Estimating mutation rates under heterogeneous stress responses

Lucy Lansch-Justen[1]*, **Meriem El Karoui**[2,3,4], **Helen K. Alexander**[1,3]*

1 Institute of Ecology and Evolution, School of Biological Sciences, University of Edinburgh, Edinburgh, Scotland, United Kingdom, 2 Institute of Cell Biology, School of Biological Sciences, University of Edinburgh, Edinburgh, Scotland, United Kingdom, 3 Centre for Engineering Biology, University of Edinburgh, Edinburgh, Scotland, United Kingdom, 4 Bacterial Systems Biology and Anti Microbial Resistance, Laboratoire de Biologie et Pharmacologie Appliquée, École Normale Supérieure Paris-Saclay, Gif-sur-Yvette, France

* lucy.lanju@googlemail.com (LLJ); helen.alexander@ed.ac.uk (HKA)

OPEN ACCESS

Citation: Lansch-Justen L, El Karoui M, Alexander HK (2024) Estimating mutation rates under heterogeneous stress responses. PLoS Comput Biol 20(5): e1012146. https://doi.org/10.1371/journal.pcbi.1012146

Editor: Mark M. Tanaka, University of New South Wales, AUSTRALIA

Received: November 27, 2023

Accepted: May 8, 2024

Published: May 28, 2024

Peer Review History: PLOS recognizes the benefits of transparency in the peer review process; therefore, we enable the publication of all of the content of peer review and author responses alongside final, published articles. The editorial history of this article is available here: https://doi.org/10.1371/journal.pcbi.1012146

Data Availability Statement: The complete annotated documentation of the computational analyses of this study is archived on Zenodo, https://doi.org/10.5281/zenodo.11174801.

Abstract

Exposure to environmental stressors, including certain antibiotics, induces stress responses in bacteria. Some of these responses increase mutagenesis and thus potentially accelerate resistance evolution. Many studies report increased mutation rates under stress, often using the standard experimental approach of fluctuation assays. However, single-cell studies have revealed that many stress responses are heterogeneously expressed in bacterial populations, which existing estimation methods have not yet addressed. We develop a population dynamic model that considers heterogeneous stress responses (subpopulations of cells with the response *off* or *on*) that impact both mutation rate and cell division rate, inspired by the DNA-damage response in *Escherichia coli* (SOS response). We derive the mutant count distribution arising in fluctuation assays under this model and then implement maximum likelihood estimation of the mutation-rate increase specifically associated with the expression of the stress response. Using simulated mutant count data, we show that our inference method allows for accurate and precise estimation of the mutation-rate increase, provided that this increase is sufficiently large and the induction of the response also reduces the division rate. Moreover, we find that in many cases, either heterogeneity in stress responses or mutant fitness costs could explain similar patterns in fluctuation assay data, suggesting that separate experiments would be required to identify the true underlying process. In cases where stress responses and mutation rates are heterogeneous, current methods still correctly infer the effective increase in population mean mutation rate, but we provide a novel method to infer distinct stress-induced mutation rates, which could be important for parameterising evolutionary models.

Author summary

How does environmental stress, especially from antibiotics, affect mutation rates in bacteria? This question has often been examined by estimating mutation rates using fluctuation assays, an experiment dating back to Luria and Delbrück in the 1940s. In this study, we consider variation in stress responses within bacterial populations, as revealed by recent

Funding: This work was supported by the UKRI Biotechnology and Biological Sciences Research Council (BBSRC) grant number BB/T00875X/1 and a University of Edinburgh Principal's Career Development PhD Scholarship to LLJ, a Wellcome Trust Investigator Award 205008/Z/16/Z to MEK, and a Royal Society University Research Fellowship URF/R1/191269 to HKA. The funders had no role in study design, data collection and analysis, decision to publish, or preparation of the manuscript.

Competing interests: The authors have declared that no competing interests exist.

single-cell studies, which is neglected in currently available mutation-rate estimation methods. Our approach involves a population dynamic model inspired by the DNA-damage response in *E. coli* (SOS response). It accounts for a subpopulation with high expression of the stress response, which increases the mutation rate and decreases the division rate of a cell. We use computer simulations to generate synthetic fluctuation assay data. Notably, we find that over a wide range of scenarios, existing models and our heterogeneous-response model cannot be distinguished using fluctuation assay data alone. This emphasises the need for separate experiments to uncover the true underlying processes. Nevertheless, when stress responses are known to be heterogeneous, our study offers a novel method for accurately estimating mutation rates specifically associated with the high expression of the stress response. Uncovering the heterogeneity in stress-induced mutation rates could be important for predicting the evolution of antibiotic resistance.

Introduction

Bacteria are commonly exposed to adverse conditions, such as starvation, sub-optimal temperatures or toxins, including antibiotics. To cope with these conditions, bacteria have evolved a range of stress responses that enhance viability under stress, often at the expense of a lower growth rate. Some of these response pathways also increase mutagenic mechanisms by, for example, increasing the expression of error-prone DNA polymerases or down-regulating error-correcting enzymes [1, 2]. It has been proposed that this so-called 'stress-induced mutagenesis' (SIM) in bacterial cells could accelerate the evolution of populations that are poorly adapted to their environment [3–6]. Consequently, inhibiting bacterial stress responses has been suggested to prevent antibiotic resistance evolution and gained some experimental support [7–9].

Several studies report increased mutation rates in bacterial populations exposed to sub-lethal antibiotic concentrations [8, 10–15]. These mutation rates have been typically measured with fluctuation assays. This experiment (see, for example, [16] for a protocol) involves inoculating several parallel cultures at a small population size and growing them under permissive conditions for several hours, typically overnight. During this *growth phase*, mutations occur randomly, and the experiment is designed to minimise selection on mutant cells. Subsequently, each culture is plated on strong selective media such that only mutant cells can grow and form a colony. The mutation rate to the chosen selective marker is estimated from the distribution of the number of mutant colonies on the plates, the *mutant count distribution*; see [17] for a summary of estimation methods. The experiment is repeated to quantify the mutation-rate increase associated with stress, by exposing the cultures to a stressor during the growth phase. Then, the *stress-induced* mutation rate is estimated and compared with the mutation rate under permissive conditions. However, stress impacts the growth of bacterial cells in several ways, which are neglected in commonly applied estimation methods, potentially leading to biased estimates of the mutation rate. For instance, increased cell death leads to overestimating the mutation rate [18]. Another effect that has not yet been addressed is within-population heterogeneity in stress responses.

In recent years, single-cell experiments have revealed extensive heterogeneity in the expression of stress responses in bacterial populations [8, 19–28]. Heterogeneity can arise for various reasons, including stochastic expression of genes involved in stress responses, especially where the corresponding proteins are initially present in small numbers [20–22], phenotypic variability in the stability of key regulators [25], or micro-environmental variation in cell-to-cell

interactions [28]. Positive and negative feedback loops are common features of stress response regulatory networks, which can generate, amongst other features, cell-to-cell variation [29]. In some cases, a subpopulation of cells showing elevated stress responses has been directly associated with a higher rate of DNA mismatches or higher mutant frequency [8, 20–22, 24, 26].

In addition to mutagenic mechanisms, stress responses can alter cell division and death rates. For example, the widely studied SOS response, which leads to the transcriptional induction of approximately 40 genes after exposure to DNA damage, involves inhibition of cell division, filamentation and induction of error-prone DNA polymerases that could increase mutation rate [30, 31]. Single-cell studies using fluorescent reporters for the SOS response in *E. coli* have revealed that its expression is highly heterogeneous. Under certain conditions, a subpopulation of cells with a very high level of SOS compared to the rest of cells with lower expression levels has been observed, and this heterogeneity can be approximated as a bimodal response [19, 21, 27]. Overall, heterogeneously expressed stress responses are, therefore, likely to impact both bacterial population dynamics and mutational input during the growth phase of a fluctuation assay, and it is unclear whether estimation methods that neglect heterogeneity in stress responses produce reliable results.

In this study, we present a population dynamics model that considers within-population heterogeneity in stress responses. Motivated by the SOS response, we describe two discrete subpopulations of cells, where high expression of the stress response is associated with both a higher mutation rate and a lower division rate than in cells with low expression. We derive the resulting mutant count distribution in the total population and implement maximum likelihood estimation of the mutation-rate increase associated with the induction of the stress response. We test the performance of our method using stochastic simulations of fluctuation assays under permissive and stressful conditions, including robustness to biologically realistic model deviations such as mutant fitness costs and cell death. We also apply formal model comparison to assess whether within-population heterogeneity could be detected from fluctuation assays alone.

Model and methods

Studying stress-induced mutagenesis with fluctuation assays requires a pair of experiments: one with a growth phase under permissive conditions (as a baseline for comparison) and one under 'stressful' conditions, where a stressor such as a low dose of antibiotic (which is supposed to induce a mutagenic stress response in the cells) is added during the growth phase. In addition to performing the experiments, researchers have to decide on a mathematical model of the underlying dynamics, including the population dynamics of non-mutants and mutants during the growth phase, and how these dynamics change under exposure to stress. This then allows them to estimate the model parameters, most importantly mutation rates, and assess increases in mutation rates due to stress. Many studies of SIM to date, for example [8, 11, 14], have implicitly assumed that the stress response is homogeneous, i.e. the stressful condition results in a population-wide elevation of the mutation rate. In contrast, our new model considers within-population heterogeneity in stress responses and mutation rates.

In the following, we recap what we call the *standard model* used in a classical fluctuation assay and extensions particularly relevant to stress. Then, we formalise the *homogeneous-response model*, a version of which is considered in the aforementioned studies of SIM, and introduce our new *heterogenenous-response model* with a detailed description of the population dynamic model under heterogeneous stress responses and the derivation of the resulting mutant count distribution. Next, we describe our model fitting and parameter estimation approach using maximum likelihood estimation and summarise the inference parameters.

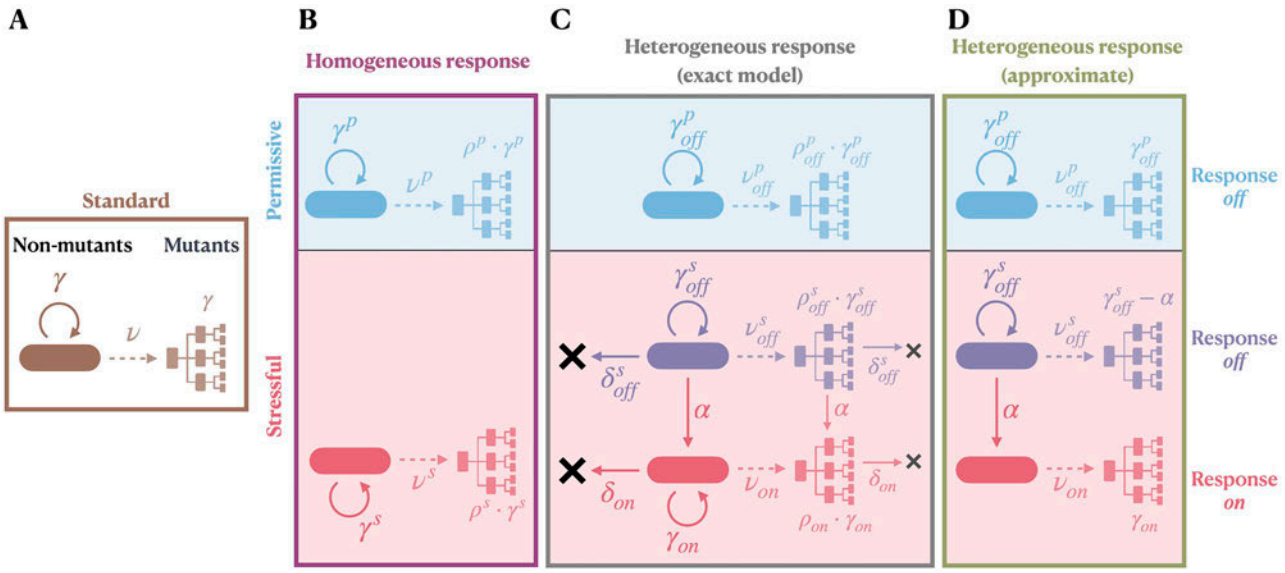

Fig 1. Schematic illustrating the standard model of fluctuation assays and models of homogeneous and heterogeneous responses to stress. In the standard model (**A**), non-mutants are assumed to grow exponentially (rate γ), mutations to arise randomly (rate ν per cell per unit time), and mutants to divide stochastically (birth rate γ). In models of homogeneous stress responses (**B**), it is assumed that both fluctuation assays under permissive (superscript *p*, light blue) and stressful (superscript *s*, light red) conditions can be described by the standard model, with optional differential fitness of mutants compared to non-mutants (factor ρ). In our model of heterogeneous stress responses, on the other hand, we assume that the induction of the stress response (rate α) results in the separation into two subpopulations: response-*off* (subscript *off*, dark purple) and response-*on* (subscript *on*, red). When simulating under the heterogeneous-response model, we use the exact model (**C**), optionally extended by cell death (rate δ) and differential mutant fitness (ρ), where explicitly specified. For inference, we fit the approximate heterogeneous-response model (**D**). For the homogeneous-response model, we use the same version for both simulation and inference.

https://doi.org/10.1371/journal.pcbi.1012146.g001

Finally, we describe the simulations to generate synthetic mutant count data, and how we evaluate the estimation methods using these data.

For schematics of the models used in simulation and inference, see Fig 1. The complete documentation of the computational methods can be found in the **README** at https://github.com/LucyL-J/Quantifying-SIM.

The standard model of fluctuation assays and extensions relevant to stress

Classically, fluctuation assays have been described using what we refer to as the *standard model* (Fig 1A). In the standard model, the non-mutant population is assumed to grow exponentially during the growth phase, while the occurrence of mutations and the division of mutant cells are treated stochastically. On selective plates, it is assumed that every mutant cell (but no non-mutant cell) forms a visible colony. Many extensions of this standard model have been developed, briefly reviewed, for example, in [32]. Here, we describe two extensions particularly relevant to stress: accounting for cell death and allowing mutant cells to have a different fitness than non-mutant cells during the growth phase. The latter can become important when resistance allowing growth on the selective plates also confers an advantage to the stressor (for example, due to cross-resistance) or when mutants carry a fitness cost. Together, these two extensions result in the following population dynamic model. The non-mutant population grows exponentially,

$$N(t) \quad N_i e^{\lambda t} \tag{1}$$

with initial population size N_i and population growth rate λ. Mutations occur according to a

time-inhomogeneous Poisson process with rate $\nu N(t)$. Note that ν describes the mutation rate to the phenotype of interest selected on the plates in the fluctuation assay (mutations per cell per unit time, also called instantaneous mutation rate). The dynamics of each mutant cell M are captured by a continuous-time linear birth-death process [33] with birth rate b and death rate d:

$$\begin{cases} M \to MM, & \text{rate } b \\ M \to \varnothing, & \text{rate } d, \end{cases} \tag{2}$$

implying that mutants have a different fitness than non-mutants if $b - d \neq \lambda$.

For such dynamics, defining the per-generation mutation rate as $\mu := \frac{\nu}{\lambda}$, the differential fitness of mutants as $\rho := \frac{b-d}{\lambda}$ and the extinction probability of mutants as $\epsilon := \frac{d}{b}$, the resulting distribution of the number of mutants when the population reaches a final population size N_f has been derived [34]: Assuming $N_f \gg N_i$ (neglecting initial population size effects), the probability-generating function (PGF) $G(z)$, a mathematically-convenient representation of the mutant count distribution, is given by

$$G(z) \quad \exp\left[\quad \mu N_f(1 \quad \epsilon) F\left(\begin{matrix} 1, \frac{1}{\rho} \\ 1 + \frac{1}{\rho} \end{matrix} ; \frac{z \quad \epsilon}{z \quad 1} \right) \right] \tag{3}$$

with F being the hypergeometric function. Note that z is a dummy variable in the PGF with no physical meaning, and $G(z)$ does not directly give the probability of observing a specific mutant count, but the probabilities can be calculated from $G(z)$ [34]. In the case where mutants have the same fitness as non-mutants and do not undergo cell death, the equation simplifies to:

$$G(z) \quad \exp\left[\mu N_f \frac{(1 \quad z)\log(1 \quad z)}{z} \right], \quad \text{for } \rho \quad 1, \epsilon \quad 0 \tag{4}$$

Formalisation of the homogeneous-response model

The *homogeneous-response model* assumes that stress and stress responses impact mutation, division and death rates on a population-wide level. This implies that the dynamics under stressful conditions can, as under permissive conditions, be captured by the standard model (with optional extensions) as described above, simply substituting different parameter values (Fig 1B). Under permissive conditions (parameters denoted with a superscript p), assuming no cell death, the non-mutant population grows exponentially, $n^p(t) = n^p(0)e^{\gamma^p t}$, with division rate γ^p; mutations occur at rate $\nu^p n^p(t)$ and mutants develop according to a pure birth process with rate $\rho^p \cdot \gamma^p$.

Under stressful conditions (parameters denoted with a superscript s), the population grows as $n^s(t) = n^s(0)e^{(\gamma^s - \delta^s)t}$ with a different growth rate caused by a change in division rate γ^s or a non-zero death rate δ^s or both. Mutations also occur at a different rate $\nu^s n^s(t)$, and the dynamics of mutants are given by a birth-death process with birth rate $\rho^s \cdot \gamma^s$ and death rate δ^s.

Therefore, the stress response results in a population-wide change in the per-division mutation rate, $\mu^p \quad \frac{\nu^p}{\gamma^p} \to \mu^s \quad \frac{\nu^s}{\gamma^s}$; potentially the differential fitness of mutants, $\rho^p \to \rho^s$; and potentially a non-zero extinction probability of mutants, $\epsilon^s \quad \frac{\delta^s}{\gamma^s}$. The PGFs for the mutant count distributions under permissive and stressful conditions in the homogeneous-response model

are thus given by

$$G^{p}_{\mathrm{hom}}(z) \quad \exp\left[\ \mu^{p} N^{p}_{f} F\left(\begin{matrix}1,\ \dfrac{1}{\rho^{p}}\\ 1+\dfrac{1}{\rho^{p}}\end{matrix};\dfrac{z}{z\quad 1}\right)\right] \tag{5}$$

$$G^{s}_{\mathrm{hom}}(z) \quad \exp\left[\ \mu^{s} N^{s}_{f}(1\quad \epsilon^{s}) F\left(\begin{matrix}1,\ \dfrac{1}{\rho^{s}}\\ 1+\dfrac{1}{\rho^{s}}\end{matrix};\dfrac{z\quad \epsilon^{s}}{z\quad 1}\right)\right]. \tag{6}$$

By applying standard mutation-rate estimation methods to both the fluctuation assay under permissive and the one under stressful conditions, studies of SIM to date have implicitly applied such a homogeneous-response model.

Detailed description of the heterogeneous-response model

In contrast, our *heterogeneous-response model* considers within-population heterogeneity in the expression of the stress response under stressful conditions. Specifically, we suppose the population can be divided into two subpopulations: one with a low expression level of the stress response (here referred to as response switched *off*, even if strictly speaking the response is not fully *off* but very low) and the other with a high expression level (here referred to as response switched *on*). Each sub-population is associated with its own mutation rate and division rate. We adopt most of the same assumptions of the standard model while focusing on the specific effect of within-population heterogeneity upon induction of stress responses (Fig 1C).

Under permissive conditions, we assume that all cells have the response switched *off*, neglecting any stochastic switching in the absence of a stressor, and therefore, continue to use the standard model (with optional differential mutant fitness). In particular, the population grows exponentially, $n^{p}_{off}(t) \quad e^{\gamma^{p}_{off} t}$ with growth rate given by the division rate γ^{p}_{off}, mutations arise at rate $v^{p}_{off} n^{p}_{off}(t)$ and mutants develop according to a pure birth process with rate $\rho^{p}_{off} \cdot \gamma^{p}_{off}$. The PGF of the mutant count distribution is given by

$$G^{p}_{\mathrm{het}}(z) \quad \exp\left[\ \mu_{off} N^{p}_{f} F\left(\begin{matrix}1,\ \dfrac{1}{\rho^{p}_{off}}\\ 1+\dfrac{1}{\rho^{p}_{off}}\end{matrix};\dfrac{z}{z\quad 1}\right)\right], \tag{7}$$

where $\mu_{off} \coloneqq \frac{v^{p}_{off}}{\gamma^{p}_{off}}$ describes the *per-division* mutation rate, which equals the *per-generation* rate as, under permissive conditions, the population growth is solely determined by cell division.

Population dynamic model under heterogeneous stress responses. Upon exposure to stressful conditions, cells induce a stress response with a constant switching rate α, leading to the emergence of a response-*on* subpopulation. Inducing the stress response alters the mutation rate of the cells but potentially also their division and death rates. We assume that, as long as the stress persists, cells do not switch the response *off* again.

Non-mutant population dynamics. We model the population sizes over time of the non-mutant response-*off* and response-*on* subpopulations, n^{s}_{off} and n_{on}, respectively, with coupled

differential equations:

$$\dot{n}^s_{off} \quad (\gamma^s_{off} \quad \delta^s_{off} \quad \alpha) n^s_{off}, \tag{8}$$

$$\dot{n}_{on} \quad \alpha n^s_{off} + (\gamma_{on} \quad \delta_{on}) n_{on}, \tag{9}$$

Here, γ^s_{off} is the division rate of the response-*off* subpopulation under stress (which can be different than under permissive conditions, γ^p_{off}) and δ^s_{off} its death rate, γ_{on} and δ_{on} are the division and death rates of the response-*on* subpopulation, and α is the switching rate. The solution to these equations is given by

$$n^s_{off}(t) \quad n^s_{off}(0) e^{(\gamma^s_{off} \quad \delta^s_{off} \quad \alpha)t} \tag{10}$$

$$n_{on}(t) \quad \frac{\alpha n_{off}(0)}{\gamma^s_{off} \quad \delta^s_{off} \quad \alpha \quad (\gamma_{on} \quad \delta_{on})} \left(e^{(\gamma^s_{off} \quad \delta^s_{off} \quad \alpha)t} \quad e^{(\gamma_{on} \quad \delta_{on})t} \right) + n_{on}(0) e^{(\gamma_{on} \quad \delta_{on})t} \tag{11}$$

with $n^s_{off}(0)$ and $n_{on}(0)$ denoting the initial numbers of response-*off* and response-*on* cells, respectively.

This approach assumes that the non-mutants, including the initially small response-*on* subpopulation, can be treated deterministically. We test the validity of this assumption using stochastic simulations (section A in S1 File): we simulate switching *on* of the response as a time-inhomogeneous Poisson process and the growth dynamics of the response-*on* subpopulation as a continuous-time linear birth-death process. Then, we compare the resulting population size with Eq 11. We find that deviations from the deterministic prediction are negligible for a wide range of switching rates and division rates of response-*on* cells and for zero and small initial sizes of the response-*on* subpopulation (Fig A in S1 File). Therefore, throughout the rest of this study, we treat non-mutants deterministically.

Mutant population dynamics. We consider mutations in the response-*off* and the response-*on* subpopulation to occur according to time-inhomogeneous Poisson processes and treat the dynamics of the resulting mutants stochastically. Mutations arise in each subpopulation at rates $v^s_{off} n^s_{off}(t)$ and $v_{on} n_{on}(t)$, respectively. Importantly, mutation is not linked to cell division, but rather to chromosome replication. Expression of the SOS response, for example, inhibits cell division, but cells continue growing, leading to filamentation. Due to the continuation of chromosome replication, filamented cells may contain multiple chromosomes [35]. We neglect the possibility that these intracellular dynamics introduce heterogeneities amongst cells within the response-on subpopulation or over time and assume that the per-cell mutation rate (v_{on}) is constant. Experiments show that under prolonged low-level stress, multinucleated filamented cells can 'bud' viable, normal-sized progeny cells from their tips, some of which contain mutated chromosomes [35]. Although our model remains a simplification of this process, the experimental evidence indicates that response-*on* cells, even if largely non-dividing, can generate mutant offspring.

At the same time, since the selective agent on the plates is normally chosen to be unrelated to the stressor applied in the growth phase (e.g. two different antibiotics with no cross-resistance), we assume that mutation itself does not alter the stress response. For response-*off* cells, this implies that mutants can induce the response equivalently to non-mutants. Nonetheless, mutations might affect the fitness during the growth phase. Together, these assumptions result in a continuous-time two-type branching process describing the mutant response-*off* and response-*on* subpopulations, defined by the respective birth rates $\rho^s_{off}\gamma^s_{off}$ and $\rho_{on}\gamma_{on}$, respective

death rates δ^s_{off} and δ_{on}, and switching at rate α:

$$\begin{cases} M_{off} \rightarrow M_{off}\, M_{off}, & \text{rate } \rho^s_{off}\gamma^s_{off} \\ M_{off} \rightarrow \varnothing, & \text{rate } \delta^s_{off} \\ M_{off} \rightarrow M_{on}, & \text{rate } \alpha \\ M_{on} \rightarrow M_{on}\, M_{on}, & \text{rate } \rho_{on}\gamma_{on} \\ M_{on} \rightarrow \varnothing, & \text{rate } \delta_{on}. \end{cases} \tag{12}$$

On selective plates, where the stressor (which was applied during the growth phase) is no longer present, we assume that response-*on* mutant cells can resume division. Therefore, we continue to adopt the standard model assumption that every mutant cell forms a visible colony upon selective plating.

Derivation of the mutant count distribution. To derive an analytical expression for the mutant count distribution, we make several approximations, resulting in the approximate heterogeneous-response model depicted in Fig 1D. First, we approximate Eq 11 as

$$\hat{n}_{on}(t) \quad \frac{\alpha n^s_{off}(0)}{\gamma^s_{off} \quad \delta^s_{off} \quad \alpha \quad (\gamma_{on} \quad \delta_{on})} e^{(\gamma^s_{off} \quad \delta^s_{off} \quad \alpha)t}. \tag{13}$$

This approximation is valid when the initial population size of the response-*on* subpopulation is comparably small, $n_{on}(0) \ll n_{off}(0)$, and its growth is slower than the growth of the response-*off* subpopulation, $\gamma_{on} \quad \delta_{on} \ll \gamma^s_{off} \quad \delta^s_{off} \quad \alpha$. As a consequence of this approximation, the total population grows exponentially with a *population growth rate* of

$$\lambda^s \quad \gamma^s_{off} \quad \delta^s_{off} \quad \alpha, \tag{14}$$

and the response-*on* subpopulation makes up a constant fraction of

$$f_{on}(t) \quad \frac{n_{on}(t)}{n_{on}(t) + n_{off}(t)} \quad \frac{\alpha}{\gamma^s_{off} \quad \delta^s_{off} \quad (\gamma_{on} \quad \delta_{on})} \quad : f^*_{on} \tag{15}$$

In the exact model given by the Eqs 10 and 11, the fraction of the response-*on* subpopulation changes with time until the stationary fraction f^*_{on} is reached, but we assume that the fraction at the end of the growth phase, $f_{on}(t_f)$, is a good approximation of f^*_{on} and for the rest of this study, we refer to it as simply the fraction of response-*on* cells f_{on}. Note that, even if response-*on* cells have zero division rate, the response-*on* subpopulation grows exponentially with the population growth rate λ^s due to the induction of the stress response in response-*off* cells.

We define the *relative switching rate* as

$$\tilde{\alpha} := \frac{\alpha}{\gamma^s_{off} \quad \delta^s_{off}} \tag{16}$$

and the *relative fitness* of response-*on* compared to response-*off* cells under stressful conditions as

$$r_{on} := \frac{\gamma_{on} \quad \delta_{on}}{\gamma^s_{off} \quad \delta^s_{off}} \tag{17}$$

and thereby obtain

$$f_{on} \quad \frac{\tilde{\alpha}}{1 \quad r_{on}}. \tag{18}$$

This allows us to rewrite the population growth rate as a function of the division rate γ^s_{off} and the extinction probability $\epsilon^s_{off} := \frac{\delta^s_{off}}{\gamma^s_{off}}$ of response-*off* cells, and the fraction f_{on} and relative fitness r_{on} of the response-*on* subpopulation

$$\lambda^s \quad \gamma^s_{off} \quad \delta^s_{off} \quad \alpha \quad \gamma^s_{off}(1 \quad \epsilon^s_{off})(1 \quad f_{on}(1 \quad r_{on})), \tag{19}$$

and to calculate the per-generation mutation rates of response-*off* and response-*on* cells

$$\frac{\nu^s_{off}}{\lambda^s} \quad \frac{\nu^s_{off}}{\gamma^s_{off}(1 \quad \epsilon^s_{off})(1 \quad f_{on}(1 \quad r_{on}))} \quad \frac{\mu_{off}}{(1 \quad \epsilon^s_{off})(1 \quad f_{on}(1 \quad r_{on}))} \tag{20}$$

$$\frac{\nu_{on}}{\lambda^s} \quad \frac{\nu_{on}}{\gamma^s_{off}(1 \quad \epsilon^s_{off})(1 \quad f_{on}(1 \quad r_{on}))} \quad \frac{\mu_{on}}{(1 \quad \epsilon^s_{off})(1 \quad f_{on}(1 \quad r_{on}))} \tag{21}$$

with $\mu_{on} := \frac{\nu_{on}}{\gamma^s_{off}}$. Importantly, we assume here that the per-division mutation rate of response-*off* cells is the same under stressful as under permissive conditions, $\mu_{off} \quad \frac{\nu^s_{off}}{\gamma^s_{off}} \quad \frac{\nu^p_{off}}{\gamma^p_{off}}$.

In an additional approximation to derive the mutant count distribution, we neglect the induction of the stress response in the mutants and assume that mutations have no fitness effect. For mathematical convenience, we consider switching as a reduction in the division rate of response-*off* mutants by α instead (birth rate equal to $\gamma^s_{off} \quad \alpha$). With this assumption, the dynamics of response-*off* and response-*on* mutant lineages are independent birth-death processes. For response-*on* cells, the relative fitness of mutants ρ_{on} (relative to the population growth rate) can be expressed via

$$\rho_{on} \quad \frac{\gamma_{on} \quad \delta_{on}}{\lambda^s} \quad \frac{r_{on}}{1 \quad f_{on}(1 \quad r_{on})}. \tag{22}$$

With these approximations (see Fig 1D), the mutant counts in the response-*off* and response-*on* subpopulations are two independent stochastic processes, each following the standard model, with differential mutant fitness in the case of the response-*on* cells. Therefore, we can substitute the appropriate parameters into Eq 3 to obtain PGFs for the mutant counts, $G^s_{off}(z)$ and $G_{on}(z)$, respectively:

$$G^s_{off}(z) \quad \exp\left[\frac{\mu_{off}}{1 \quad f_{on}(1 \quad r_{on})}(1 \quad f_{on})N^s_f \frac{(1 \quad z)\log\left(\frac{1 \quad z}{1 \quad \epsilon^s_{off}}\right)}{z \quad \epsilon^s_{off}}\right] \tag{23}$$

$$G_{on}(z) \quad \exp\left[\frac{\mu_{on}}{1 \quad f_{on}(1 \quad r_{on})}\frac{1 \quad \epsilon_{on}}{1 \quad \epsilon^s_{off}} f_{on} N^s_f F\left(\begin{matrix} 1, \frac{1 \quad f_{on}(1 \quad r_{on})}{r_{on}} \\ 1 + \frac{1 \quad f_{on}(1 \quad r_{on})}{r_{on}} \end{matrix}; \frac{z \quad \epsilon_{on}}{z \quad 1}\right)\right]. \tag{24}$$

Finally, the total mutant count distribution is given by the sum of the contributions of response-*off* and response-*on* subpopulations, with its PGF $G^s_{\text{het}}(z)$ given by the product $G^s_{off}(z) \cdot G_{on}(z)$.

In the case of $\gamma_{on} = 0$, the contribution to the mutant count from the response-*on* subpopulation follows a Poisson distribution, and (without cell death, implying $r_{on} = 0$) the PGF of total mutant count distribution reduces to

$$G^s_{\text{het}}(z) \quad \exp\left[\overbrace{\mu_{off} N^s_f \frac{(1 \quad z)\log(1 \quad z)}{z}}^{\text{Response-}off\text{ contribution}} + \overbrace{\mu_{on} \frac{f_{on}}{1 \quad f_{on}} N^s_f (z \quad 1)}^{\text{Response-}on\text{ contribution}}\right] \tag{25}$$

$$\exp\left[\mu_{off} N^s_f \left(\frac{(1 \quad z)\log(1 \quad z)}{z} + \frac{\mu_{on} f_{on}}{\mu_{off}(1 \quad f_{on})}(z \quad 1)\right)\right]. \tag{26}$$

$G^s_{\text{het}}(z)$ no longer depends on the mutation rate (μ_{on}) and fraction (f_{on}) of response-*on* cells separately, but rather on the composite parameter

$$\mathcal{S} := \frac{\mu_{on} f_{on}}{\mu_{off}(1 \quad f_{on})} \tag{27}$$

which gives the ratio of mutation supply coming from the response-*on* compared to the response-*off* subpopulation, with $\mathcal{S} \quad 0$ implying no heterogeneity in mutation rates.

For the purpose of comparison, we also define the increase in population mean mutation rate under stressful compared to permissive conditions:

$$\bar{M} := \frac{(1 \quad f_{on})\mu_{off} + f_{on}\mu_{on}}{\mu_{off}}, \tag{28}$$

which is directly comparable to the increase in mutation rate in the homogeneous-response model, $\frac{\mu^s}{\mu^p}$, since μ^p and μ^s are population-wide rates.

Example mutant count distributions for the homogeneous and heterogeneous-response models are shown in Fig B in S1 File.

Model fitting and parameter estimation using maximum likelihood

We use a maximum likelihood approach to estimate the model parameters from fluctuation assay data. For a given model (homogeneous or heterogeneous), we find the set of model parameters θ for which the observed mutant counts are most likely. Importantly, we consider mutant count data concurrently from a pair of fluctuation assays: one under permissive and the other under stressful conditions. In our heterogeneous-response model, there is at least one shared parameter between conditions (μ_{off}); therefore, we consider the joint likelihood function. Note, however, that if there are no shared parameters between conditions (as is the case for some of the homogeneous-response models), the inference can be carried out separately.

We define a log-likelihood function

$$\ln \mathcal{L}(\theta \mid x^p, x^s) \quad \sum_{i \quad 0}^{m^p} x^p(i) \ln[p^p_i(\theta)] + \sum_{i \quad 0}^{m^s} x^s(i) \ln[p^s_i(\theta)] \tag{29}$$

as the natural logarithm of the probability of observing the mutant count distributions x^p and

Table 1. Parameters in the inference.

Symbol	Definition	Cond.	Model	In the inference
N_f^p	Final population size	P	(a-e)	Fixed
N_f^s	Final population size	S	(a-e)	Fixed
μ^p	Population-wide mutation rate	P	(a-c)	Inferred
μ^s	Population-wide mutation rate	S	(a-c)	Inferred
ρ^p	Differential mutant fitness	P	(a)	Fixed = 1
			(c)	Inferred
ρ^s	Differential mutant fitness	S	(a)	Fixed = 1
			(c)	Inferred
$\rho^p = \rho^s$	Differential mutant fitness	P+S	(b)	Jointly inferred
ϵ^s	Extinction probability mutants	S	(a-c)	Fixed = 0
μ_{off}	Mutation rate response-*off* cells	P+S	(d-e)	Jointly inferred
$\mathcal{S}$	Mutation-supply ratio	S	(d-e)	Inferred
f_{on}	Fraction response-*on* cells	S	(d)	Fixed
			(c)	Inferred if $r_{on} \neq 0$
r_{on}	Relative fitness response-*on* cells	S	(d)	Fixed (= 0)
			(e)	Inferred
μ_{on}	Mutation rate response-*on* cells	S	(d-e)	Calculated*
ϵ_{off}^s, ϵ_{on}	Extinction probabilities mutants	S	(d-e)	Fixed = 0

The different inference models are homogeneous-response (a) without, (b) with constrained or (c) with unconstrained differential mutant fitness, and heterogeneous-response with (d) zero or (e) non-zero division rate of response-*on* cells. In the inference, each parameter is either set to a fixed value or inferred, with the exception of the mutation rate of response-*on* cells, which is calculated from $\mathcal{S}$, μ_{off} and f_{on}. Parameters which appear in both permissive (P) and stressful (S) conditions are jointly inferred.

https://doi.org/10.1371/journal.pcbi.1012146.t001

x^s under permissive and stressful conditions, respectively, for a given model with parameters θ. Here, m^p and m^s represent the maximal observed numbers of mutant colonies, and $x^p(i)$ and $x^s(i)$ are the number of plates with i mutant colonies under permissive and stressful conditions, respectively. The p_i^p and p_i^s give the probabilities to observe i mutant colonies under permissive and stressful conditions, respectively, calculated from the PGFs of the mutant count distributions using recursive formulas described in [34]. Then, we use the default optimisation algorithm implemented in the Julia [36] package Optim.jl (https://julianlsolvers.github.io/Optim.jl/stable/), to find the parameters that maximise this log-likelihood function. The parameters that are estimated depend on the specific model that is considered, as described below and summarised in Table 1.

The complete documentation of all inference algorithms can be found in the file called **inference.jl** at https://github.com/LucyL-J/Quantifying-SIM.

Parameters in the inference.

Homogeneous-response model. In the homogeneous-response model, the mutant count distributions (Eqs 5 and 6) depend on the per-division mutation rates, final population sizes, and, optionally, differential mutant fitness under permissive and stressful conditions, as well as the extinction probability of mutants under stress. All parameters must either be set as inference parameters, or set to a fixed value, which could be the default value or as measured in a separate experiment. In our implementation, the per-division mutation rates, μ^p and μ^s, are inferred to calculate the increase in mutation rate associated with the stress, that is, $\frac{\mu^s}{\mu^p}$. The final population sizes under permissive and stressful conditions, N_f^p and N_f^s, are set to fixed

values, as they would typically be measured through plating a few cultures on non-selective media and colony counting. Moreover, we set the extinction probability of mutants under stress, ϵ^s, to zero because we neglect cell death in the inference, which is in common with most existing approaches, but see [18].

For the differential fitness of mutants compared to non-mutants, ρ^p and ρ^s, we consider three cases corresponding to different versions of the homogeneous-response model: (a) mutants have the same fitness as non-mutants, $\rho^p = \rho^s = 1$; (c) mutants have a different fitness than non-mutants (*unconstrained*) and two separate values, ρ^p and ρ^s, are inferred; or (b) mutants have a different fitness than non-mutants, but the effect is constrained to be equal under permissive and stressful conditions, $\rho^p = \rho^s$. For the models (a) and (c), the mutant count distributions under permissive and stressful conditions have no joint parameters and can, therefore, be considered separately by using existing estimation methods: (a) corresponds to the standard model and (c) to the standard model with differential mutant fitness (implemented, for example, in [37]). Studies to date have followed such an approach to estimate the increase in mutation rate. Model (b), on the contrary (with constrained differential mutant fitness, arguably a reasonable null model), represents a new version of the homogeneous-response model, which is first implemented here. In this case, we estimate the model parameters by jointly maximising the log-likelihood function given in Eq 29. In the main Results, we consider all three homogeneous-response models (a-c); in section M in S1 File, we repeat the analysis for constrained mutant fitness only, i.e. models (a-b).

Heterogeneous-response model. In the heterogeneous-response model, the mutant count distributions under permissive (Eq 7) and stressful conditions (Eqs 23 and 24), depend on the per-division mutation rates of response-*off* and response-*on* cells, the extinction probabilities of response-*off* and response-*on* mutants under stress, the fraction and relative fitness of response-*on* compared to response-*off* cells, and the total final population sizes under permissive and stressful conditions. The mutation rate of response-*off* cells, μ_{off}, appears as a parameter in both the mutant count distributions under permissive and under stressful conditions, and the joint inference crucially relies on our assumption that, even though the division rate itself might change under stress, the *per-division* mutation rate of response-*off* cells is the same under both conditions. As for the homogeneous-response model, we assume that the final population sizes, N_f^p and N_f^s, are known from plating on non-selective medium. Moreover, we neglect cell death, which implies $\epsilon_{off}^s \quad \epsilon_{on} \quad 0$, but test the robustness of this assumption.

For the relative fitness of response-*on* cells, we consider two different model versions of the approximate heterogeneous-response model: (d) as a default, we set $r_{on} = 0$, inspired by the SOS response in *E. coli*, which inhibits cell division, or to a small non-zero value that we assume is measured in a separate experiment (section H in S1 File); and (e) we infer r_{on}. Similarly, for the fraction of the response-*on* subpopulation, we (i) assume that it is a known quantity measured in a separate experiment (e.g. microscopy or flow cytometry), or (ii) set it as an inference parameter.

Ultimately, we are interested in quantifying the relative increase in mutation rate associated with induction of the stress response, that is, $\frac{\mu_{on}}{\mu_{off}}$. To do so we need to estimate the mutation rate of response-*on* cells, μ_{on}. However, we do not directly infer this parameter; instead, we infer the composite parameter of the mutation-supply ratio $\mathcal{S}$ defined in Eq 27, from which we calculate μ_{on}. The reason for this approach is that for $r_{on} = 0$, the mutant count distribution under stress does not depend separately on μ_{on} and f_{on} but only on $\mathcal{S}$ (together with μ_{off} and N_f^s); see Eq 26. This also implies that, for $r_{on} = 0$ and when the fraction of the response-*on*

subpopulation is unknown, μ_{on} and thus $\frac{\mu_{on}}{\mu_{off}}$ cannot be calculated. In this case, we report estimates of $\mathcal{S}$ instead as an indicator of heterogeneity.

Confidence intervals using profile likelihood. In addition to the maximum-likelihood estimates, we calculate 95% confidence intervals using a profile likelihood approach (section E in S1 File). The confidence interval for each parameter contains all values such that, after optimisation over the remaining inference parameters, the likelihood does not significantly drop according to a likelihood ratio test.

Evaluating inference methods on simulated data

We test our estimation method using simulated fluctuation assay data: For chosen ranges of parameter values, we perform stochastic simulations of the population dynamics during the growth phases of a pair of fluctuation assays, one under permissive and the other under stressful conditions. From the resulting mutant count distributions, we infer the respective parameters under heterogeneous and homogeneous-response models and compare the estimated with the true simulated parameters, as well as perform model selection. For most of this study, we simulate under the heterogeneous-response model, but we repeat part of the analysis for simulation under the homogeneous-response model (sections K and N in S1 File).

The complete documentation of all population dynamic functions can be found in the file called **population_dynamics.jl** at https://github.com/LucyL-J/Quantifying-SIM.

Simulation methods. To simulate the growth phase under permissive conditions, we consider exponential growth of the non-mutant population (Eq 1) and implement the occurrence of mutations as a time-inhomogeneous Poisson process with rate proportional to the population size using a standard approach described, for example, in [38]. We treat mutant cells stochastically by using Gillespie's algorithm [39] to simulate the pure birth process described by Eq 2 with zero death rate. In the case of the homogeneous-response model, the population growth rate is given by the division rate, γ^p, the mutation rate per cell per unit time by ν^p and the birth rate of mutants by $\rho^p \cdot \gamma^p$. Similarly, for the heterogeneous-response model, the rates are given by the respective rates of response-*off* cells (γ^p_{off}, ν^p_{off} and $\rho^p_{off} \cdot \nu^p_{off}$).

For the homogeneous-response model, we simulate the growth phase under stressful conditions using the same algorithm but with different rates (γ^s, ν^s, $\rho^s \cdot \gamma^s$). To simulate stressful conditions under the heterogeneous-response model, we use Eqs 10 and 11 (setting $n_{on}(0) = 0$) to describe the growth of the response-*off* and response-*on* subpopulations, and implement the occurrence of mutations as two independent time-inhomogeneous Poisson processes with rates proportional to the subpopulation sizes ($n^s_{off}(t)$ and $n_{on}(t)$, respectively) and the mutation rates per cell per unit time (ν^s_{off} and ν_{on}). We simulate the mutant dynamics stochastically as a two-type branching process described by Eq 12 using Gillespie's algorithm.

In all simulations, we set the duration t_f of the growth phase such that the expected number of *mutations* (not *mutants*) is constant across the considered parameter ranges (section C in S1 File). In our main results, we take $c = 50$ parallel cultures per assay, which is readily feasible if culturing on a 96-well plate; see, for example, [16] for a protocol. In sections D and N in S1 File, we also examine the sensitivity of the results to the number of parallel cultures by considering smaller numbers c.

Accuracy and precision of parameter estimates. Generally, we evaluate the accuracy and precision of all estimation methods by simulating pairs of fluctuation assays, estimating the parameters of the inference model and comparing the respective estimates with the true values; repeated $R = 100$ times for each parameter set simulated. We consider the deviation from the true value of the median estimate across the simulations as a measure of the accuracy of the estimation and the variation as a measure of the precision. In particular, we calculate the

median of the relative error across the R replicates,

$$\mathrm{RE} \quad \frac{\mathrm{median}\left(\left\{\frac{\mu_{on}}{\mu_{off}}\right\}_{\mathrm{est}} \quad \left(\frac{\mu_{on}}{\mu_{off}}\right)_{\mathrm{true}}\right)}{\left(\frac{\mu_{on}}{\mu_{off}}\right)_{\mathrm{true}}}. \tag{30}$$

Here, a positive or negative relative error implies over- or underestimation, respectively. Moreover, we calculate the coefficient of variation across the R replicates,

$$\mathrm{CV} \quad \frac{\mathrm{std}\left(\left\{\frac{\mu_{on}}{\mu_{off}}\right\}_{\mathrm{est}}\right)}{\mathrm{mean}\left(\left\{\frac{\mu_{on}}{\mu_{off}}\right\}_{\mathrm{est}}\right)}. \tag{31}$$

where 'std' denotes standard deviation. Where we calculate confidence intervals (section E in S1 File), we also use the median width of the confidence intervals as a measure of precision.

To plot the estimated parameters across the $R = 100$ simulations, we use boxplots, where each box shows the median and interquartile range with whiskers extending to 1.5 times the interquartile range and any outliers outside that range represented as dots. To summarise the confidence intervals on each of the $R = 100$ estimates, we plot the median maximum likelihood estimate with error bars extending to the medians of the lower and upper bounds of the 95% confidence intervals.

Model selection: Heterogeneous versus homogeneous response. We also evaluate whether it is possible to identify the heterogeneity of stress responses from mutant count data alone. In this case, we suppose we do not have separate experimental data showing heterogeneity and, therefore, do not have an estimate of f_{on}. For this purpose, we simulate fluctuation assays under the (exact) heterogeneous-response model and under the homogeneous-response model (sections K and N in S1 File) and, then, fit the different homogeneous (a-c) and (approximate) heterogeneous-response models (d-e). For model selection, we use a combination of likelihood-ratio test (LRT) and Akaike information criterion (AIC). The AIC is defined as

$$\mathrm{AIC} \quad 2(k \quad \ln \mathcal{L}) \tag{32}$$

where k is the number of inferred parameters of the model. Within the set of models (a-c) and within the set (d-e), the models are nested and we use LRTs to determine the best heterogeneous/homogeneous-response model within each set first. However, we cannot use LRT to select between the sets (a-c) and (d-e) because these models are not nested. Therefore, between the two best models, we select the one with the lowest AIC. However, if the difference in AIC is within ±2, we say that the AICs are comparable, and neither of the models can be selected. We also consider the Bayesian information criterion (BIC) as an alternative second selection step (section N in S1 File).

Results

We aim to estimate the increase in mutation rate associated with the induction of the stress response when this response is heterogeneously expressed across the bacterial population. In particular, we consider cases in which the population can be divided into two discrete subpopulations: one with a low expression level (response *off*) and the other with a high expression level (response *on*). The key principle of our method is to jointly infer their mutation rates from mutant count data obtained from a pair of fluctuation assays under permissive and stressful conditions. For the latter, we need to disentangle the contributions from the

response-*off* and response-*on* subpopulations. The success of this method relies on the changing shape of the mutant count distribution under stress, which occurs if there is a highly mutating but slowly dividing response-*on* subpopulation (Fig B in S1 File).

To evaluate the performance of our method, we use simulated mutant count data to compare the estimated parameters with the true simulated ones. First, we explore how the accuracy and precision of our method depend on the model parameters by simulating and inferring under the same model. Then, we test the robustness of our method to model deviations by simulating under a more complex model than used in the inference. Finally, we determine under what conditions the heterogeneous-response model can be distinguished from the homogeneous-response model assumed in currently available methods by inferring under both models and comparing how well they fit simulated data.

In all simulations, we set the initial population size to 10^4 and the initial fraction of the response-*on* subpopulation to zero. Moreover, we consider the duration of the growth phase such that the expected number of mutations equals one. This way, the resulting number of resistant mutant colonies on each selective plate is usually within an experimentally countable range of zero to a couple hundred (section C in S1 File). Table 2 summarises the default parameters used in the simulations, while parameters that vary are specified in the relevant Results section. For each parameter combination, we simulate $R = 100$ pairs of fluctuation assays under permissive and stressful conditions, with $c = 50$ parallel cultures per assay. We also test the sensitivity of our method's performance to the number of parallel cultures (section D in S1 File) and repeat the model selection analysis for smaller numbers of parallel cultures ($c = 20, 10$) in section N in S1 File. Generally, we assume that the final population sizes in permissive and stressful conditions (N_f^p and N_f^s, respectively) and the fraction of the response-*on* subpopulation under stress (f_{on}) are known from separate experimental measurements, except for the last Results section where we infer without a separate estimate of f_{on}.

Estimation of the mutation-rate increase is accurate and precise for sufficiently large response-*on* mutation supply

First, we evaluate our novel inference method's performance in the best-case scenario; that is, we simulate and infer under the same model: a model of heterogeneous stress responses without cell death, with mutant fitness equal to non-mutant fitness, and with zero division rate of response-*on* cells. We simulate for a range of mutation rates in response-*on* cells, $\nu_{on} \in [10^{-5}, 10^{-8}]\ h^{-1}$ and switching rates $\alpha \in [0.001, 0.1]\ h^{-1}$. Note that the per-division mutation rate μ_{on} and the per-unit-time rate ν_{on} are equivalent here because we set the division rate γ_{off}^s to one.

For the inference, we consider the same model as used in the simulations with the only exception that we neglect switching *on* the stress response in mutants and initial population size effects; for a comparison of the exact and approximated heterogeneous-response model, see Model and methods. For each set of mutant count data, we infer the mutation rate of response-*off* cells (μ_{off}) and the mutation-supply ratio ($\mathcal{S}$), which defines the relative contribution of response-*on* cells to the total mutation supply (Eq 27). From these estimates, we calculate the stress-induced mutation-rate increase, i.e. $\frac{\mu_{on}}{\mu_{off}}$. To quantify the accuracy of our method, we calculate the median of the relative error of our estimated mutation-rate increases (Eq 30). Additionally, we use the coefficient of variation across the estimates (Eq 31) to quantify our method's precision.

Comparing the estimated with the true mutation-rate increase $\frac{\mu_{on}}{\mu_{off}}$, we find that the accuracy and precision improve with increasing $\frac{\mu_{on}}{\mu_{off}}$ and relative switching rate $\tilde{\alpha}$ (Fig 2B and 2C). For example, for $\tilde{\alpha} \quad 0.05$, when $\frac{\mu_{on}}{\mu_{off}} \geq 25$, 95% of estimates lie within 2–fold of the true mutation-rate increase and the estimation is unbiased (Fig 2A). For smaller $\frac{\mu_{on}}{\mu_{off}}$, on the other hand, the

Table 2. Parameters used in the simulations unless explicitly specified otherwise.

Symbol	Cond.	Definition	Numerical value
γ^p_{off}	P	Division rate response-*off* cells	$1\ h^{-1}$
ρ^p_{off}	P	Differential mutant fitness response-*off* cells	1
ν^p_{off}	P	Mutations per unit time response-*off* cells	$10^{-8}\ h^{-1}$
γ^s_{off}	S	Division rate response-*off* cells	$1\ h^{-1}$
ρ^s_{off}	S	Differential mutant fitness response-*off* cells	1
ν^s_{off}	S	Mutations per unit time response-*off* cells	$10^{-8}\ h^{-1}$
δ^s_{off}	S	Death rate response-*off* cells	$0\ h^{-1}$
γ_{on}	S	Division rate response-*on* cells	$0\ h^{-1}$
ρ_{on}	S	Differential mutant fitness response-*on* cells	1
ν_{on}	S	Mutations per unit time response-*on* cells	$10^{-6}\ h^{-1}$
δ_{on}	S	Death rate response-*on* cells	$0\ h^{-1}$
α	S	Switching rate	$0.05\ h^{-1}$

For simplicity, we set the division rate of response-*off* cells under permissive (P) and stressful (S) conditions to $1\ h^{-1}$. The switching rate for the SOS response in *E. coli* has been estimated using single-cell imaging [27]. The mutation rate is based on rifampicin resistance, a selective marker commonly used in fluctuation assays. In *E. coli*, the number of point mutations conferring rifampicin resistance has been estimated to be 79 [40] and the mutation rate between $0.2 \cdot 10^{-10}$ and $5 \cdot 10^{-10}$ nucleotides per generation in permissive conditions [41], yielding a mutation rate of $\nu^p_{off}, \nu^s_{off} \approx 10^{-8}$ per unit time for response-*off* cells. Meanwhile, the mutation rate under induction of the stress response (ν_{on}) is set to a default of 100 times higher, comparable to the increase associated with genetic mutators [41, 42].

https://doi.org/10.1371/journal.pcbi.1012146.t002

variation in the estimates becomes large. Nonetheless, if the mutation-rate increase is estimated to be >25, the true increase is very likely to be >10, and conversely, if the mutation-rate increase is estimated close to zero ($<10^{-3}$), it is very likely to be <10.

The mutation-supply ratio, which is defined $\mathcal{S} := \frac{\mu_{on}}{\mu_{off}} \frac{f_{on}}{1\ f_{on}}$ (approximately given by the product of $\frac{\mu_{on}}{\mu_{off}}$ and $\tilde{\alpha}$ for small α and small r_{on}) determines our method's performance. For $\mathcal{S} \gg 1$, the contribution of the response-*on* subpopulation is dominating. In contrast, for $\mathcal{S} \ll 1$, the response-*on* subpopulation contributes very little to the total mutant count. Overall, in the best-case scenario and for the parameter regime considered here, $\mathcal{S} \sim \mathcal{O}(1)$ or greater is sufficient for an accurate and precise estimate of the mutation-rate increase.

We also evaluate the sensitivity of our method's performance to the number of parallel cultures (Fig C in S1 File). For smaller c, the precision of our method worsens compared to $c = 50$, but the estimation of $\frac{\mu_{on}}{\mu_{off}}$ remains accurate for sufficiently large $\mathcal{S} \sim \mathcal{O}(1)$ or greater.

In addition to the maximum likelihood estimates, we calculate 95% profile likelihood confidence intervals on the estimates of the mutation-rate increase (Fig D in S1 File). We find that the median width of the confidence intervals increases with decreasing $\frac{\mu_{on}}{\mu_{off}}$ and $\tilde{\alpha}$, in a similar way as the CV of the estimates for $R = 100$ repeated simulations shown in Fig 2C. Moreover, we confirm that the true value for the mutation-rate increase lies outside of the confidence interval in < 5% of the simulations.

Cell death has a limited impact on estimates

Our inference model accounts for changes in mutation and division rates upon induction of the stress response but neglects other potential consequences of the stress, such as cell death.

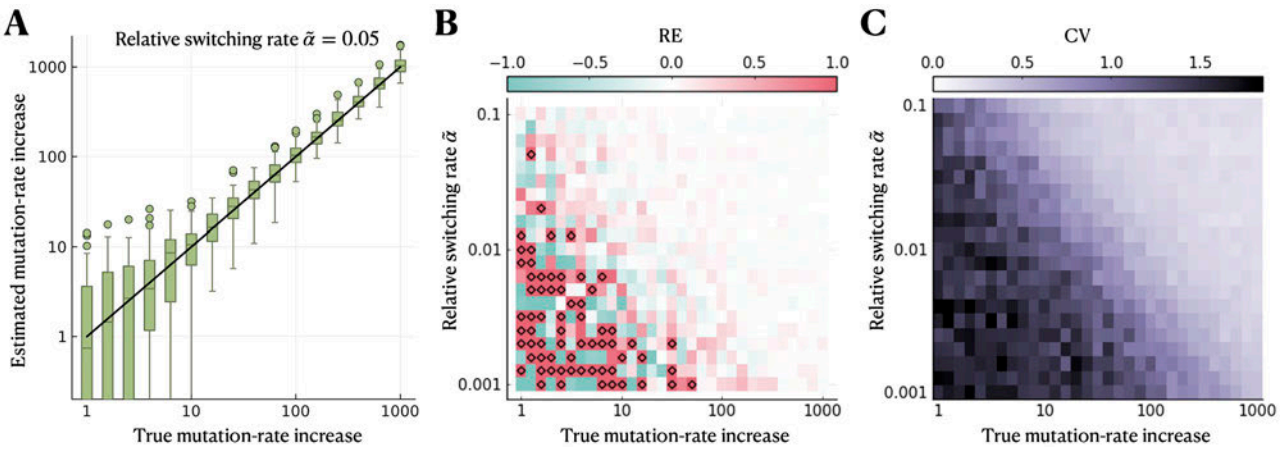

Fig 2. Estimation of the mutation-rate increase is accurate and precise when the mutation-supply ratio is sufficiently large. We simulate using the simplest model of heterogeneous stress responses (without cell death or differential mutant fitness and with zero division rate of response-*on* cells) and infer the mutation-rate increase $\frac{\mu_{on}}{\mu_{off}}$ assuming the same model in the inference. **A** Estimated compared to true $\frac{\mu_{on}}{\mu_{off}}$ for a range of values of $\frac{\mu_{on}}{\mu_{off}}$ and a relative switching rate of $\tilde{\alpha} = 0.05$. **B** Median relative error of estimated compared to true mutation-rate increase for a range of $\frac{\mu_{on}}{\mu_{off}}$ and $\tilde{\alpha}$. Over/underestimation is shown in red/blue, and diamonds indicate a relative error greater than one. **C** Coefficient of variation across estimates. The parameter ranges used in the simulations are $\nu_{on} \in [10^{-5}, 10^{-8}]\ h^{-1}$ and $\alpha \in [0.001, 0.1]\ h^{-1}$.

https://doi.org/10.1371/journal.pcbi.1012146.g002

Previous work showed that the occurrence of cell death, if neglected in the inference model, leads to overestimation of mutation rate [18]. Therefore, we asked whether neglecting cell death has a similar effect in the case of heterogeneous stress responses. For this purpose, we simulate fluctuation assays under an extended model of heterogeneous stress responses with cell death. We consider the cases that (i) only response-*off* cells are affected by cell death, (ii) only response-*on* cells are affected, or (iii) all cells are affected equally, using parameter ranges of $\delta^s_{off},\ \delta_{on} \in [0.0,\ 0.5]\ h^{-1}$.

Interestingly, we find that any biases in the estimated mutation-rate increase depend on which subpopulation is affected by cell death. If only response-*off* cells die, the mutation-rate increase is overestimated for sufficiently large death rates (Fig 3A). On the other hand, if only response-*on* cells die, the mutation-rate increase is underestimated (Fig 3B). The estimation remains unbiased if both subpopulations are equally affected by cell death. However, the variation in the estimates increases for large death rates (Fig 3C). From the contribution of the response-*on* subpopulation to the mutant count given in Eq 24, it can be seen that the effects of cell death in response-*off* and response-*on* cells partly cancel each other out. This result also holds for a smaller switching rate (Fig E in S1 File).

We test another biologically realistic model deviation: the fitness of mutants differs from non-mutants during the growth phase (Fig F in S1 File). We find that neglecting this effect in the inference causes very little bias in the estimates for either a fitness advantage or a fitness cost of mutations.

Estimation remains accurate when response-*on* cells have a small to moderate division rate

So far, we considered response-*on* cells not to divide at all during the growth phase, motivated by the SOS response. However, the division rate of response-*on* cells might be non-zero, especially if cells are exposed to a very low level of DNA damage (in the case of SOS) or for other stress responses. As a default setting, our inference method sets the relative fitness of response-

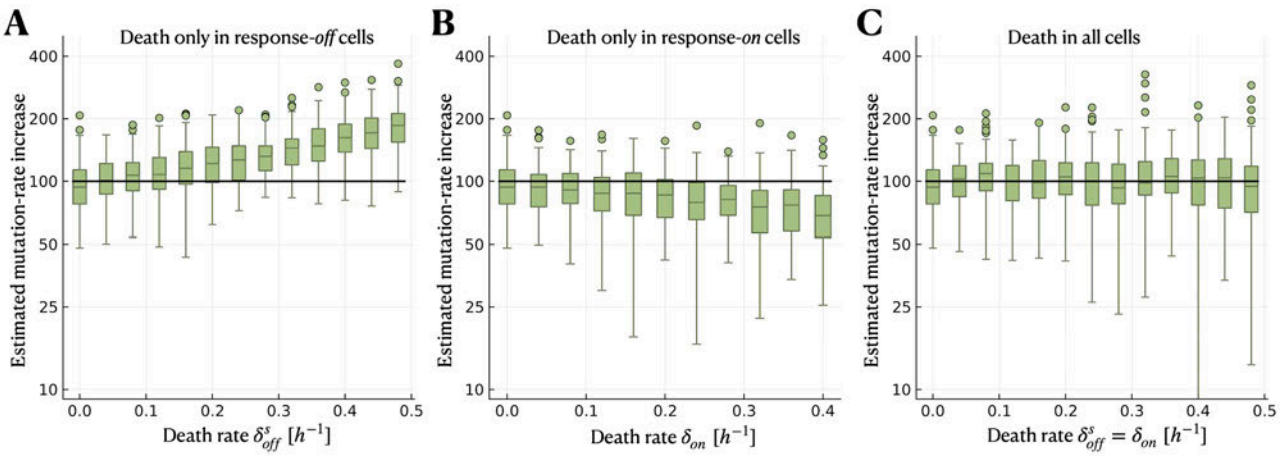

Fig 3. Cell death has limited impact on the estimation of the mutation-rate increase. We simulate using the heterogeneous-response model (without differential mutant fitness and with zero division rate of response-*on* cells) but with cell death. However, we neglect cell death in the model used for inference. The black solid lines indicate the true mutation-rate increase used in the simulations. **A** Estimated mutation-rate increase when only response-*off* cells are affected by cell death, **B** when only response-*on* cells are affected by cell death, and **C** when all cells are affected by cell death equally. The parameter ranges used in the simulations are $\delta^s_{off},\ \delta_{on} \in [0.0,\ 0.5]\ h^{-1}$ (with $\gamma^s_{off} = 1\ h^{-1}$).

https://doi.org/10.1371/journal.pcbi.1012146.g003

on cells to zero ($r_{on} = 0$), but it also allows us to estimate r_{on} as an inference parameter. In the following, we evaluate the performance of our inference method when true $r_{on} > 0$, specifically the impact on the estimated mutation-rate increase.

We simulate under the heterogeneous-response model with a non-zero division rate of response-*on* cells, considering a parameter range of $\gamma_{on} \in [0, 1]\ h^{-1}$ (with $\gamma_{off} = 1\ h^{-1}$). Note that the relative fitness of response-*on* cells r_{on} is equivalent to their division rate γ_{on} because we consider no cell death here. We consider two different inference approaches. In one case, we infer the mutation rate μ_{off}, the mutation-supply ratio $\mathcal{S}$ and the relative fitness of response-*on* cells r_{on}. Alternatively, we infer only μ_{off} and $\mathcal{S}$ while setting $r_{on} = 0$. We estimate the mutation-rate increase $\frac{\mu_{on}}{\mu_{off}}$ in both cases and compare it to the true value. In the first case, we also compare the estimated with the true r_{on}.

We find that the estimation of the mutation-rate increase remains accurate for small to moderate relative fitness r_{on}. For larger $r_{on} \to 1$, on the other hand, the mutation-rate increase is underestimated, yet more accurate and precise if r_{on} is also inferred (Fig 4A). The estimate of r_{on} itself is also underestimated for larger r_{on} (Fig 4B).

We also evaluate the performance when r_{on} is set to the true value in the inference. Interestingly, this increases the accuracy and precision of the estimate of $\frac{\mu_{on}}{\mu_{off}}$ only slightly compared to when r_{on} is inferred (Fig G in S1 File). The reason lies in the approximation made to derive the mutant count distribution (Eq 13), which is no longer valid as $r_{on} \to 1$.

Model selection between heterogeneous and homogeneous response is often inconclusive

In many cases, it may not be known *a priori* whether the stress response is heterogeneously expressed across the population or whether, in contrast, all cells respond similarly. We want to determine whether distinguishing these two models is possible using mutant count data from fluctuation assays alone. To do so, we simulate fluctuation assays under the heterogeneous-response model for a range of relative fitness of response-*on* cells, r_{on}. For the inference, we use

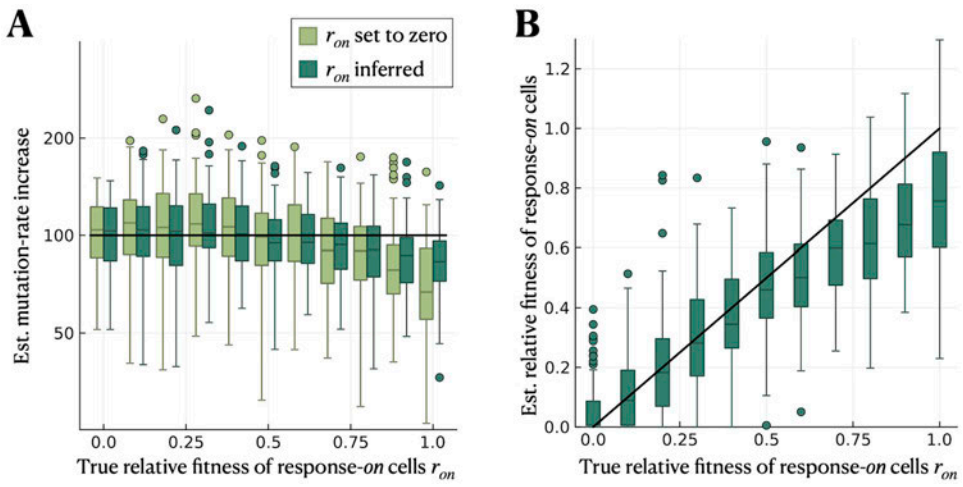

Fig 4. Estimation of the mutation-rate increase remains accurate when response-*on* cells have a small to moderate relative fitness. We simulate using the heterogeneous-response model (without cell death or differential mutant fitness) with $r_{on} \geq 0$ being the relative fitness of response-*on* cells compared to response-*off* cells. We consider two cases for the inference: (i) setting r_{on} to zero and only inferring μ_{off} and $\mathcal{S}$, and (ii) inferring r_{on} in addition. **A** Estimated mutation-rate increase $\frac{\mu_{on}}{\mu_{off}}$ for both cases and a range of relative fitness of response-*on* cells. The solid black line indicates the true value of $\frac{\mu_{on}}{\mu_{off}}$. **B** Estimated compared to true relative fitness of response-*on* cells in inference case (ii). The parameter range used in the simulations is $\gamma_{on} \in [0, 1]$ in h^{-1}.

https://doi.org/10.1371/journal.pcbi.1012146.g004

both the heterogeneous- and homogeneous-response models and compare how well they fit the data. We use the same simulation data as in the previous section (parameter range $\gamma_{on} \in [0, 1]\ h^{-1}$). However, we suppose that the fraction of the response-*on* subpopulation f_{on} is unknown. Therefore, when using the heterogeneous-response model in the inference, we either set $r_{on} = 0$ (in which case f_{on} drops out of the equations) and infer only μ_{off} and $\mathcal{S}$, or set f_{on} and r_{on} as additional inference parameters. Note that, if f_{on} is not inferred, the mutation-rate increase $\frac{\mu_{on}}{\mu_{off}}$ can no longer be calculated, see Eq 26.

We perform model selection between the heterogeneous and the homogeneous-response models using a combination of the likelihood ratio test (LRT) and the Akaike Information Criterion (AIC), which consider how well the models reproduce the data while penalising the number of model parameters. For the homogeneous-response model, we consider three cases: (a) without differential mutant fitness (inference parameters: μ^p and μ^s), (b) with differential mutant fitness, but constrained to be equal under permissive and stressful conditions (inference parameters μ^p, μ^s and $\rho^p = \rho^s$) and (c) with unconstrained differential mutant fitness (inference parameters: μ^p, μ^s, ρ^p and ρ^s). For the heterogeneous-response model, we consider two cases: (d) zero relative fitness of response-*on* cells (inference parameters: μ_{off} and $\mathcal{S}$) and (e) non-zero relative fitness of response-*on* cells (inference parameters: μ_{off}, $\mathcal{S}$, f_{on} and r_{on}). We use LRTs to select the best homogeneous model (a-c) and the best heterogeneous model (d-e) within each of these sets of nested models. Then, we use the AIC to select between the best homogeneous and the best heterogeneous-response model, which are not nested. If the difference in AIC is less than two, we say neither model is clearly selected.

After applying this two-step model selection, we find that the heterogeneous-response model is selected in the majority of cases (around 75% for $r_{on} = 0$) when the relative fitness of response-*on* cells is small (Fig 5A). For increasing r_{on}, however, the homogeneous-response model without differential mutant fitness is selected with increasing frequency until it is selected for the majority of simulations for large r_{on}. The other models are selected for only a

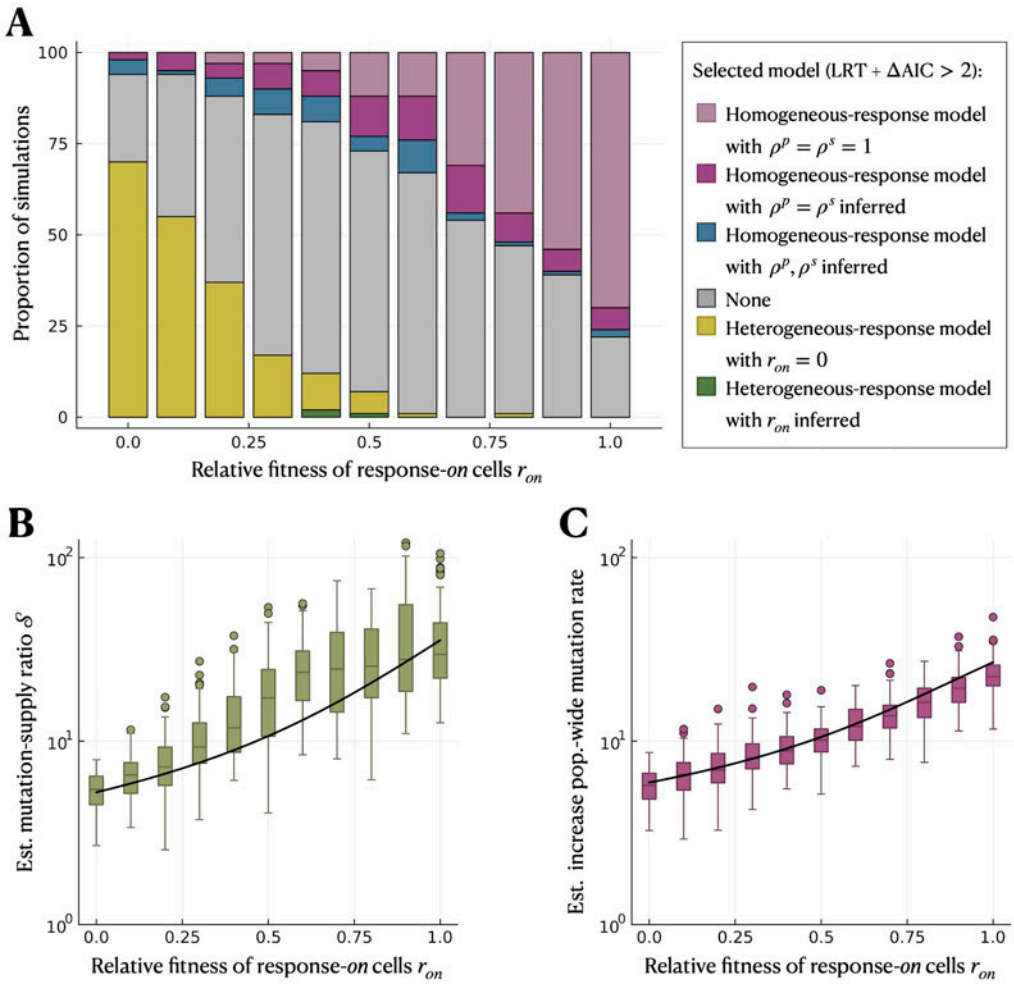

Fig 5. The heterogeneous-response model is selected only when response-*on* cells have a small relative fitness. We simulate under the heterogeneous-response model for a range of relative fitness of response-*on* cells, r_{on}. In the inference, we use (d) the heterogeneous-response model with $r_{on} = 0$ (yellow) and (e) the heterogeneous-response model with r_{on} and f_{on} as inference parameters (dark green) to infer the mutation rate of response-*off* cells, μ_{off}, and mutation-supply ratio, $\mathcal{S}$. We also use the homogeneous-response model (a) without differential mutant fitness ($\rho^p = \rho^s = 1$; light purple), (b) with constrained differential mutant fitness ($\rho^p = \rho^s$ inferred; dark purple) and (c) with unconstrained differential mutant fitness (ρ^p, ρ^s inferred; blue) to infer the population-wide mutation rates under permissive and stressful conditions, μ^p and μ^s, and, for (b) and (c), additionally ρ^p and ρ^s. **A** Model selection using LRT and AIC. **B** Estimated mutation-supply ratio, $\mathcal{S}$, by the best heterogeneous-response model. **C** Estimated increase in mutation rate, $\frac{\mu^s}{\mu^p}$, by the best homogeneous-response model. The black lines in **B** and **C** indicate the true values of $\mathcal{S}$ and the increase in population mean mutation rate, M, respectively. The parameter range used in the simulations is $\gamma_{on} \in [0, 1]\ h^{-1}$.

https://doi.org/10.1371/journal.pcbi.1012146.g005

small number of simulations. Over the whole parameter range, there is a substantial fraction of cases in which no model can be selected, with the highest proportion of ≈50% for intermediate r_{on}. This implies that heterogeneity in stress responses with sufficiently large $\mathcal{S}$ can in principle be detected, but only if the division rate of response-*on* is very small (or zero).

Comparing the mutation-supply ratio $\mathcal{S}$ $\frac{\mu_{on} f_{on}}{\mu_{off}(1 - f_{on})}$ estimated by the best heterogeneous-response model with its true value, we find that the estimate is accurate and precise for small r_{on}, but with a slight loss in precision for larger r_{on} (Fig 5B). This means that even without a

separate estimate of f_{on}, the magnitude of the heterogeneity in mutation rates (in the form of $\mathcal{S}$) can be captured.

We also compare the estimated increase in mutation rate $\frac{\mu^s}{\mu^p}$ from the best homogeneous-response model with the true increase in population mean mutation rate under the simulated heterogeneous-response model, given by $\bar{M}$ $\frac{(1\ f_{on})\mu_{off}+f_{on}\mu_{on}}{\mu_{off}}$. Interestingly, the inferred $\frac{\mu^s}{\mu^p}$ is an accurate and precise estimate of $\bar{M}$ over the whole range of r_{on}, with only a slight underestimation for large r_{on} (Fig 5C). For $r_{on} \to 1$ and assuming no cell death, accurate estimation of $\bar{M}$ is expected because the probability generating function (PGF) of the mutant count distribution reduces to

$$G^s_{\text{het}}(z) \quad \exp\left[\left(\mu_{off}(1 \quad f_{on}) + \mu_{on}f_{on}\right)N^s_f\frac{(1 \quad z)\log(1 \quad z)}{z}\right], \tag{33}$$

This distribution is equivalent to the homogeneous-response model without differential mutant fitness (Eq 6), which is selected as the best homogeneous-response model for most simulations. For small r_{on}, on the other hand, homogeneous-response models with differential mutant fitness are selected more often, and they (falsely) infer an increasingly severe mutant cost under stressful conditions as $r_{on} \to 0$ (Fig H in S1 File), despite mutations not having a cost in the simulations.

We repeat the analysis for a smaller mutation-rate increase, $\frac{\mu_{on}}{\mu_{off}}$ 10, and find that the heterogeneous-response model is selected less often, only in around 25% of the simulations for $r_{on} = 0$ (Fig I in S1 File), implying that small mutation-rate increases are most likely not picked up through model selection. We also perform model selection when using smaller numbers of parallel cultures ($c = 20, 10$) in the inference, and find that, overall, model selection is less informative for smaller c (Fig M in S1 File).

Finally, we check for the rate of false positives where the heterogeneous-response model is incorrectly selected in the absence of heterogeneity, by simulating under versions of the homogeneous-response model and performing model selection. We find that, when simulating under the homogeneous-response model with constrained mutant fitness, the homogeneous-response model is selected in almost all cases independent of the increase in mutation rate (Fig N in S1 File). Therefore, if the mutant fitness is the same under permissive and stressful conditions, the risk of false positives is negligible. When simulating under the homogeneous-response model with unconstrained mutant fitness, on the other hand, there are more cases in which no model or the heterogeneous-response model is selected (Fig O in S1 File).

When simulating under the homogeneous-response model without an increase in mutation rate ($\frac{\mu^s}{\mu^p}$ 1) and with small mutant fitness costs, no model can be selected in most cases, but both heterogeneous and homogeneous-response models correctly infer that there is no increase in mutation rate, corresponding to $\mathcal{S}$ 0 and $\bar{M}$ 1, respectively (Fig J in S1 File).

Discussion

Since its introduction 80 years ago, the standard model behind the fluctuation assay has been extended numerous times to overcome limitations and make it more biologically realistic. Extensions particularly relevant for quantifying stress-induced mutagenesis include considering cell death [18, 43] and differential mutant fitness [44]. In this study, we addressed a so-far overlooked limitation of fluctuation analysis: heterogeneity in the expression of stress responses, which single-cell studies have recently demonstrated. Our population dynamic model considers that only a subpopulation of cells (fraction f_{on}) have the stress response

switched *on* and the remainder of the population switched *off*. This allows us to estimate the relative increase in mutation rate associated with the induction of the stress response, $\frac{\mu_{on}}{\mu_{off}}$.

We tested our estimation method with simulated mutant count data, which confirmed accurate and precise estimation of $\frac{\mu_{on}}{\mu_{off}}$ for sufficiently large mutation-supply ratio defined as $\mathcal{S} := \frac{f_{on}}{1 - f_{on}} \frac{\mu_{on}}{\mu_{off}}$ (Fig 2). $\mathcal{S}$ depends on the mutation-rate increase itself and the fraction of the response-*on* subpopulation. While $\frac{\mu_{on}}{\mu_{off}}$ is inherent to the stress response, f_{on} could potentially be increased through experimental design. For example, increasing the antibiotic concentration has been shown to increase the rate of switching *on* the stress response and thus the fraction of the response-*on* subpopulation [27]. Our results suggest that mutation rate estimates would be more accurate at higher antibiotic concentrations, all else being equal. Increasing antibiotic concentration could, however, also increase cell death. We neglect cell death in our inference, but we showed that our method is robust to this model deviation up to moderate death rates when cell death affects response-*off* and response-*on* subpopulations equally (Fig 3C).

We used model selection with a combination of likelihood-ratio tests and AIC to evaluate whether a signal of mutation-rate heterogeneity can be detected from fluctuation assays alone. The chances of detecting heterogeneity are highest when response-*on* cells are non- or only slowly-dividing ($r_{on} \ll 1$). For moderate switching rates and a mutation-rate increase of $\frac{\mu_{on}}{\mu_{off}} \geq 100$, the heterogeneous-response model is selected over homogeneous-response models in the majority of the simulated experiments (Fig 5A). However, with increasing r_{on} (> 0.25), the heterogeneous-response model is only rarely selected. A smaller mutation-rate increase $\frac{\mu_{on}}{\mu_{off}} \geq 10$ also cannot effectively be detected by model selection (Fig I in S1 File). Generally, model selection with fewer than $c \approx 50$ parallel cultures per fluctuation assay will be very difficult to interpret even for the best-case parameter range (Fig M in S1 File).

Our results suggest that heterogeneity in stress responses may have been overlooked when using fluctuation assays, and these data should be complemented with additional experiments to support or rule out alternative explanations. For example, mutants arising in the fluctuation assay can be isolated and their relative fitness compared to non-mutants measured with a pair of competitive fitness assays under permissive and stressful conditions. This measurement would allow researchers to check whether mutant fitness values estimated from the homogeneous-response model fit (ρ^p and ρ^s) are reasonable. In particular, a large difference in estimated ρ^p and ρ^s may alternatively indicate the presence of a slowly-dividing and highly-mutating subpopulation (Fig H in S1 File). Constraining $\rho^p = \rho^s$, arguably a reasonable null model, increases the fraction of simulated experiments in which the heterogeneous model is selected (Fig L in S1 File).

If there is reason to suspect heterogeneity in the stress response, experimentalists can test this hypothesis directly by engineering fluorescent reporters into the bacterial strain of interest and measuring the response on a single-cell level, e.g. by flow cytometry [8, 9, 24] or microscopy [8, 19, 20]. These experiments would provide an independent estimate of the fraction of the response-*on* subpopulation to further constrain the heterogeneous-response model and allow calculation of $\frac{\mu_{on}}{\mu_{off}}$. In reality, multiple factors causing deviation from the standard fluctuation assay model (e.g. heterogeneous stress responses, differential mutant fitness, and cell death) will likely operate simultaneously. Since it is not feasible to reliably estimate a large number of parameters from fluctuation assay data alone, separate experiments become important to decide which deviation(s) are most relevant to incorporate into the fluctuation analysis.

Interestingly, the homogeneous-response model performs well in estimating the increase in population mean mutation rate (Fig 5C). Therefore, mutation rate estimates from previous

studies that neglect heterogeneity in stress-induced mutagenesis, such as [8, 11, 14], can simply be interpreted as population-wide averages. However, these studies may underestimate the true extent of mutagenesis associated with the expression of the stress response if it is only induced by a subpopulation of cells. Estimating not only the increase in population mean but also heterogeneity in mutation rate, as is possible with our method, could be important for parameterising evolutionary models, such as predictions of antibiotic resistance evolution. Theoretical modelling suggests that single-locus adaptation can be accurately captured by the population mean mutation rate, but within-population variation (even for a fixed population mean) can speed up multi-locus adaptation [45]. However, this previous model did not incorporate any coupling of changes in mutation rate to changes in cell division or death rates, as would be expected in the case of stress responses. Therefore, an important direction for future work is to assess when the pleiotropic effects of realistic stress responses truly accelerate evolution.

Our approach to quantifying stress-induced mutagenesis assumes that the expression of the stress response is bimodal and can reasonably be modelled as either switched *off* or *on*. To a reasonable approximation, this expression pattern has been observed for the SOS response, particularly in slow-growth conditions [27]. In other conditions or for other stress responses, it might be more appropriate to model the expression as a unimodal distribution. We expect, however, that this increase in model complexity would make parameter inference more challenging. Similarly, for simplicity, we neglect stochastic induction of the stress response under permissive conditions. Low levels of stress-response expression have been reported, for example, due to spontaneous DNA breakage [46, 47]. We expect our method to be robust to low levels of stress response induction under permissive conditions since, in this case, the subpopulation with elevated stress response level will be negligibly small. This also implies, though, that with our method we cannot effectively quantify heterogeneity in mutation rates in unstressed conditions.

To be able to derive an analytical expression for the mutant count distribution, we made a series of approximations, the most important one being that cells with stress response switched *on* have a net growth rate ($\gamma_{on} - \delta_{on}$) much lower than that of *off* cells (γ^s_{off} δ_{off} α). For the SOS response, this approximation is valid, as induction of the response inhibits cell division. However, it might be violated for other stress responses, particularly if they protect cells from death, resulting in $\delta_{on} < \delta_{off}$. In this case, our approximation is no longer valid, and therefore, parameter estimation using our method is expected to be less accurate. Nonetheless, the estimated mutation-rate increase is robust to relative fitness of response-*on* cells r_{on} $\frac{\gamma_{on}}{\gamma^s_{off}} \frac{\delta_{on}}{\delta^s_{off}}$ up to ≈75% and is only marginally improved by inferring r_{on} rather than setting it to zero (Fig 4A).

We also assume response-*on* cells do not switch the response *off* so long as the stress remains present during a fluctuation assay's comparably short growth phase. In particular, this assumption implies that the model cannot capture stress responses that are transiently expressed and associated with pulse-like mutagenesis even under continued exposure to the stressor, such as the oxidative stress response [48]. Our model could be adapted for stress responses where induction of the response is associated with a *decrease* in mutation rate along with increased cell viability, such as the adaptive (Ada) response to DNA alkylation damage, which also exhibits within-population heterogeneity in timing of induction [22, 23]. However, this situation would require a different parameterisation of the model, in which our current analytical approximations break down and the potential for parameter inference would need to be re-tested. Overall, developing models tailored to other stress responses offers an interesting direction for future work.

In summary, we have presented and validated a new method for inferring stress-induced increases in mutation rate from fluctuation assays. Importantly, however, both a heterogeneous stress response and a homogeneous response with mutant fitness costs can generate similar patterns in fluctuation assay data (Fig B in S1 File), which calls for further experiments to distinguish these models. While the homogeneous-response model can estimate the increase in population mean mutation rate, our new method of inferring heterogeneous mutation rates would be crucial for accurately characterising the mutagenic effects of stress responses and parameterising models of multi-locus adaptation. In future work, we aim to incorporate our new method into user-friendly tools for application to experimental data, similar to existing R packages [37, 49] and web tools [16, 32, 50, 51] for fluctuation analysis.

Supporting information

S1 File. Supplementary information. Mathematical derivations, example mutant count distributions, sensitivity analysis, 95% confidence intervals, parameter estimation and model selection for additional parameter ranges, and comparison of model selection procedures.
(PDF)

Acknowledgments

The authors are grateful for helpful feedback on the mathematical results received from Tibor Antal and for the discussion and inspiration provided by the Alexander and El Karoui labs.

Author Contributions

Conceptualization: Lucy Lansch-Justen, Meriem El Karoui, Helen K. Alexander.

Formal analysis: Lucy Lansch-Justen.

Funding acquisition: Meriem El Karoui, Helen K. Alexander.

Investigation: Lucy Lansch-Justen.

Methodology: Lucy Lansch-Justen, Meriem El Karoui, Helen K. Alexander.

Software: Lucy Lansch-Justen.

Supervision: Meriem El Karoui, Helen K. Alexander.

Validation: Lucy Lansch-Justen, Helen K. Alexander.

Visualization: Lucy Lansch-Justen.

Writing – original draft: Lucy Lansch-Justen.

Writing – review & editing: Lucy Lansch-Justen, Meriem El Karoui, Helen K. Alexander.

References

1. Friedberg EC, Walker GC, Siede W, Wood RD, Schultz RA, Ellenberger T. Mutagenesis and Translesion Synthesis in Prokaryotes. In: DNA Repair and Mutagenesis. Washington, DC, USA: ASM Press; 2014. p. 509–568. Available from: http://doi.wiley.com/10.1128/9781555816704.ch15.
2. Foster PL. Stress-Induced Mutagenesis in Bacteria. Critical Reviews in Biochemistry and Molecular Biology. 2007; 42(5):373–397. https://doi.org/10.1080/10409230701648494 PMID: 17917873
3. Bjedov I, Tenaillon O, Gérard B, Souza V, Denamur E, Radman M, et al. Stress-Induced Mutagenesis in Bacteria. Science. 2003; 300(5624):1404–1409. https://doi.org/10.1126/science.1082240 PMID: 12775833

4. Tenaillon O, Denamur E, Matic I. Evolutionary significance of stress-induced mutagenesis in bacteria. Trends in Microbiology. 2004; 12(6):264–270. https://doi.org/10.1016/j.tim.2004.04.002 PMID: 15165604
5. Ram Y, Hadany L. The evolution of stress-induced hypermutation in asexual populations. Evolution. 2012; 66(7):2315–2328. https://doi.org/10.1111/j.1558-5646.2012.01576.x PMID: 22759304
6. Ram Y, Hadany L. Stress-induced mutagenesis and complex adaptation. Proceedings of the Royal Society B: Biological Sciences. 2014; 281 (1792). https://doi.org/10.1098/rspb.2014.1025 PMID: 25143032
7. Cirz RT, Chin JK, Andes DR, de Crécy-Lagard V, Craig WA, Romesberg FE. Inhibition of Mutation and Combating the Evolution of Antibiotic Resistance. PLoS Biology. 2005; 3(6):e176. https://doi.org/10.1371/journal.pbio.0030176 PMID: 15869329
8. Pribis JP, García-Villada L, Zhai Y, Lewin-Epstein O, Wang AZ, Liu J, et al. Gamblers: An Antibiotic-Induced Evolvable Cell Subpopulation Differentiated by Reactive-Oxygen-Induced General Stress Response. Molecular Cell. 2019; 74(4):785–800.e7. https://doi.org/10.1016/j.molcel.2019.02.037 PMID: 30948267
9. Zhai Y, Pribis JP, Dooling SW, Garcia-Villada L, Minnick PJ, Xia J, et al. Drugging evolution of antibiotic resistance at a regulatory network hub. Science Advances. 2023; 9(25):eadg0188. https://doi.org/10.1126/sciadv.adg0188 PMID: 37352342
10. WU YL, SCOTT EM, PO ALW, TARIQ VN. Development of resistance and cross-resistance in Pseudomonas aeruginosa exposed to subinhibitory antibiotic concentrations. APMIS. 1999; 107(1-6):585–592. https://doi.org/10.1111/j.1699-0463.1999.tb01596.x PMID: 10379686
11. Gillespie SH, Basu S, Dickens AL, O'Sullivan DM, McHugh TD. Effect of subinhibitory concentrations of ciprofloxacin on Mycobacterium fortuitum mutation rates. Journal of Antimicrobial Chemotherapy. 2005; 56(2):344–348. https://doi.org/10.1093/jac/dki191 PMID: 15956099
12. Henderson-Begg SK, Livermore DM, Hall LMC. Effect of subinhibitory concentrations of antibiotics on mutation frequency in Streptococcus pneumoniae. Journal of Antimicrobial Chemotherapy. 2006; 57 (5):849–854. https://doi.org/10.1093/jac/dkl064 PMID: 16531433
13. Baharoglu Z, Mazel D. Vibrio cholerae Triggers SOS and Mutagenesis in Response to a Wide Range of Antibiotics: a Route towards Multiresistance. Antimicrobial Agents and Chemotherapy. 2011; 55 (5):2438–2441. https://doi.org/10.1128/AAC.01549-10 PMID: 21300836
14. Kohanski MA, DePristo MA, Collins JJ. Sublethal Antibiotic Treatment Leads to Multidrug Resistance via Radical-Induced Mutagenesis. Molecular Cell. 2010; 37(3):311–320. https://doi.org/10.1016/j.molcel.2010.01.003 PMID: 20159551
15. Gutierrez A, Laureti L, Crussard S, Abida H, Rodríguez-Rojas A, Blázquez J, et al. β-lactam antibiotics promote bacterial mutagenesis via an RpoS-mediated reduction in replication fidelity. Nature Communications. 2013; 4. https://doi.org/10.1038/ncomms2607 PMID: 23511474
16. Krašovec R, Richards H, Gomez G, Gifford DR, Mazoyer A, Knight CG. Measuring Microbial Mutation Rates with the Fluctuation Assay. Journal of Visualized Experiments. 2019; 2019(153):1–9. PMID: 31840662
17. Foster PL. Methods for determining spontaneous mutation rates. Methods in enzymology. 2006; 409:195–213. https://doi.org/10.1016/S0076-6879(05)09012-9 PMID: 16793403
18. Frenoy A, Bonhoeffer S. Death and population dynamics affect mutation rate estimates and evolvability under stress in bacteria. PLOS Biology. 2018; 16(5):e2005056. https://doi.org/10.1371/journal.pbio.2005056 PMID: 29750784
19. McCool JD, Long E, Petrosino JF, Sandler HA, Rosenberg SM, Sandler SJ. Measurement of SOS expression in individual Escherichia coli K-12 cells using fluorescence microscopy. Molecular Microbiology. 2004; 53(5):1343–1357. https://doi.org/10.1111/j.1365-2958.2004.04225.x PMID: 15387814
20. Mrak P, Podlesek Z, van Putten JPM, Žgur-Bertok D. Heterogeneity in expression of the Escherichia coli colicin K activity gene cka is controlled by the SOS system and stochastic factors. Molecular Genetics and Genomics. 2007; 277(4):391–401. https://doi.org/10.1007/s00438-006-0185-x PMID: 17216493
21. Kamenšek S, Podlesek Z, Gillor O, Žgur-Bertok D. Genes regulated by the Escherichia coli SOS repressor LexA exhibit heterogenous expression. BMC Microbiology. 2010; 10(1):283. https://doi.org/10.1186/1471-2180-10-283 PMID: 21070632
22. Uphoff S, Lord ND, Okumus B, Potvin-Trottier L, Sherratt DJ, Paulsson J. Stochastic activation of a DNA damage response causes cell-to-cell mutation rate variation. Science. 2016; 351(6277):1094–1097. https://doi.org/10.1126/science.aac9786 PMID: 26941321
23. Uphoff S. Real-time dynamics of mutagenesis reveal the chronology of DNA repair and damage tolerance responses in single cells. Proceedings of the National Academy of Sciences. 2018; 115(28):E6516–E6525. https://doi.org/10.1073/pnas.1801101115 PMID: 29941584

24. Woo AC, Faure L, Dapa T, Matic I. Heterogeneity of spontaneous DNA replication errors in single isogenic Escherichia coli cells. Science Advances. 2018; 4(6):2–10. https://doi.org/10.1126/sciadv.aat1608 PMID: 29938224

25. Jones EC, Uphoff S. Single-molecule imaging of LexA degradation in Escherichia coli elucidates regulatory mechanisms and heterogeneity of the SOS response. Nature Microbiology. 2021. https://doi.org/10.1038/s41564-021-00930-y PMID: 34183814

26. Vincent MS, Uphoff S. Cellular heterogeneity in DNA alkylation repair increases population genetic plasticity. Nucleic Acids Research. 2021; 49(21):12320–12331. https://doi.org/10.1093/nar/gkab1143 PMID: 34850170

27. Jaramillo-Riveri S, Broughton J, McVey A, Pilizota T, Scott M, El Karoui M. Growth-dependent heterogeneity in the DNA damage response in Escherichia coli. Molecular Systems Biology. 2022; 18(5):1–14. https://doi.org/10.15252/msb.202110441 PMID: 35620827

28. Choudhary D, Lagage V, Foster KR, Uphoff S. Phenotypic heterogeneity in the bacterial oxidative stress response is driven by cell-cell interactions. Cell Reports. 2023; 42(3):112168. https://doi.org/10.1016/j.celrep.2023.112168 PMID: 36848288

29. Lagage V, Uphoff S. Pulses and delays, anticipation and memory: seeing bacterial stress responses from a single-cell perspective. FEMS microbiology reviews. 2020; 44(5):565–571. https://doi.org/10.1093/femsre/fuaa022 PMID: 32556120

30. Friedberg EC, Walker GC, Siede W, Wood RD, Schultz RA, Ellenberger T. The SOS Responses of Prokaryotes to DNA Damage. In: DNA Repair and Mutagenesis. Washington, DC, USA: ASM Press; 2014. p. 463–508. Available from: http://doi.wiley.com/10.1128/9781555816704.ch14.

31. Baharoglu Z, Mazel D. SOS, the formidable strategy of bacteria against aggressions. FEMS Microbiology Reviews. 2014; 38(6):1126–1145. https://doi.org/10.1111/1574-6976.12077 PMID: 24923554

32. Łazowski K. Efficient, robust, and versatile fluctuation data analysis using MLE MUtation Rate calculator (mlemur). Mutation Research—Fundamental and Molecular Mechanisms of Mutagenesis. 2023; 826 (April). PMID: 37104996

33. Feller W. Die Grundlagen der Volterraschen Theorie des Kampfes ums Dasein in wahrscheinlichkeitstheoretischer Behandlung. Acta Biotheoretica. 1939; 5(1):11–40. https://doi.org/10.1007/BF01602932

34. Keller P, Antal T. Mutant number distribution in an exponentially growing population. Journal of Statistical Mechanics: Theory and Experiment. 2015; 2015(1):P01011. https://doi.org/10.1088/1742-5468/2015/01/P01011

35. Bos J, Zhang Q, Vyawahare S, Rogers E, Rosenberg SM, Austin RH. Emergence of antibiotic resistance from multinucleated bacterial filaments. Proceedings of the National Academy of Sciences. 2015; 112(1):178–183. https://doi.org/10.1073/pnas.1420702111 PMID: 25492931

36. Bezanson J, Edelman A, Karpinski S, Shah VB. Julia: A Fresh Approach to Numerical Computing. SIAM Review. 2017; 59(1):65–98. https://doi.org/10.1137/141000671

37. Mazoyer A, Drouilhet R, Despréaux S, Ycart B. flan: An R Package for Inference on Mutation Models. The R Journal. 2017; 9(1):334. https://doi.org/10.32614/RJ-2017-029

38. GABBIANI F, COX SJ. Stochastic Processes. In: Mathematics for Neuroscientists. Elsevier; 2010. p. 251–266. Available from: http://www.worldscientific.com/doi/abs/10.1142/9789813148963_0008 https://linkinghub.elsevier.com/retrieve/pii/B9780123748829000162.

39. Gillespie DT. Exact stochastic simulation of coupled chemical reactions. The Journal of Physical Chemistry. 1977; 81(25):2340–2361. https://doi.org/10.1021/j100540a008

40. Garibyan L. Use of the rpoB gene to determine the specificity of base substitution mutations on the Escherichia coli chromosome. DNA Repair. 2003; 2(5):593–608. https://doi.org/10.1016/S1568-7864(03)00024-7 PMID: 12713816

41. Lee H, Popodi E, Tang H, Foster PL. Rate and molecular spectrum of spontaneous mutations in the bacterium Escherichia coli as determined by whole-genome sequencing. Proceedings of the National Academy of Sciences of the United States of America. 2012; 109(41). https://doi.org/10.1073/pnas.1210309109 PMID: 22991466

42. Marinus MG. DNA methylation and mutator genes in Escherichia coli K-12. Mutation Research/Reviews in Mutation Research. 2010; 705(2):71–76. https://doi.org/10.1016/j.mrrev.2010.05.001 PMID: 20471491

43. Vasse M, Bonhoeffer S, Frenoy A. Ecological effects of stress drive bacterial evolvability under subinhibitory antibiotic treatments. ISME Communications. 2022; 2(1). https://doi.org/10.1038/s43705-022-00157-w PMID: 37938266

44. Zheng Q. Estimation of Rates of Non-neutral Mutations When Bacteria are Exposed to Subinhibitory Levels of Antibiotics. Bulletin of Mathematical Biology. 2022; 84(11):131. https://doi.org/10.1007/s11538-022-01085-5 PMID: 36178523

45. Alexander HK, Mayer SI, Bonhoeffer S. Population Heterogeneity in Mutation Rate Increases the Frequency of Higher-Order Mutants and Reduces Long-Term Mutational Load. Molecular Biology and Evolution. 2016; 34(2):244. https://doi.org/10.1093/molbev/msw244

46. Jeanine M P, Susan M R. Spontaneous DNA breakage in single living Escherichia coli cells. Nature Genetics. 2007; 39(6):797–802. https://doi.org/10.1038/ng2051

47. Vincent MS, Uphoff S. Bacterial phenotypic heterogeneity in DNA repair and mutagenesis. Biochemical Society Transactions. 2020; 48(2):451–462. https://doi.org/10.1042/BST20190364 PMID: 32196548

48. Lagage V, Chen V, Uphoff S. Adaptation delay causes a burst of mutations in bacteria responding to oxidative stress. EMBO reports. 2023; 24(1). https://doi.org/10.15252/embr.202255640 PMID: 36397732

49. Zheng Q. rSalvador: An R package for the fluctuation experiment. G3: Genes, Genomes, Genetics. 2017; 7(12):3849–3856. https://doi.org/10.1534/g3.117.300120 PMID: 29084818

50. Hall BM, Ma CX, Liang P, Singh KK. Fluctuation AnaLysis CalculatOR: a web tool for the determination of mutation rate using Luria–Delbrück fluctuation analysis. Bioinformatics. 2009; 25(12):1564–1565. https://doi.org/10.1093/bioinformatics/btp253 PMID: 19369502

51. Gillet-Markowska A, Louvel G, Fischer G. bz-rates: A Web Tool to Estimate Mutation Rates from Fluctuation Analysis. G3 Genes|Genomes|Genetics. 2015; 5(11):2323–2327. https://doi.org/10.1534/g3.115.019836 PMID: 26338660

What's next? Application to experimental data!

Our estimation method had always been intended for the analysis of experimental data. With my second supervisor Meriem El Karoui, we discussed the possibility of performing our own experiments. But then we came across a recent meta-analysis of fluctuation assay data [71] and decided to re-analyse these experiments instead. After scanning the data, we realised that we needed to additionally implement partial plating. Moreover, our estimation analysis up until this point had been under the assumption that there was stress-induced mutagenesis (with the question of whether or not there was heterogeneity in stress responses). For the data we intended to re-analyse, this assumption was not necessarily true. Therefore, we decided to include a 'null model' of no stress-induced mutagenesis in our estimation and model selection procedure. The variation in experimental design and antimicrobials used in the experiments also sparked new research questions.

Chapter 3

Support for stress-induced mutagenesis and heterogeneous stress responses in experimental fluctuation assay data

3.1 Introduction

Antibiotic resistance is a major global health threat, and the rapid emergence and spread of resistance has closely followed each discovery of a new antibiotic. It is important to understand how genetic mutations arise that allow bacteria to survive antibiotic treatment, a research area to which the fluctuation assay has contributed significantly.

The fluctuation assay, originally designed to test whether mutations arise spontaneously and at random, or are induced by and directed towards a selective pressure [54], has a simple experimental setup (see [47] for a protocol): Several parallel cultures are inoculated and grown, typically overnight, in permissive conditions (*the growth phase*). Then, each culture is plated on a plate with selective medium (often an antibiotic) where only resistant mutant cells can grow. The resistant colonies are counted, giving the so-called *mutant count distribution*. When the first fluctuation assay was performed, the shape of the mutant count distribution, with large variation in the colony counts between plates, provided evidence that mutations arise spontaneously during the growth phase [54]. At the same time, the experiment yielded the first quantitative estimate of the mutation rate in bacteria, and is used almost exclusively for this purpose today.

Fluctuation assays are used in many fields of research, including antimicrobial resistance, evolutionary genetics, DNA repair and genotoxicity, see [20] for a review. At the intersection of all these fields lies the topic of stress-induced mutagenesis (SIM), which is the concern of this work. SIM describes how exposure to environmental stressors, such as antibiotics or biocides at low concentrations, induces stress responses in bacteria. This can lead to an increase in DNA damage followed by the upregulation of error-prone DNA repair mechanisms and, thereby, to an increase in mutation rate. Several studies report SIM in bacteria, particularly when exposed to low levels of stress such as low antibiotic concentrations, using fluctuation assays to estimate and compare mutation rates [76, 28, 33, 3, 45, 31, 62].

Since the invention of the fluctuation assay, there have been huge improvements in the mathematical and computational methods to estimate the mutation rate. Today, there are a range of reliable and easy-to-use tools available, see for example [51] for a recent review. Moreover, the original population dynamic model behind the fluctuation assay has been extended in various ways to make it more biologically realistic or to adapt it to specific scenarios. For example, the mutant count distribution has been derived for the case that there is cell death, that mutant cells have a different fitness than non-mutant cells, and that only part of each culture is plated on the selective media.

In our previous work, we additionally proposed an estimation approach particularly relevant for studying SIM: Addressing cell-to-cell heterogeneity in the induction of stress responses [50], which has been revealed by recent single-cell studies [59, 61, 40, 70, 69, 74, 62, 39, 73, 38, 13]. We introduced a population dynamic model inspired by the DNA-damage response in *E. coli* (SOS response), which captures heterogeneity in stress responses in the form of a slowly dividing and highly mutating subpopulation. Using simulated fluctuation assay data, we showed that this model allows us to estimate the specific increase in mutation rate associated with the induction of the stress response, if the fraction of this response-*on* subpopulation has been measured. However, we also found that either heterogeneity in stress responses or mutants having a different fitness than non-mutants results in a similar shape of the mutant count distribution and, therefore, are difficult to distinguish from fluctuation assay data alone. Moreover, we showed that neglecting heterogeneity in stress responses effectively leads to an accurate estimation of the increase in population-mean mutation rate, but not in the mutation rate specifically associated with cells inducing the stress response.

In this work, we now apply our estimation method [50] to published experimental data from studies using fluctuation assays to quantify SIM. We extended the population dynamic models to include partial plating because many studies do not plate the entire culture onto the selective plates. We also defined a null model to test whether there is statistical evidence for SIM in the first place. Moreover, we converted our method into a user-friendly R tool, freely available at `https://github.com/LucyL-J/estimu`.

3.2 Models and methods

3.2.1 Meta-analysis of previous experimental studies

We re-analysed published fluctuation assay data that fulfilled our requirement of performing at least one fluctuation assay where the parallel cultures were exposed to a concentration of an antibiotic or antimicrobial chemical below the minimum inhibitory concentration (MIC) and one untreated control assay. We excluded studies for which no raw data was available and studies in which cultures were allowed to recover in fresh antibiotic-free medium after exposure during the growth phase and before plating, as this protocol deviates from the standard fluctuation assay protocol in a way that cannot adequately be captured by existing population dynamic models.

To identify relevant data, we used a recent meta-analysis [71] which gathered such fluctuation assay data from 10 studies [3, 14, 15, 25, 30, 34, 37, 60, 64, 68], as well as performed their own experiments [71], but we excluded studies that used a regrowth protocol [37, 64]. Additionally, we included two more recently published studies [10, 65]. In total, we considered 11 studies which performed 94 fluctuation assays using 5 different bacterial species and 25 antimicrobials.

We classified these antimicrobials by their target [43], which represents a broader classification than antibiotic class and allows us to include antimicrobial chemicals (technically not antibiotics), see Table 3.1. Antimicrobials binding to the 70S ribosome make the largest group by the number of experiments using them, followed by antimicrobials binding to DNA gyrase (Fig 3.1).

Antibiotic	Abbreviation	Class	Target
Mitomycin	MMC	Anti-tumor/-neoplastic	DNA directly
Ciprofloxacin	Cip	Quinolone	DNA gyrase
Nalidixic acid	Nal		
Norfloxacin	Nor		
Novobiocin	Novo	Aminocoumarin	
Trimethoprim	Trim	Antimetabolite	Dihydrofolate
Rifampicin	Rif	Rifamycin	RNA polymerase
Chloramphenicol	Cm	Amphenicol	70S Ribosome
Erythromycin	Ery	Macrolide	
Amikacin	Ami	Aminoglycoside	
Gentamycin	Gen		
Kanamycin	Kan		
Neomycin	Neo		
Tobramycin	Tob		
Streptomycin	Strep		
Spectinomycin	Spec	Aminocyclitol	
Tetracycline	Tet	Tetracycline	
Ampicillin	Amp	Penicillin	Penicillin-binding protein
Penicillin	Pen		
Ceftazidime	Cef	Cephalosporin	
Imipenem	Imi	Carbapenem	
Benzalkonium chloride	BAC	Disinfectant	Cell membrane diretly
Chlorhexidine digluconate	CHX		
Didecyldimethyl-ammoniumchlorid	DDAC		
Copper	Cu		Multiple targets via generation of toxic reactive species (TRS)
Hydrogen peroxide	H_2O_2		
Metronidazole	Met	Nitroimidazole	
Nitrofurantoin	Nitro	Nitrofuran	
Optochin	Opto	Quinine-derivative	ATPase

Table 3.1: Classification of the antimicrobials used in the re-analysed experiments (with respective abbreviations) by antibiotic class and target.

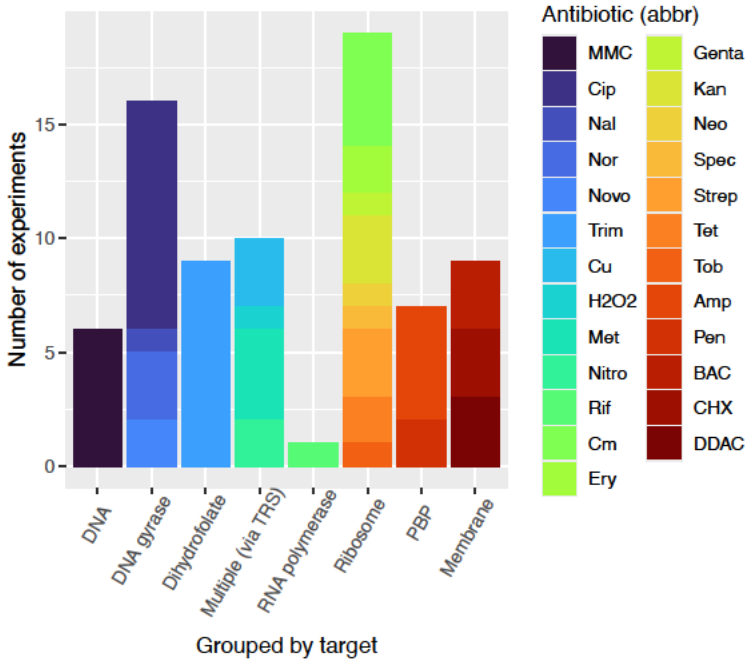

Figure 3.1: Antimicrobials used in the re-analysed experiments, grouped by their target, see Table 3.1.

For each experiment, we extracted raw data necessary for the inference: resistant mutant colony counts together with the fraction of the culture that was plated and the final population size at the end of the growth phase for the untreated (UT) and antimicrobial (S for stressed) fluctuation assay, respectively. Note that we assume the final population sizes were measured without uncertainty, in common with all existing mutation-rate estimation tools but undoubtedly a simplifying assumption.

We also extracted metadata on the antibiotic concentration (in $\frac{\mu g}{mL}$, and in units of the respective MIC if available, Appendix Table B.1), growth medium, duration of the growth phase, selective marker, and bacterial species and strain (Table 3.2). Most studies used an *E. coli* wild-type (wt) strain (MG1655 or the derived strain TD2158). Bacterial species other than *E. coli* were *A. baylyi* and *B. subtilis* [65], *P. aeruginosa* (strain PA01 [68] and the more virulent PA14 [34]), and *S. pneumoniae* [14]. Three studies compared a wild-type and a mutant strain: [15] and [60] used an *E. coli* MG1655 wild-type and SulA-deletion strain (ΔSulA); [68] used a *P. aeruginosa* PA01 wild-type and LexA-deficient strain (LexAd).

From the raw data, we additionally extracted the number of parallel cultures (for the UT and for the S conditions). If the study used *E. coli* and measured the expression of the DNA-damage response (SOS response), we recorded any qualitative or quantitative measurements provided in the study (not shown in Table 3.2 but can be found in the file **meta_data.csv** at `https://github.com/LucyL-J/estimu`).

In cases where several biological replicates (i.e. multiple fluctuation assays under the same conditions) were performed, we pooled the replicates together due to our requirement of always pairing exactly one stressed (antimicrobial-treated) with one untreated fluctuation assay and such pairing being ambiguous otherwise. This pairing also implied that if a study tested more than one antimicrobial but performed only one untreated control, we re-used the data from untreated fluctuation assay for each antimicrobial treatment. Overall, we were left with 77 pairs of fluctuation assays, which we defined as *experiments*, to analyse. To each experiment, we assigned a unique identifier consisting of '1stauthor_antimicrobial_X'. X describes a condition other than the antimicrobial, which was varied by the authors, such as the selective marker, the duration of the growth phase, the bacterial species or strain, or the drug concentration.

We show the estimation results for all bacterial species and strains. However, we restricted some of our analyses to experiments using *E. coli* wild-type strains MG1655 and TD2158 (44 out of 77) to be able to compare estimated parameters meaningfully.

Study	Species strain (mutant)	Antimicrobial applied in the S condition ([$\frac{\mu g}{mL}$])	#cultures (UT, S)	Growth phase	Selective plates
Baharoglu et al. [3]	*E. coli* MG1655	Amp (0.05), Cm (0.15), Cip (0.05), Kan (0.2), MMC, Neo (0.1), Rif (0.05), Spec (0.2), Tet (0.15), Tob (0.1), Trim (0.05)	(3, 2-3)	$24h$ in MH	40% on Rif
Bulssico et al. [10]	*E. coli* TD2158	Cip (0.01)	(236, 240)	$20h$ in LB	100% on Rif
Cortes et al. [14]	*S. pneumoniae* D39	Cm (3.0), Ery (0.09), Pen (0.024)	(29-30, 18-31)	$7.5h$ in BHI	100% on Opto, 100% on Rif
Dapa et al. [15]	*E. coli* MG1655 (ΔSulA)	MMC (1.0)	(62-65, 18)	$24h$ in LB, $48h$ in LB	4% on Rif
Frenoy et al. [25]	*E. coli* MG1655	H_2O_2 (0.034), Kan (3.0), Nor (0.05)	(153, 71-158)	$24h$ in LB	20% on Rif
Giroux et al. [30]	*E. coli* MG1655	Trim (0.04)	(30, 30)	$24h$ in LB	2% on Tet
Hocquet et al. [34]	*P. aeruginosa* PA14	Met (50.0)	(3, 3)	$24h$ in LB	0.0002% on Ami, 0.2% on Cef, 0.02% on Cip, 0.002% on Imi
Mo et al. [60]	*E. coli* MG1655 (wt and ΔSulA)	Amp (2.0), Cip (0.01), MMC (0.5), Nitro (2.0), Novo (16.0), Strep (2.0), Trim (0.032)	(6, 6)	$48h$ in LB	1% on Rif
Schmidt et al. [65]	*A. baylyi* ADP1	BAC (0.24), CHX (0.002), Cip (0.036), Cu (1.0), DDAC (0.02), Trim (16.0)	(48, 48)	$25h$ in M9G	100% on Rif
	B. subtilis 3610	BAC (0.0012), CHX (0.012), Cip (0.008), Cu (0.004), DDAC (0.0002), Trim (0.004)			
	E. coli MG1655	BAC (0.03), CHX (0.012), Cip (0.0006), Cu (0.025), DDAC (0.01), Trim (0.2),			
Torres-Barcelo et al. [68]	*P. aeruginosa* PA01 (wt and LexAd)	Cip (0.048)	(12, 12)	$24h$ in M9KB	4% on Rif
Vasse et al. [71]	*E. coli* MG1655	Amp (1.0 and 3.2), Cm (0.15 and 1.5), Cip (0.005), Kan (1.6), MMC (1.0), Nal (1.0), Nor (0.005 and 0.05), Strep (5.0), Tet (0.15), Trim (0.005 and 0.05)	(23, 11-12)	$24h$ in LB	40% on Rif

Table 3.2: Bacteria, antimicrobials, number of parallel cultures, duration of the growth phase and growth medium, and plated fraction and the selective medium used in the respective studies. In some studies, the number of parallel cultures varied, both within and between the untreated (UT) and the antimicrobial-treated (S for stressed) conditions. Most studies used nutrient-rich media: Mueller-Hilton (MH), lysogeny broth (LB), brain heart infusion (BHI). Two studies used minimal media, supplemented with either glucose (M9G) [65] or kasugamycin and bovine serum albumin (M9KB) [68]. The concentration of MMC was missing in [3].

3.2.2 Models of stress-induced mutagenesis (SIM)

We analysed each experiment (pair of fluctuation assays, antimicrobial-treated compared to untreated condition) under three different scenarios: (i) there is no increase in per-division mutation rate due to the antimicrobial, (ii) the antimicrobial leads to a population-wide increase in mutation rate, and (iii) the antimicrobial results in the emergence of a subpopulation of cells with increased mutation (and decreased division) rate. Fig 3.2 shows a schematic of how we model these scenarios. Case (i) corresponds to the null model of stress not influencing the mutation rate. Case (ii) corresponds to a model of homogeneous stress responses, and case (iii) corresponds to a model of heterogeneous stress responses with induction in only a small subpopulation, as we introduced in our previous work [50].

General model structure: All models we use share the same basic structure, in common with the majority of models used in mutation-rate estimation from fluctuation assays [51]: an exponentially growing non-mutant population (or subpopulations with the stress response *off/on* in the case of the heterogeneous-response model) with population growth rate λ. Cell death is neglected and, therefore, the population growth rate λ is equal to the cell division rate γ. Mutations occur randomly at rate μ per cell division, and each mutant cell grows stochastically according to a pure birth process with the birth (cell division) rate b. Optionally, we also consider a differential mutant fitness, i.e. mutant cells having a different division rate than non-mutant cells, described by the ratio $\rho := \frac{b}{\lambda}$. When only a fraction of the whole culture is plated (plating efficiency E), we assume that each mutant cell, independently, has the same probability E to end up on the plate and form a colony.

Null model (no stress-induced mutagenesis): In our null model, we assume that cells do not induce a mutagenic stress response and, despite the division rate potentially being impacted by the antimicrobial, the *per-division* mutation rate does not change, i.e. $\mu_0 = \mu_s$ (subscript 0 for the untreated control and subscript S for the stressed condition under antimicrobial treatment). The same applies to the mutant fitness: even if $\rho_0 \neq 1$, it remains unchanged regardless of the presence of the antimicrobial, i.e. $\rho_0 = \rho_s$. This assumption is reasonable as long as resistance to the antibiotic used

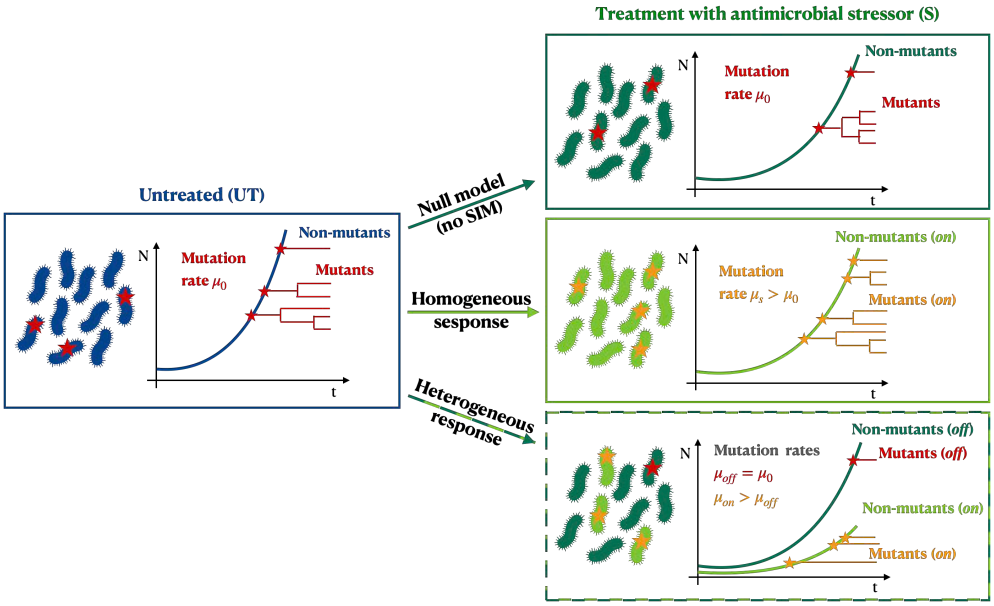

Figure 3.2: Models of SIM. In the untreated condition (UT), the non-mutant population grows exponentially with rate λ_0 given by the division rate $= \gamma_0$. Mutations occur randomly at per-division rate μ_0, and mutant lineages grow stochastically with differential fitness ρ_0 (compared to the non-mutant population). Under treatment with an antimicrobial stressor (S), we consider three possibilities: **Null model (no SIM):** Non-mutants grow exponentially with potentially reduced division rate, $\lambda_s = \gamma_s \leq \gamma_0$. Mutations occur randomly at the same per-division rate μ_0, and mutants grow stochastically with the same differential fitness ρ_0 as in the UT condition. **Homogeneous response:** Non-mutants grow exponentially with potentially reduced division rate $\lambda_s = \gamma_s \leq \gamma_0$. Mutations occur randomly at an increased per-division mutation rate $\mu_s > \mu_0$. Mutants grow stochastically with differential fitness ρ_s, which can be $\neq \rho_0$. **Heterogeneous response:** Response-*off* non-mutants divide at rate γ_{off} and switch to the response-*on* state at rate α. Response-*on* non-mutants have a zero or very low division rate $\gamma_{on} \ll \gamma_{off}$ relative to response-*off* non-mutants, $r_{on} := \gamma_{on}/\gamma_{off}$. The total population grows exponentially at rate $\lambda_s \approx \gamma_{off} - \alpha$, and the response-*on* subpopulation makes up a stationary fraction f^*_{on}. In response-*off* cells, mutations occur at the same per-division mutation rate $\mu_{off} = \mu_0$, and mutants grow stochastically with the same differential fitness $\rho_{off} = \rho_0$. In response-*on* cells, mutations occur at a high per-(response-*off*)-division rate $\mu_{on} > \mu_{off}$, and response-*on* mutants grow stochastically with differential fitness $\rho_0\gamma_{on}/(\gamma_{off} - \alpha)$. **For all models:** We assume that the initial population size is much smaller than the final population size at the end of the growth phase, $N_i \ll N_f$, and neglect cell death. Each mutant cell is plated on a selective plate with a probability given by the plating efficiency E.

on the selective plate does not confer any advantage or disadvantage in the presence of the antimicrobial stressor used during the growth phase, in particular, that there is no cross-resistance.

For models of SIM, we distinguish between stress responses that are expressed homogeneously and ones that are expressed heterogeneously across the bacterial population.

Homogeneously expressed stress responses: In the homogeneous-response model, we assume that all cells in a population respond to the antimicrobial in the same way: a population-wide increase in per-division mutation rate under antimicrobial treatment compared to untreated conditions, $\mu_0 \to \mu_s$, and optionally, a population-wide change in differential mutant fitness, $\rho_0 \to \rho_s$.

Heterogeneously expressed stress responses: In the heterogeneous-response model, we assume within-population heterogeneity in the stress response. In particular, in our heterogeneous-response model, the antimicrobial treatment results in the emergence of a response-*on* subpopulation (subscript on), which expresses the stress response. Switching to the response-*on* state happens at a rate α, and after an initial equilibration phase, the response-*on* subpopulation makes up a (stationary) fraction f^*_{on} of the total population. Induction of the stress response in these response-*on* cells results in an increased mutation rate $\mu_{on} > \mu_{off}$ and zero/decreased division rate, r_{on}, relative to response-*off* cells. This model is inspired by the SOS response in *E. coli*, which is heterogeneously expressed within populations [59, 40, 38]. Moreover, the SOS response includes the induction of error-prone DNA polymerases and inhibits cell division but not DNA replication, implying that mutations can still occur, potentially at an increased rate [4, 26]. For more details of the model, see [50].

3.2.3 Parameter estimation and confidence intervals

We used a maximum-likelihood approach to estimate the model parameters under the different models. That is, for each experiment and each model, we determined the set of parameters for which the likelihood of the observed mutant count distribution in the untreated condition together with the one under antimicrobial treatment is maximal. Using a profile-likelihood approach, we also calculated 95% confidence intervals around the maximum-likelihood estimates.

Here, we extended our previous work [50] in three ways: by implementing inference under the above-described null model, by allowing a fixed (not estimated) differential mutant fitness in the heterogeneous-response model, and by including partial plating into all models. The latter closely follows the implementation by [51], and details can be found in the file **mutantcountdistributions.jl** at `https://github.com/LucyL-J/estimu`.

Null model: Under the null model, we jointly infer the mutation rate, which remains unchanged under antimicrobial treatment $\mu_0 = \mu_s$. In general, the differential mutant fitness can be set to fixed values in the inference if it is known from separate experiments. Because estimates of the mutant fitness are not available for the data analysed here, we either set $\rho_0 = \rho_s = 1$, or consider it as an additional joint inference parameter $\rho_0 = \rho_s$, under the assumption that differential fitness is not affected by the antimicrobial treatment. This results in one, or optionally two, inference parameters.

Homogeneous-response model: In the homogeneous-response model, there are a minimum of two inference parameters: the mutation rates under untreated and antimicrobial treatment, μ_0 and μ_s. Optionally, we also infer the differential mutant fitness, either as a joint parameter (constrained to be equal regardless of the treatment, $\rho_0 = \rho_s$) or as two separate parameters, ρ_0 and ρ_s. Under the homogeneous-response model, we quantify stress-induced mutagenesis as the increase in population-wide mutation rate $\bar{M} := \frac{\mu_s}{\mu_0}$.

Heterogeneous-response model: In the heterogeneous-response model, the mutation rate of response-*off* cells, μ_{off}, is assumed to be the same regardless of the treatment and is, therefore, jointly inferred from untreated and treatment conditions. Response-*on* cells, on the other hand, appear only under antimicrobial treatment. We have to distinguish two cases, depending on the relative division rate of response-*on* cells, r_{on}. When $r_{on} = 0$, we cannot infer the mutation rate μ_{on} and fraction f_{on} of response-*on* cells separately (see [50]). Instead, we infer as a second composite parameter, the mutation-supply ratio defined as

$$S := \frac{\mu_{on} f_{on}}{\mu_{off}(1 - f_{on})}, \tag{3.1}$$

SIM	Model version	Inference parameters	Abbr.
Null (no SIM)	without diff. mutant fitness	μ_0	N_0
	with diff. mutant fitness (constrained)	μ_0, ρ_0	N_1
Homogeneous	without diff. mutant fitness	μ_0, μ_s	HOM_0
	with diff. mutant fitness (constrained)	μ_0, μ_s, $\rho_0 = \rho_s$	HOM_1
	with diff. mutant fitness (unconstrained)	μ_0, μ_s, ρ_0, ρ_s	HOM_2
Heterogeneous	zero rel. division rate *on*-cells	μ_{off}, S	HET_0
	non-zero rel. division rate *on*-cells	μ_{off}, S, r_{on}	HET_1
		μ_{off}, S, r_{on}, f_{on}	HET_2

Table 3.3: Models of SIM, subdivided into specific model versions, with a list of parameters inferred in each model version, and the abbreviation for the model version used in section 3.2.4.

which measures how many mutations originate in the response-*on* subpopulation compared to the response-*off* subpopulation. When $r_{on} \neq 0$, we can set r_{on} and f_{on} as inference parameters (in addition to μ_{off} and S) and subsequently calculate μ_{on}, giving in total four inference parameters.

If an estimate for the fraction of response-*on* cells is available from a separate experiment, the mutation rate of response-*on* cells can be calculated even if $r_{on} = 0$. Alternatively, r_{on} can be inferred, with a total of three inference parameters in that case.

In principle, mutants can have a different fitness than non-mutants in our heterogeneous-response model. However, we implemented only the model version with differential mutant fitness set as a fixed value in the inference and not as an inference parameter itself. Since estimates of mutant fitness are not available in the studies analysed here, we set $\rho_{off} = \rho_0 = 1$ here. Under the heterogeneous-response model, we quantify stress-induced mutagenesis either as the specific increase in mutation rate associated with the induction of the stress response, i.e. $\frac{\mu_{on}}{\mu_{off}}$ (in the case of non-zero r_{on} or known f_{on}), or as the mutation-supply ratio S (for $r_{on} = 0$ and f_{on} unknown).

Table 3.3 summarises all inference models and model versions with their respective abbreviations.

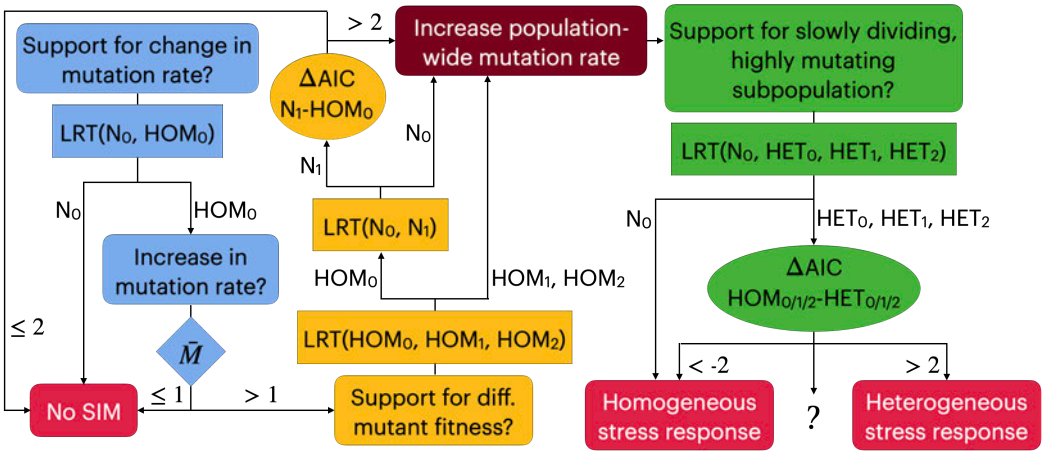

Figure 3.3: Model selection procedure. First, we tested for an increase in mutation rate (blue), followed by tests for differential mutant fitness (yellow). Finally, we compared between homogeneous and heterogeneous stress responses (green).

3.2.4 Model selection

For each experiment (pair of fluctuation assays, antimicrobial-treated compared to untreated condition), we also evaluated which of the above-described models best explains the mutant count data using a multi-step model selection procedure, summarised in Fig 3.3.

Support for SIM: As a first step, we determined whether there is significant evidence for stress-induced mutagenesis. For this purpose, we evaluated first whether there was support for a change in mutation rate due to the antimicrobial, while neglecting any differential mutant fitness, by performing an LRT between the model versions N_0 and HOM_0. If HOM_0 was selected, we checked that the fold-change in mutation rate was indeed greater than one. If yes, we then tested whether there was support for a differential mutant fitness in addition to an increase in mutation rate by performing successive LRTs between the model versions HOM_0, HOM_1 and HOM_2. If either HOM_1 or HOM_2 had significant support in these LRTs, we chose the respective version as the best homogeneous-response model version and classified this as support for SIM.

However, if HOM_0 was selected by the LRTs (no significant support for HOM_1 or HOM_2), we additionally checked whether a differential mutant fitness in the absence of a change in mutation rate could present an alternative explanation by performing an LRT between N_0 and N_1. If this test was significant, i.e. either a differential mutant

fitness (but without a change in mutation rate) *or* an increase in mutation rate (but without differential mutant fitness) could explain the fluctuation assay data, we used the Akaike information criterion (AIC) to select between the scenarios. Here, we cannot use an LRT because these models are not nested. If the difference in AIC between N_1 and HOM_0 was greater than two, we selected HOM_0 as the best homogeneous-response model version with support for SIM. Otherwise, we classified the data as being without significant support for SIM.

Homogeneous vs. heterogeneous response: If we found significant support for SIM, we determined if a homogeneous or heterogeneous stress response better explains this increase in (population-wide) mutation rate. Here, we performed successive LRTs between the model versions N_0, HET_0, HET_1 (if an estimate of f_{on} was available), and HET_2 to determine whether there was support for population heterogeneity in SIM in the form of a highly mutating but slowly dividing response-*on* subpopulation. In the case that there was no such support (N_0 was selected), we classified the data to be better explained by the homogeneous-response model.

On the other hand, if either HET_0 or HET_2 (or HET_1 if applicable) had significant support in these LRTs, we chose the respective version as the best heterogeneous-response model version. Subsequently, we used the AIC to select between the best homogeneous-response model version (as selected previously) and the best heterogeneous-response model version (again, we cannot use an LRT because these models are not nested). If the difference in AIC between the best homogeneous- and the best heterogeneous-response model version was smaller than minus two, we selected the homogeneous-response model; if the difference was greater than two, we selected the heterogeneous-response model. On the other hand, if the absolute difference in AIC was smaller than two, we considered the model selection inconclusive and selected none of the models.

Here, we chose the AIC with a threshold of $|\Delta\text{AIC}| < 2$ as a selection criterion because it provided the best trade-off between false positive and false negative selection of the heterogeneous-response model in our previous simulation study [50]. Arguably, the value of two represents a rather weak threshold. However, we expected the signal of heterogeneity in stress responses to be weak itself and not possible to be picked up at all for a stricter criterion.

3.2.5 estimu: an R tool to ESTimate Increases in MUtation rates

We performed all our analysis using our R tool estimu, available at `https://github.com/LucyL-J/estimu`. Estimation of stress-induced mutagenesis is done via the function

```
estimu(mc_UT, Nf_UT, mc_S, Nf_S, plateff, fit_m=1.,
       f_on=FALSE, rel_div_on=0., mod="selection", criterion="AIC")
```

which takes as input the observed mutant counts mc_UT and final population size Nf_UT of the untreated fluctuation assay and the mutant counts mc_S and final population size Nf_S observed under antimicrobial treatment, as well as the plating efficiency plateff. The differential mutant fitness fit_m, the fraction f_on of the response-*on* subpopulation and the relative division rate r_on of response-*on* cells can be given as additional input if known from separate experiments.

It is possible to estimate parameters under one specific model (“null", “homogeneous", “heterogeneous") or to compare all models and select the best using the above-described multi-step model selection (“selection"). If the differential mutant fitness and/or the relative division rate of the response-*on* cells are specified, the respective input values are fixed during the model selection process. The selection criterion can be changed from “AIC" to “BIC" (the Bayesian information criterion), although we only present results using AIC here.

The estimation function outputs a data frame with maximum-likelihood estimates and 95% confidence intervals of all the model parameters for each model used in the inference, and an additional data frame with log-likelihood, AIC and BIC values and the results of the model selection procedure if applicable.

Example: Input the observed mutant counts, final population sizes and plating efficiency.

```
mc_UT <- c(80, 0, 9, 3, 11, 0, 0, 1, 0, 3, 5, 1, 1, 2, 0, 0, 1)
Nf_UT <- 1E09
mc_S <- c(10, 2, 4, 0, 0, 0, 0, 1, 1, 2, 1, 1, 0, 2, 1, 0, 1)
Nf_S <- 1.6E08
plateff <- 1
```

Performing model selection between all models via executing the ‘estimu’ function with the option mod=“selection"

```
[1] "Model used for inference: Heterogeneous (zero division rate on-cells)"
[[1]]
                      parameter condition           status          MLE  lower_bound  upper_bound
1       Mutation rate off-cells      UT+S jointly inferred 1.032803e-09 5.678150e-10 1.681530e-09
2                Mutant fitness        UT     set to input 1.000000e+00 1.000000e+00 1.000000e+00
3                Mutant fitness         S     set to input 1.000000e+00 1.000000e+00 1.000000e+00
4         Mutation-supply ratio         S         inferred 4.880225e+00 1.690687e+00 1.179641e+01
5        Mutation rate on-cells         S calc. from 1,4&6 9.576595e-08 4.129363e-08 1.688635e-07
6             Fraction on-cells         S     set to input 5.000000e-02 5.000000e-02 5.000000e-02
7   Rel. division rate on-cells         S     set to input 0.000000e+00 0.000000e+00 0.000000e+00
8   Rel. mutation rate on-cells         S   calc. from 4&6 9.272428e+01 3.212305e+01 2.241318e+02
9 Fold change mean mutation rate      S/UT   calc. from 4&6 5.586214e+00 2.556153e+00 1.215659e+01

[[2]]
                                    model selection_result       LL      AIC      BIC
1 Heterogeneous (zero division rate on-cells)               - -69.44947 142.8989 145.9517
```

Figure 3.4: Output of the estimation function 'estimu' in R. In this example, the model used in the inference is the heterogeneous-response model with a relative division rate of response-*on* cells set to zero (the default) and a fraction of response-*on* cells set to the fixed value $f_{on} = 0.05$ in the inference. The first output data frame gives information about the model parameters: to which condition they apply (untreated (UT) or stressed (S), or a combination of the two), and whether they are set to a fixed value, inferred or calculated from other parameters. For the inferred parameters, the maximum likelihood estimate and lower/upper bound of 95% confidence intervals are returned. The second output data frame contains the log-likelihood (LL) of the model, as well as AIC and BIC values.

```
estimu(mc_UT, Nf_UT, mc_S, Nf_S, plateff, mod="selection", criterion="AIC")
"Significant support for SIM"
"Selected model: Heterogeneous (zero division rate on-cells)"
"Estimated parameters under all models are:"
    ...
```

prints the model selection result and returns the estimated parameters under all the models used in the process (not shown here).

Moreover, model parameters can be input as fixed values if they are known from a separate experiment. In this example, parameters are estimated specifically under the heterogeneous-response model for a fixed fraction of the response-*on* subpopulation given by 5%,

```
estimu(mc_UT, Nf_UT, mc_S, Nf_S, plateff, mod="heterogeneous", f_on=0.05)
"Model used for inference: Heterogeneous (zero division rate on-cells)"
...
```

which prints the model used in the inference and returns the estimated parameters, log-likelihood, AIC and BIC values (Fig 3.4).

Detailed information can be found in the **README** at `https://github.com/LucyL-J/estimu`.

3.3 Results

We re-analysed published fluctuation assay data from 11 studies that tested whether antimicrobial treatment changes the mutation rate [3, 10, 14, 15, 25, 30, 34, 37, 60, 65, 68, 71]. To begin with, we applied inference models without heterogeneity in stress responses, as they have been used in any previous study of stress-induced mutagenesis (SIM). The change in (population-wide) mutation rate due to stress estimated under these models is similar to the change in population-mean mutation rate even if the stress response was actually heterogeneous [50]. Here, we quantified the confidence intervals around the estimated fold-change in mutation rate under stress and tested whether it was significantly greater than one, indicating statistical support for SIM (section 3.3.1), which had been missing in most previous analyses. Moreover, we evaluated whether the antimicrobial target is associated with the magnitude of the increase by comparing antimicrobials targeting DNA or DNA gyrase with ribosome-targeting ones (section 3.3.2). For subsequent analyses, we narrowed the experiments down to the cases that statistically support SIM. Using one of these experiments (treatment with the DNA-damaging antibiotic norfloxacin) as an example, we applied and compared estimation results of homogeneous- and heterogeneous-response models in detail (section 3.3.3). We also assessed whether models of homogeneous or heterogeneous stress responses best explain the data for the remaining experiments with significant support for SIM (section 3.3.4). For all our analyses, we neglect the potential effect of cell death, which could, however, be relevant under stressful conditions.

3.3.1 Not all experiments that estimate an increase in mutation rate significantly support SIM

First, we estimated the fold-change in population-wide mutation rate for all 77 experiments, using a model of homogeneous stress responses without differential mutant fitness (model version HOM_0, see Table 3.3). As we have shown in our previous work, this estimate accurately reflects the change in the population-mean mutation rate (except for a slight underestimation of at most around 20%) even if stress responses were actually heterogeneous.

In 56 out of 77 experiments, the population-wide mutation rate was estimated to increase under the antimicrobial treatment compared to untreated (maximum-likelihood estimate $\bar{M} > 1$, dots in Fig 3.5, top). This result is consistent with [71], who analysed 53 of the 77 shown experiments already in this regard. In their analysis, the authors found an increase in mutation rate in 41 out of these 53 experiments, as well as in 19 out of 24 other experiments that we did not consider here. They concluded that antibiotic treatment led to a systematic increase in mutation rate. However, the authors reported only maximum-likelihood estimates without calculating confidence intervals or testing for significance.

We calculated 95% confidence intervals around the estimated fold-change in population-wide mutation rate using a profile likelihood approach and found that, in some cases, they span several orders of magnitude (error bars in Fig 3.5, top). A linear model indicated that the experimental design could be responsible. In particular, a small plating efficiency caused significantly wider CIs (Appendix Fig B.1).

Moreover, not all experiments with a maximum-likelihood estimate $\bar{M} > 1$ actually significantly support the hypothesis of SIM. Applying model selection using likelihood-ratio tests and the AIC (see section 3.2.4 for details), we tested whether an increase in mutation rate explains the data significantly better than our null hypothesis of no change in mutation rate. We also considered a differential mutant fitness, i.e. mutants having a different fitness than non-mutants, as an alternative explanation for the observed mutant count data. Interestingly, we found that only 34 out of the 56 experiments with an estimated $\bar{M} > 1$ showed significant support for an increased population-wide mutation rate compared to the null model (Fig 3.5, bottom).

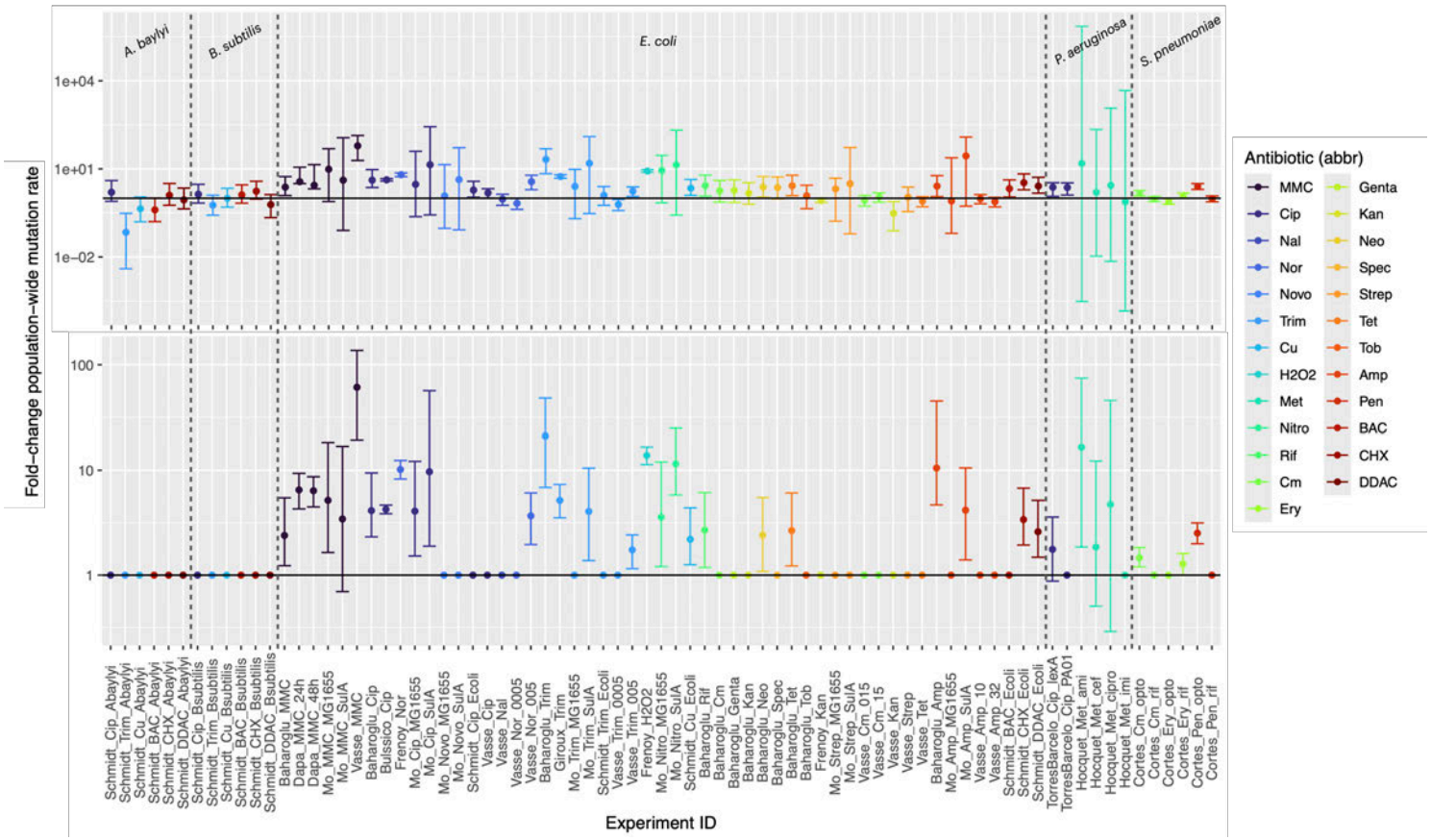

Figure 3.5: Estimated fold-change in mutation rate under antimicrobial treatment for all re-analysed experiments. For each experiment (uniquely identified by their ID, see section 3.2.1 and Table 3.2), the maximum-likelihood estimate of the population-wide mutation rate $\bar{M}$ with the 95% profile likelihood confidence intervals are shown. The model used in the inference is the homogeneous-response model without differential mutant fitness, HOM_0 (top), and the best homogeneous-response model in the case of support for SIM according to our model selection procedure (bottom).

Notably, the experiments with significant support for SIM might still include false positives. A statistical analysis of which factors impact the detection of SIM (generalised linear mixed model in Appendix Eq B.2) indicated that the odds of detecting SIM are higher when using fewer parallel cultures (Appendix Fig B.2).

Our observation emphasises the importance of uncertainty quantification. Even though previous authors concluded broad support for SIM, the evidence might not be statistically significant in many cases, and prone to false positives when few parallel cultures are used.

3.3.2 Antimicrobials directly targeting DNA or DNA-gyrase increase mutation rates

Due to differences in mode of action, we expect that certain antimicrobials have the potential to increase mutation rates while others might not. We classified antimicrobials according to their target (see section 3.2.1). Out of all the antimicrobials studied, four directly target DNA or DNA-gyrase: ciprofloxacin, mitomycin, nalidixic acid and norfloxacin. We expected that these antimicrobials could increase the mutation rate because they directly cause DNA damage. We compared these antimicrobials with those targeting the ribosome: chloramphenicol, erythromycin, gentamicin, kanamycin, neomycin, spectinomycin, streptomycin, tetracycline and tobramycin. Ribosome-targeting antibiotics inhibit protein synthesis and do not directly damage DNA; therefore, we do not necessarily expect an increase in mutation rate.

We restricted this analysis to experiments that used the *E. coli* wild-type strains MG1655 or TD2158. The majority of experiments were done on these strains (44 out of 77), and this restriction allowed us to meaningfully compare the estimated values of $\bar{M}$ without having to account for differences in the mechanism of action of antimicrobials or stress responses across different bacterial species or mutant strains. Out of the 44 experiments with wild-type *E. coli* strains, 13 used an antimicrobial directly targeting DNA or DNA gyrase, and 14 used a ribosome-targeting one.

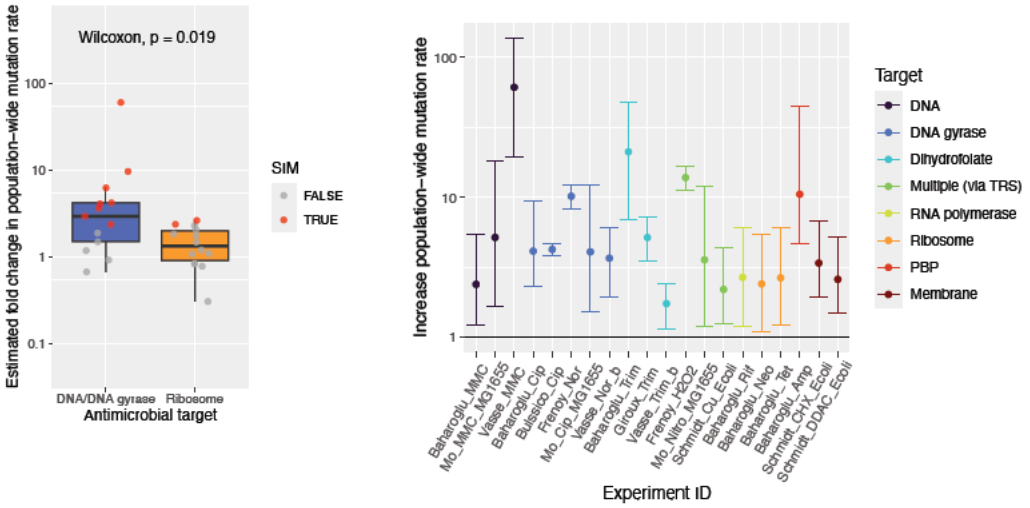

Figure 3.6: Stress-induced mutagenesis is impacted by the antimicrobial target. Fold-change in population-wide mutation rate of DNA/DNA-gyrase compared to ribosome-targeting antibimicrobials in wild-type *E. coli*, estimated under the homogeneous-response model without differential mutant fitness, HOM_0 (left). Red dots corresponds to experiments with significant support for SIM. Estimated increase in population-wide mutation rate for all wild-type *E. coli* experiments with a significant increase in population-wide mutation rate (right). The experiments are sorted by the antimicrobial target. The estimation was done under the best homogeneous-response model according to our model selection procedure.

Comparing these two groups, we observed that the direct DNA/DNA-gyrase targeting antimicrobials led to a significantly larger increase in population-wide mutation rate $\bar{M}$ than ribosome-targeting antimicrobials (Wilcoxon, $p = 0.019$), confirming our hypothesis that the antimicrobial target impacts the change in mutation rate (Fig 3.6, left). The median increase in population-wide mutation rate due to direct DNA/DNA-gyrase targeting antimicrobials was $\bar{M} = 2.97$, compared to $\bar{M} = 1.35$ for ribosome-targeting ones.

We also analysed the 20 experiments on wild-type *E. coli*, which showed significant support for an increased population-wide mutation rate compared to the null model (shown in Fig 3.6, right), regarding the antimicrobial target. In 8 out of 20 cases, the antimicrobial used directly targeted DNA/DNA-gyrase, but in only 2 cases the ribosome. This means that, overall, 62% of the experiments on *E. coli* using directly DNA/DNA-gyrase targeting antimicrobials supported SIM, compared to around 14% of experiments using ribosome-targeting antimicrobials; a significantly lower percent-

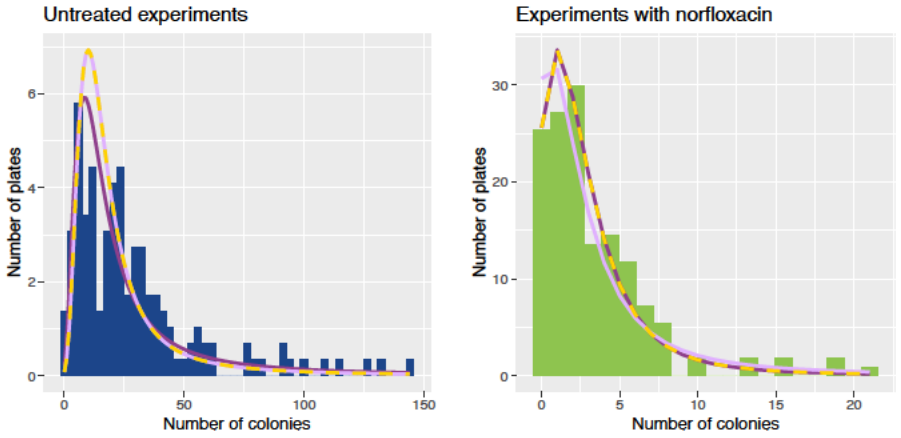

Figure 3.7: Mutant count distributions and model fits for the example experiment using norfloxacin [25]. For the untreated experiments (left) and the experiments with norfloxacin treatment (right), the mutant count distributions show the total number of plates for which a certain number of resistant colonies were counted. The lines are the model fits of the homogeneous-response model without differential mutant fitness, i.e $\rho_0 = \rho_s = 1$ (light violet), of the homogeneous-response model with unconstrained mutant fitness, i.e. ρ_0, ρ_s inferred separately (dark purple), and of the heterogeneous-response model with non-zero relative division rate of response-*on* cells and without differential mutant fitness (yellow).

age (Pearson's Chi-squared test with Yates' continuity correction, p = 0.032). The generalised linear mixed model (Appendix Eq B.2) confirmed these findings: The odds of detecting SIM were significanlty lower for ribosome-targeting antimicrobials than for ones targeting DNA/DNA-gyrase (Appendix Fig B.2).

3.3.3 Comparing estimates under homogeneous and heterogeneous stress responses: example case norfloxacin

As a case study, we delved deeper into one of the experiments with significant SIM, performed by [25]. The authors treated *E. coli* MG1655 populations with $50 ng/mL$ of norfloxacin during the growth phase of the fluctuation assay and subsequently plated $E = 20\%$ of each culture ($c_s = 158$ parallel cultures after pooling biological replicates together) onto selective media with a high rifampicin concentration. In the control assays, cultures ($c_0 = 153$) were grown without treatment before plating $E = 20\%$ on rifampicin plates. The observed mutant count distributions under norfloxacin and untreated conditions are shown as histograms in Fig 3.7.

Norfloxacin is a fluoroquinolone, binding to DNA gyrase and thereby causing DNA damage and inducing the SOS-response in *E. coli*, which is why we expected this experiment to show evidence of SIM. Indeed, using a model of homogeneous stress responses without differential mutant fitness, HOM_0, as in section 3.3.1, we found an estimated increase in population-wide mutation rate (from $\mu_0 = 8.3 \cdot 10^{-9}$ to $\mu_s = 5.26 \cdot 10^{-8}$) of around 6.3-fold within 95% confidence intervals of $[5.3, 7.5]$-fold (model fit shown as light violet lines in Fig 3.7). This model was also preferred when applying a likelihood-ratio test (LRT) over a model without a change in mutation rate, N_0.

Next, we tested whether including a differential mutant fitness, i.e. mutant cells having a different division rate than non-mutant cells, significantly improves the model fit and should be taken into account when estimating the increase in mutation rate. We fitted (i) a model of homogeneous stress responses with differential mutant fitness but constrained to be equal in both the antimicrobial treatment and the untreated experiment, HOM_1, and (ii) a model of homogeneous stress responses with differential mutant fitness without any such constraint, HOM_2. Applying LRTs, we found that the homogeneous model with unconstrained differential mutant fitness, HOM_2, was selected and provided the best explanation of the homogeneous-response models (model fit shown as dark purple lines in Fig 3.7). Under this model, the increase in population-wide mutation rate was estimated to be around 10.2-fold (95% CI: $[7.8, 13.2]$-fold), increasing from $\mu_0 = 6.6 \cdot 10^{-9}$ to $\mu_s = 6.7 \cdot 10^{-8}$. At the same time, the differential mutant fitness was estimated to be $\rho_0 = 1.2$ in the untreated condition, but $\rho_s = 0.74$ for the experiment with added norfloxacin. This latter estimate would imply that mutant cells, in this case carrying rifampicin resistance, are 20% fitter than non-mutant cells when growing in LB but are 25% less fit when growing in the presence of norfloxacin, resulting in a mutant fitness ratio of $\frac{\rho_s}{\rho_0} = 0.62$ (95% CI: $[0.5, 0.76]$). As we showed in our previous work [50], a large discrepancy in differential mutant fitness between conditions estimated under this model can instead be an indicator of heterogeneity in stress responses and, hence, mutation rates.

Therefore, we also fitted models of heterogeneous stress responses (see 3.2.2 for details) to the mutant count data. We found that a model where the highly-mutating response-*on* subpopulation has a low but non-zero division rate, HET_2 (model fit shown as a yellow line in Fig 3.7), explains the data best out of the two considered heterogeneous-response models, HET_0 and HET_2. These characteristics, a high mutation rate coupled with a low division rate, are consistent with induction of the DNA-damage response (SOS response) in *E. coli*. Under this model, the mutation rate of

response-*off* cells was estimated as $\mu_{off} = 8.3 \cdot 10^{-9}$, which closely matches the estimate under the homogeneous-response model of the mutation rate in the untreated experiment. For the fluctuation assay with added norfloxacin, the mutation-supply ratio was estimated to be around $S = 30$ (95% CI: $[21, 68]$), implying that the response-*on* subpopulation contributes almost 30-times as many mutations as the rest of the population.

We cannot precisely infer the fraction of response-*on* cells (f_{on}) due to unidentifiability (implying that the 95% confidence intervals span the whole range $0 \leq f_{on} \leq 1$). Nonetheless, we can consider plausible values for f_{on} and calculate the resulting increase in mutation rate specific to the induction of the stress response, $\frac{\mu_{on}}{\mu_{off}}$. If the fraction of response-*on* cells was around $f_{on} = 64\%$, as estimated for *E. coli* exposed to ciprofloxacin at $10 ng/mL$ [10], the induction of the stress response would lead to an around 16-fold increase in mutation rate. However, if the fraction of the response-*on* subpopulation was smaller, for example, $f_{on} = 5\%$ as observed for *E. coli* exposed to $3 ng/mL$ of ciprofloxacin [38]), the induction of the stress response would lead to an estimated increase in mutation rate of almost 570-fold.

As a final step, we performed model selection between the best homogeneous- and heterogeneous-response models. Using the AIC, we found that the homogeneous-response model with unconstrained differential mutant fitness is clearly selected ($|\Delta\text{AIC}| > 12$). However, when we constrained the differential mutant fitness to be equal under exposure to norfloxacin and untreated, arguably a reasonable null assumption, we found the opposite: the heterogeneous-response model with low non-zero relative division rate of response-*on* cells was selected ($|\Delta\text{AIC}| > 5$).

This example highlights the importance of considering which model is used to estimate mutation rates under antimicrobial treatment and examining whether all estimated parameters are reasonable. If deemed necessary, additional experiments can be performed. For example, fitness assays competing mutants against non-mutants under antimicrobial treatment and untreated conditions can help decide whether the discrepancy in the estimates for ρ_s and ρ_0 is realistic. Alternatively, if a specific stress response is suspected to cause the increase in mutation rate, proteins associated with the induction of the response can be fluorescently labelled and fluorescence microscopy used to check for heterogeneity in the expression of the stress response. An estimate of the fraction of the response-*on* subpopulation, f_{on}, would also allow researchers to accurately estimate the specific increase in mutation rate associated with the induction of the response.

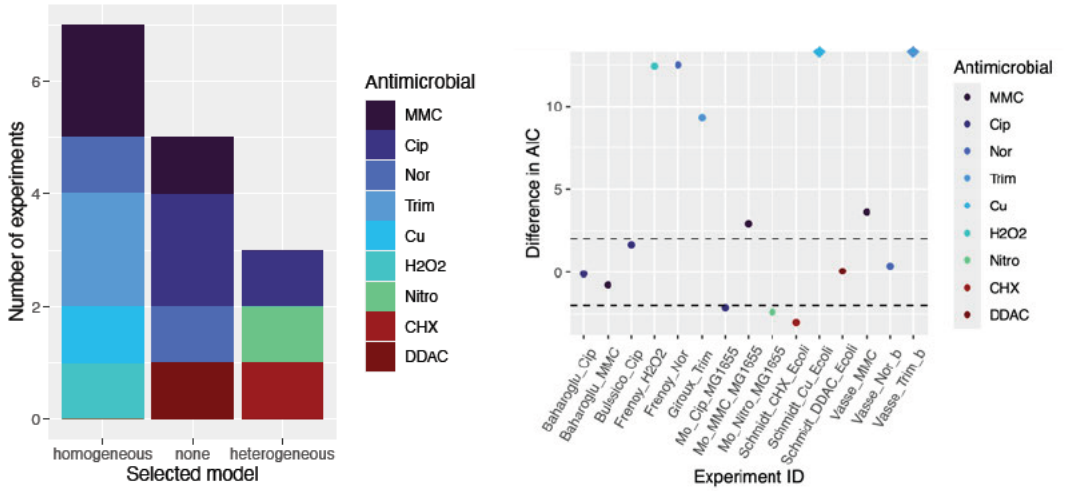

Figure 3.8: Model selection between models of homogeneous and heterogeneous stress responses. Number of experiments for which a homogeneous- or heterogeneous-response model or none was selected (left) and the respective differences in AIC (right). $\Delta\text{AIC} > 0$ implies that the homogeneous-response model explained the data better, and $\Delta\text{AIC} < 0$, conversely, that the heterogeneous-response model represented a better explanation. No model is selected if $|\Delta\text{AIC}| < 2$ (within the dashed lines). The cases in which we did not compare AICs (if there was support for the homogeneous-response model compared to the null model but not for the heterogeneous-response model) are shown as diamonds.

3.3.4 Experiments with indications for heterogeneous stress responses

Besides the above-described experiment, we applied the same inference and model selection procedure to the other 15 experiments, for which we found a significant increase in population-wide mutation rate $\bar{M}$ and which used a minimum of $c_s = 3$ parallel cultures. The reason for these requirements is that we had previously found model selection less reliable for smaller increases in mutation rate (as would be the case without a significant increase of $\bar{M}$) and for smaller numbers of parallel cultures [50] and Appendix Fig B.2. We set the precise threshold of $c_s = 3$ because as many as three parameters associated with antimicrobial treatment are inferred by our models.

In 3 out of the 15 experiments meeting these criteria, a model of heterogeneous stress responses was selected. In 5 cases, no model was selected ($|\Delta\text{AIC}| < 2$), and in the remaining 7 cases, a model of homogeneous stress responses better explained the data (Fig 3.8).

The three experiments for which a heterogeneous-response model was selected were ciprofloxacin at $10ng/mL$ and nitrofurantoin at $2\mu g/mL$ [60], and the disinfectant chlorhexidine digluconate at $12ng/mL$ [65].

Ciprofloxacin is a fluoroquinolone and is expected to induce the SOS response in *E. coli*, in accordance with our results. On the other hand, nitrofurantoin has an unclear mechanism of action, but it potentially targets multiple sites, including DNA, by generating reactive nitrogen species. Our results could suggest that nitrofurantoin also results in the induction of the SOS response (or another mutagenic stress response that simultaneously reduces the division rate of a cell) in a heterogeneous manner within the bacterial population.

Chlorhexidine digluconate is a disinfectant, and the concentration used resembles concentrations found in the environment [65]. In addition to estimating mutation rates using fluctuation assays, the authors of the study [65] also measured SOS-response expression. They found that the SOS response is indeed induced for chlorhexidine digluconate. However, the mechanism of action of the antimicrobial is disrupting the cell membrane, causing cell death. None of the population dynamics models we used considers cell death, which might interfere with the model selection process.

The five experiments for which no model was selected were ciprofloxacin at $50ng/mL$ and mitomycin at an unknown concentration [3], ciprofloxacin at $10ng/mL$ [10], didecyldimethylammoniumchlorid at $2ng/mL$ [65], and norfloxacin at $50ng/mL$ [71]. All of these antimicrobials either target DNA (mitomycin) or DNA gyrase (ciprofloxacin and norfloxacin) or are disinfectants that have been found to induce the SOS response (didecyldimethylammoniumchlorid), just as the three antimicrobials for which the heterogeneous-response model was selected.

As described in the previous section, a discrepancy in the estimated values for the differential mutant fitness, $\rho_s \ll \rho_0$, can be an indicator for heterogeneous stress responses as well. We also found $\rho_s \ll \rho_0$ to be the case for one other experiment, performed within the same study as our example experiment from the previous section 3.3.3 [25]: treating *E. coli* MG1655 with $34ng/mL$ of H_2O_2. This result could hint towards H_2O_2 also causing DNA damage and inducing the SOS response in a small subpopulation of cells. Notably, for the third antimicrobial tested in the study, kanamycin (which targets the ribosome), we found no statistical evidence for stress-induced mutagenesis.

Overall, even though the antimicrobials for which the heterogeneous-response model or no model was selected can be connected to the induction of the SOS response, there is no clear clustering between the antimicrobial target and the outcome of the model selection procedure.

3.4 Discussion and conclusions

In recent years, single-cell studies have revealed extensive heterogeneity in stress responses, with some responses being suspected to increase mutation rates [59, 61, 40, 70, 69, 74, 62, 39, 73, 38, 13]. In our previous work, we proposed a population dynamic model that allows us to quantify stress-induced mutagenesis (SIM) under heterogeneous stress responses from fluctuation assay data [50]. In this work, we made relevant extensions to our model, particularly allowing for partial plating of cultures, and applied our estimation method to published experimental data [3, 10, 14, 15, 25, 30, 34, 37, 60, 65, 68, 71].

In the first section 3.3.1, we applied inference models without heterogeneity in stress responses as they have been used in previous analyses. In 56 out of the 77 re-analysed experiments, we found an increase in the maximum likelihood estimate of the population-wide mutation rate $\bar{M}$. In previous studies, such an increase in $\bar{M}$ would often have been taken as evidence for SIM. However, we showed that many (22 out of 56) claimed cases of SIM actually do not have significant statistical support. We also found that the experimental design, in particular the plating efficiency (an easy-to-optimise experimental parameter), impacts the precision of the estimates and that using few parallel cultures might increase the risk of false positive detection of SIM (Appendix B.2). Researchers should take this into account when planning and analysing fluctuation assays. For example, the recently published estimation tool mlemur [51] has a useful option to calculate the necessary number of parallel cultures for a desired statistical power to detect differences in mutation rates between two conditions (corresponding to untreated versus stressed in the case of SIM).

The motivation for our analysis in the next section 3.3.2 was our intuition that SIM is most likely due to faulty DNA-damage repair. We chose to compare antimicrobials expected to cause DNA damage (antimicrobials targeting DNA or DNA gyrase), with ones that do not (ribosome-targeting antimicrobials). We confirmed that the first group increased mutation rates significantly more than the latter. This statement held when

(i) simply comparing the magnitude of the fold-change in population-wide mutation rate $\bar{M}$ under antimicrobial treatment, and (ii) comparing the percentage of cases with statistical evidence for an increase in $\bar{M}$. Overall, this could imply that the risk of emergence of resistance mutations is increased only for certain groups of antimicrobials. Arguably, most antimicrobials (such as trimethoprim [30]) will ultimately generate toxic reactive species and cause all sorts of damage inside a bacterial cell, including DNA damage. This appears to be the case particularly for disinfectants, even at low concentrations as found in the environment. Indeed, a recent study found that such disinfectants induce the SOS response in *E. coli* [65]. For other antimicrobials, however, the amount of DNA damage at low concentrations might be small.

In sections 3.3.3 and 3.3.4, we identified potential cases of heterogeneous stress responses using model selection. Most of the antimicrobials for which the heterogeneous-response model or no model was selected were DNA-damaging (either antimicrobials directly targeting DNA or DNA gyrase, or disinfectants causing various damage to bacterial cells). For some of these antimicrobials, the expression of SOS response was measured in addition to mutation rates [3, 10, 65], but these are rough estimates. It would be interesting to perform further experiments to get a more precise estimate of the fraction of response-*on* cells, as this would allow us to estimate the specific increase in mutation rate associated with induction of the response.

Moreover, for many antimicrobials that we know are DNA-damaging, no significant increase in mutation rate was detected or if so, the homogeneous-response model was selected. For example, for one of the experiments using the fluoroquinolone norfloxacin [25] considered in detail in section 3.3.3, the homogeneous-response model was selected. However, the differential mutant fitness in the stressed condition was estimated to be much smaller than in the untreated control, which can also be an indicator of heterogeneity in stress responses [50].

Another factor influencing the model selection result could be the antibiotic concentration that was used. A very low concentration might cause an increased mutation rate that is too small to be picked up. For example, in one study [65], ciprofloxacin was used at very low concentrations of $0.6\,\frac{ng}{mL}$ (0.2% MIC), and no SIM was detected, even though the study showed that the SOS response was induced. Another study tested some antimicrobials at two different concentrations [71]. For norfloxacin at $5ng/mL$, no SIM was detected, whereas at $50ng/mL$, the population-wide mutation rate increased significantly, but homogeneous- and heterogeneous-response models could not be distinguished. Moreover, our statistical analysis (Appendix Eq B.2) indicated

that the chance of detecting SIM increased significantly with increasing antimicrobial concentration (Appendix Fig B.2). Further research could investigate how the increase in population-wide mutation rate generally depends on the antimicrobial concentration for a given stress response.

In general, we know from our previous work that a sufficiently large number of parallel cultures is required to perform effective model selection between different models of SIM [50]. Future work could quantitatively address the question of how many cultures are required to distinguish homogeneous and heterogeneous stress responses, similar to the power analysis method implemented in the aforementioned estimation tool mlemur [51].

In all our analyses, we assumed that the different models, or at least one of the null/homogeneous/heterogeneous-response models, can explain the observed fluctuation assay data reasonably well. However, the complex population dynamics under stress might not be adequately captured by any of the models. Therefore, an important next step would be to implement a goodness-of-fit test to evaluate whether a model is appropriate. Alternatively, models would need to be extended, for example, by cell death or time-dependent growth rates (to describe stationary phase dynamics) [25, 58]. Due to small sample sizes in fluctuation assay data, a χ^2-goodness-o-fit test as implemented in [29] is likely not suitable. Instead, a simulation-based approach would be required, but this is outside the scope of this work.

In summary, we have demonstrated that our previously introduced computational method to estimate mutation rates under heterogeneous stress responses is readily applicable to experimental data. As we predicted, model selection using fluctuation assay data alone is often inconclusive, but can be improved by better experimental design and follow-up experiments. Finally, we encourage researchers carrying out future experiments to apply our estimation method, which we converted into a usable R-tool freely available at `https://github.com/LucyL-J/estimu`.

Chapter 4

Modelling how stress-induced mutagenesis depends on the antibiotic dose and mode of action

4.1 Motivation

Antimicrobials at widely varying concentrations can be found in many places, such as sewage, soil, or humans/livestock after antibiotic treatment. Exposure to antimicrobials induces stress responses in bacteria and can increase mutation rates, called stress-induced mutagenesis (SIM). In the previous chapter, we re-analysed published fluctuation assay data from studies that quantify the magnitude of SIM in bacteria exposed to low-dose antimicrobials [3, 10, 14, 15, 25, 30, 34, 60, 65, 68, 71].

One of these studies [71] treated wild-type *E. coli* populations with antibiotics at two different concentrations: ampicillin at $1\,\mu g/mL$ and $3.2\,\mu g/mL$, chloramphenicol at $0.15\,\mu g/mL$ and $1.5\,\mu g/mL$, and norfloxacin and trimethoprim at $5\,ng/mL$ and $50\,ng/mL$. We identified a significant increase in mutation rate for norfloxacin and trimethoprim compared to the untreated control populations, but only at the higher concentration used. This indicates that the antibiotic concentration impacts SIM, potentially having a stronger effect at higher doses.

In another study, which we did not analyse in the previous chapter due to the unavailability of raw data, the authors estimated the increase in mutation rate explicitly depending on the concentration of ciprofloxacin [62] (to our knowledge, the only study measuring the increase in mutation rate across the antibiotic concentration for > 2 concentrations within the same experimental system). Using fluctuation assays, they estimated the mutation rate of untreated *E. coli* MG1655 populations and compared it to the mutation rate under ciprofloxacin treatment of concentrations ranging from

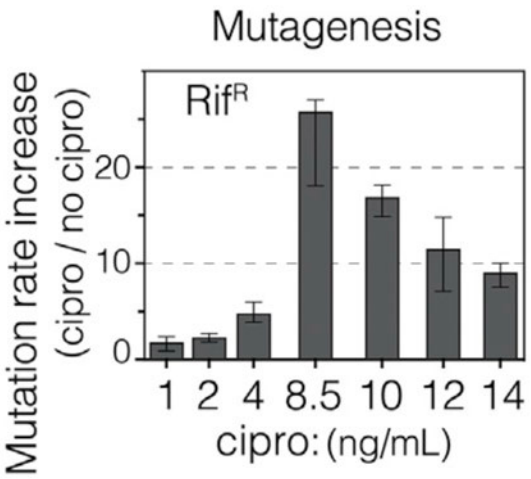

Figure 4.1: Increase in population-wide mutation rate for different ciprofloxacin concentrations [62]. The authors estimated the mutation rate to rifampicin resistance using fluctuation assays; with ciprofloxacin at various concentrations added to the media during the growth phase. Bars show the fold-change in (population-wide) mutation rate compared to the no-ciprofloxacin treatment, with error bars giving the standard deviation across biological replicates. Reprinted from [62] with permission from Elsevier.

$C = 1\,ng/mL$ to $C = 14\,ng/mL$ (MIC = $12\,ng/mL$). The authors found that the increase in mutation rate strongly increased between the concentrations of $C = 4\,ng/mL$ and $C = 8.5\,ng/mL$, that it was maximal for the latter and that it dropped off again at higher concentrations (Fig 4.1). $C = 8.5\,ng/mL$ was their observed minimum antibiotic concentration (MAC), defined as the concentration for which the population growth drops to 10%.

At the same time, the authors linked the increase in mutation rate to the expression of stress responses [62]. They also showed extensive heterogeneity in the expression of these stress responses but ignored this heterogeneity when estimating mutation rates. Our previous work showed that when ignoring heterogeneity in mutagenic stress responses, an accurate estimate of the *population-mean* mutation rate is recovered [50]. In light of these results, the non-monotonic dose-dependence observed (Fig 4.1) could reflect a change in the expression pattern of stress responses across the bacterial population, even for a concentration-independent increase in mutation rate associated with the induction of the response.

In this chapter, I mathematically explore the dose dependence of the increase in population-mean mutation rate caused by a heterogeneously expressed stress response to an antibiotic stressor. I extend our population dynamic model [50] to include the dependence of the population growth and stress-response induction on the antibiotic concentration. Ultimately, I compare different model versions based on bacteriostatic/cidal antibiotics qualitatively and quantitatively with the results observed by [62].

4.2 Model and methods

I use the population dynamic model of heterogeneous stress responses introduced in our previous work [50], which was, in turn, based on [38]. This model is motivated by the DNA damage response (SOS response) in *E. coli* and assumes that the response is induced heterogeneously among cells. This results in a highly mutating and slowly dividing subpopulation with response switched *on*. The dynamics are modelled using coupled differential equations, deterministically describing division (at rates γ_{off}, γ_{on} with $\gamma_{on} \ll \gamma_{off}$) and death (at rates δ_{off}, δ_{on}) in the response-*off* and response-*on* subpopulations, respectively; and switching from response-*off* to *on* state (at rate α):

$$\begin{cases} \dot{n}_{off} = (\gamma_{off} - \delta_{off} - \alpha) n_{off} \\ \dot{n}_{on} = \alpha n_{off} + (\gamma_{on} - \delta_{on}) n_{on}. \end{cases} \tag{4.1}$$

The solution to these equations is given by

$$\begin{cases} n_{off}(t) = n_{off}(0) \mathrm{e}^{(\gamma_{off} - \delta_{off} - \alpha)t} \\ n_{on}(t) = \frac{\alpha n_{off}(0)}{\gamma_{off} - \delta_{off} - \alpha - (\gamma_{on} - \delta_{on})} \left(\mathrm{e}^{(\gamma_{off} - \delta_{off} - \alpha)t} - \mathrm{e}^{(\gamma_{on} - \delta_{on})t} \right) + n_{on}(0) \mathrm{e}^{(\gamma_{on} - \delta_{on})t}, \end{cases} \tag{4.2}$$

with time $t = 0$ marking the onset of the stress. For $\gamma_{on} - \delta_{on} \ll \gamma_{off} - \delta_{off} - \alpha$ and $n_{on}(0) \ll n_{off}(0)$, i.e. when the relative fitness of response-*on* cells is small and only very few cells have the response switched *on* in the absence of stress, the population size of the response-*on* subpopulation can be approximated as

$$\hat{n}_{on}(t) = \frac{\alpha n_{off}(0)}{\gamma_{off} - \delta_{off} - \alpha - (\gamma_{on} - \delta_{on})} \mathrm{e}^{(\gamma_{off} - \delta_{off} - \alpha)t}. \tag{4.3}$$

In this case, the total population grows exponentially with a population growth rate of

$$\lambda = \gamma_{off} - \delta_{off} - \alpha. \tag{4.4}$$

In our model, mutations occur according to time-inhomogeneous Poisson processes with rates $n_{off}(t)\mu_{off}$ and $n_{on}(t)\mu_{on}$, respectively, where the mutation rate of response-*on* cells is assumed to be higher than of response-*off* cells, $\mu_{on} > \mu_{off}$. Importantly, we assume that, even though the division rate of response-*off* cells might be affected by the antibiotic, the *per-division* mutation rate μ_{off} is constant with respect to the antibiotic concentration. Moreover, we assume that the mutation rate of response-*on* cells is an inherent property of the stress response and, therefore, constant.

In [50], we also described the (stochastic) dynamics of mutant cells, but here, I am only interested in the deterministic quantity of the (relative) increase in population-mean mutation rate. Previously, we had defined this quantity as

$$\bar{M} := \frac{f^*_{on}\mu_{on} + (1 - f^*_{on})\mu_{off}}{\mu_{off}} \tag{4.5}$$

with f^*_{on} being the stationary fraction of response-*on* cells,

$$\begin{aligned} f^*_{on} &= \lim_{t\to\infty} \frac{n_{on}(t)}{n_{on}(t) + n_{off}(t)} \\ &= \begin{cases} \frac{\alpha}{\gamma_{off} - \delta_{off} - (\gamma_{on} - \delta_{on})}, & \text{if } \gamma_{on} - \delta_{on} < \gamma_{off} - \delta_{off} - \alpha \\ 1, & \text{else} \end{cases}. \end{aligned} \tag{4.6}$$

Here, I want to model the time dynamics in more detail, which is why I define the increase in population-mean mutation rate as a time-dependent variable

$$\bar{M}_t := \frac{f_{on}(t)\mu_{on} + (1 - f_{on}(t))\mu_{off}}{\mu_{off}} = \left(\frac{\mu_{on}}{\mu_{off}} - 1\right) f_{on}(t) + 1. \tag{4.7}$$

$\bar{M}_t$ describes how much the mutation rate, averaged over the total population, is higher due to the highly mutating subpopulation at a given time. The increase in population-mean mutation rate is proportional to the fraction of response-*on* cells.

The reason why I am interested in calculating $\bar{M}_t$ is that our previous work showed the following: When estimating the increase in mutation rate due to stress using fluctuation assays but neglecting any heterogeneity in stress responses, an accurate estimate of the increase in population-mean mutation rate $\bar{M}_{t_f}$, with t_f being the

duration of the growth phase, is recovered [50]. All studies to date that have estimated the increase in mutation rates due to stress have neglected heterogeneity in stress responses. Therefore, I need to calculate $\bar{M}_{t_f}$ depending on the antibiotic concentration to compare my modelling results with estimates from published fluctuation assay data.

In this chapter, I ask how the increase in the population-mean mutation rate depends on the concentration of an antibiotic that induces a heterogeneous stress response. To answer this question, I model how division, death, and switching rates depend on concentration, directly and indirectly through interdependencies.

4.2.1 Population growth rate: dose-response curve

I describe the dependence of the population growth rate using a dose-response curve. Generally, a dose-response curve describes how a bacterial population reacts, in this case, its growth rate when exposed to a certain dose of an antibiotic. Most dose-response curves share the feature of having a sigmoidal shape with a weak response at low doses, followed by a steeper incline/decline and a phase of flattening off. An example of a sigmoidal function is the three-parameter Hill function of the form

$$\lambda(C) = \frac{\lambda_{\text{max}}}{1 + \left(\frac{C}{\text{IC50}}\right)^h} \tag{4.8}$$

with λ_{max} being the (maximal) growth rate in the absence of the antibiotic, h the Hill coefficient describing the strength of the response and IC50 the concentration at which the population growth rate is halved. Note that for this version of the Hill function, the growth rate goes to zero for high concentrations C instead of negative values, as is the case for the four-parameter version [63]. Since, in a fluctuation assay, the cultures are inoculated at a small population size at the beginning of the growth phase and are treated with sub-MIC concentrations, I do not consider negative growth rates here.

In particular, I use the dose-response curve measured by [16], who exposed *E. coli* MG1655 populations to a range of concentrations of the DNA-damaging antibiotic ciprofloxacin and measured the exponential growth rate. They found a Hill coefficient of $h = 4$ to fit the data best. In this chapter, I will use Eq 4.8 with $h = 4$ to describe the population growth rate as a function of the drug concentration (Fig 4.3, left y-axis, green line).

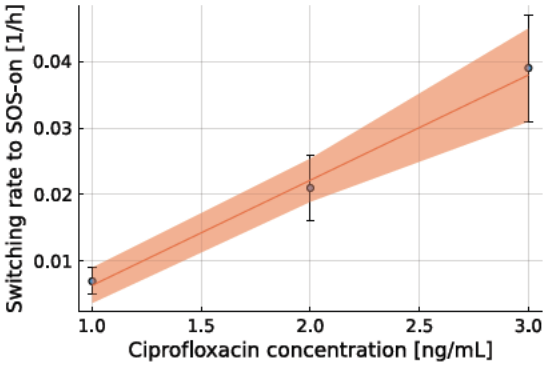

Figure 4.2: Switching rate initially increases with antibiotic concentration. For low concentrations C, the switching rate measured by [38] (blue dots $\pm$ standard deviation) increases linearly with C. I use a linear least squares approach and assume Gaussian measurement error to calculate the mean and standard deviation of the proportionality factor $s = 0.016 \pm 0.004$ (orange line and ribbon).

4.2.2 Switching rate: coupled to cell division

Next, I want to model how the rate at which cells induce the stress response depends on the antibiotic concentration they are exposed to. In fact, the switching rate has been shown to be coupled to the division rate of a cell by recent experiments using single-cell data [38]. The authors performed mother machine experiments on *E. coli* under different nutrient conditions, which allowed the cells to divide differently fast. Interestingly, they found that the rate at which *E. coli* cells induce the SOS response, increases with the division rate of the cells. The authors also exposed the bacteria to low concentrations of ciprofloxacin and, again, found that the switching rate was higher for richer media with a higher division rate. Therefore, I assume

$$\alpha \propto \gamma_{off} \tag{4.9}$$

when the antibiotic concentration C is constant. At the same time, the authors found the switching rate to increase linearly with the antibiotic concentration [38] (at least for low C, Fig 4.2). Using a linear least squares approach, and assuming Gaussian error in the switching rates measured by [38], I obtained the mean and standard deviation of the proportionality factor s (Fig 4.2). Overall, I model the switching rate as

$$\alpha(C) = s\,\gamma_{off} C, \tag{4.10}$$

with $s = 0.016 \pm 0.004$ and Gaussian uncertainty.

Note, however, that the division rate might also depend on the antibiotic concentration, $\gamma_{off}(C)$. Therefore, the dependence of α on C is not necessarily linear for higher C, which I will address later in section 4.2.4.

4.2.3 Division and death rate of response-*on* cells

I define the relative division rate of response-*on* cells as

$$r_{on} = \frac{\gamma_{on}}{\gamma_{off}} \tag{4.11}$$

and assume this value is a constant inherent property of the stress response, just as the mutation rate of response-*on* cells. Without this assumption, on which our whole model is based, exponential growth of the total population would not be given anymore.

For the death rate of response-*on* cells, I consider two scenarios: (i) it is equal to the death rate of response-*off* cells, $\delta(C)_{on} \equiv \delta_{off}(C)$, or (ii) it has a constant, but potentially non-zero value $\delta_{on} \geq 0$.

4.2.4 Antibiotic action: bacteriostatic/cidal?

Finally, I need to model how exactly the antibiotic impacts growth. The population growth rate (Eq 4.4) depends on the division, death and switching rate of response-*off* cells. I consider two extremes here.

Bactericidal antibiotics: In the first case, the antibiotic acts entirely bactericidal, i.e. the reduction in population growth as antibiotic concentration increases is caused by an increased death rate together with switching-*on* of cells. The antibiotic does not impact the division rate of response-*off* cells. Moreover, I assume that the death rate of response-*off* cells in the absence of stress is zero, $\delta_{off}(C = 0) = 0$, yielding

$$\lambda(C) = \lambda_{\max} - \delta_{off}(C) - \alpha(C) \tag{4.12}$$

$$\Rightarrow \delta_{off}(C) = \lambda_{\max}(1 - sC) - \lambda(C), \quad \alpha(C) = s\lambda_{\max}C, \tag{4.13}$$

where the division rate of response-*off* cells is given by the maximal population growth rate (in the absence of stress), $\gamma_{off} = \lambda_{\max}$.

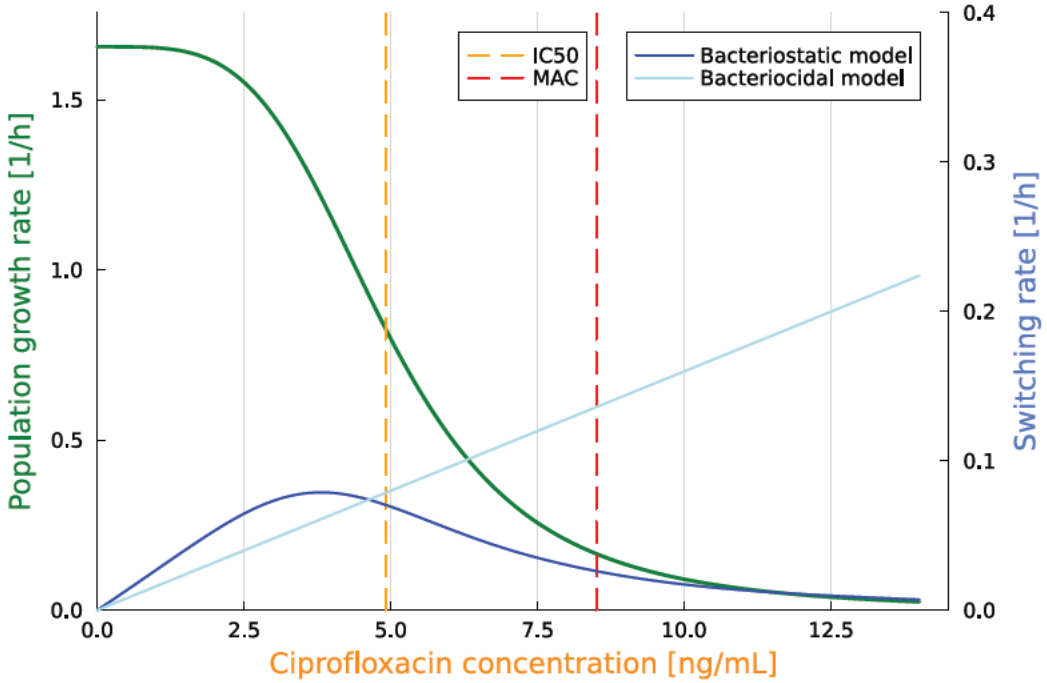

Figure 4.3: Population dynamics depending on the antibiotic concentration C. The population growth rate is assumed to decrease with C according to a Hill function dose-response curve (green line): the growth rate is halved at the IC50 (orange dashed line) and drops to 10% at the MAC (red dashed line). For a purely bacteriostatic antibiotic, the switching rate initially increases with C but decreases again for intermediate C around the IC50 and goes to zero for high C (blue line). The switching rate increases linearly with C (light blue line) for a purely bactericidal antibiotic. Parameters used here are $n_{off}(0) = 10^4$, $\lambda_{\max} = 1.66\,h^{-1}$, IC50 $= 4.9\,ng/mL$, $h = 4$, $s = 0.016 \pm 0.004$, $n_{on}(0) = 1$, $r_{on} = 0$, and $\delta_{off} = 0\,h^{-1}$, $\delta_{on} = 0\,h^{-1}$ in the case of the bacteriostatic antibiotic.

In this case, the switching rate increases linearly with the antibiotic concentration (Eq 4.13, and Fig 4.3, light blue line).

The division rate of response-*on* cells is, as for response-*off* cells, not impacted by the antibiotic and given by

$$\gamma_{on} = r_{on}\lambda_{\max}. \tag{4.14}$$

For the death rate of response-*on* cells, the two cases I consider are: (i) it is equal to the death rate of response-*off* cells,

$$\delta_{on}(C) \equiv \delta_{off}(C) = \lambda_{\max}(1 - sC) - \lambda(C), \tag{4.15}$$

and (ii) it has a concentration-independent value $\delta_{on} \equiv$ const. ≥ 0. The argument for such a simplifying assumption of a constant death rate is that induction of the stress response, in a way, protects the cells from the stressor. Even though the death rate of response-*on* cells might be non-zero, it could be independent of the level of stress.

Bacteriostatic antibiotics: On the other extreme, the antibiotic action is entirely bacteriostatic, i.e. it slows growth but does not cause cell death. Then, the reduction in the population growth rate is due to a reduction in the division rate in response-*off* cells and switching of cells to the response-*on* state. At the same time, the death rate of response-*off* cells remains $\delta_{off} \equiv 0$ (as in the absence of stress), yielding

$$\lambda(C) = \gamma_{off}(C) - \alpha(C, \gamma_{off}(C)) \tag{4.16}$$

$$\Rightarrow \gamma_{off}(C) = \frac{\lambda(C)}{1 - sC}, \quad \alpha(C) = \frac{sC\lambda(C)}{1 - sC}. \tag{4.17}$$

As a consequence, the switching rate $\alpha(C)$ initially increases with the drug concentration for low C but decreases again for intermediate C (Eq 4.17, and Fig 4.3, blue line).

Moreover, since the relative division rate of response-*on* cells is assumed to be constant with respect to antibiotic concentration, the division rate of response-*on* cells is given by

$$\gamma_{on}(C) = r_{on}\gamma_{off}(C) = \frac{r_{on}\lambda(C)}{1 - sC}. \tag{4.18}$$

The death rate of response-*on* cells also remains constant, and I consider both zero and non-zero values.

4.3 Results

I extended our population dynamic model of heterogeneous stress responses [50] to consider how parameters depend on the level of stress, i.e. antibiotic concentration C. I describe the population growth rate using a sigmoidal-shaped dose-response curve and assume the switching rate is coupled to the division rate, as indicated by experiments [38]. For the antibiotic mode of action, I consider two cases: purely bactericidal and purely bacteriostatic.

In the following, I qualitatively evaluate the dependence of the increase in population-mean mutation rate, $\bar{M}_t(C)$, on the antibiotic mode of action and concentration. $\bar{M}_t(C)$ is proportional to the fraction of the response-*on* subpopulation $f_{on}(t)$. However, since the expression for the time-dependent $f_{on}(t)$ does not allow for an intuitive interpretation, I first analytically analyse the dependence of the stationary fraction f_{on}^* on the antibiotic concentration. After that, I numerically explore the relationship between $f_{on}(t)$ and f_{on}^*. Finally, I compare model predictions of $\bar{M}_{t_f}(C)$ quantitatively with experimental estimates [62].

4.3.1 Monotonic increase of the fraction of the response-*on* subpopulation for bactericidal antibiotics

The stationary fraction f_{on}^* depends on the switching rate α and the difference between the net growth rate (defined as division minus death rate) of response-*off* and response-*on* cells, see Eq 4.6. For entirely bactericidal antibiotics, the switching rate increases linearly with the antibiotic concentration (Eq 4.13). Therefore, the stationary fraction of the response-*on* subpopulation increases monotonically with increasing antibiotic concentration, as

$$f_{on}^* = \begin{cases} \frac{sC\lambda_{\max}}{\lambda_{\max}(sC-r_{on})+\delta_{on}(C)+\lambda(C)}, & \text{if } \delta_{on}(C) < \lambda(C) - \lambda_{\max}(sC - r_{on}) \\ 1, & \text{else} \end{cases}. \quad (4.19)$$

However, the strength of the increase depends on the death rate of response-*on* cells. For a concentration-independent death rate $\delta_{on} \geq 0$, the increase in f_{on}^* has a sigmoidal shape with a sharp increase for intermediate C (Fig 4.4, left). The concentration for which the increase changes most sharply (the inflection point) depends on the value of δ_{on}: it is higher for higher δ_{on} (Appendix Fig C.1, left).

Since the response-*on* subpopulation has a very small population size at time $t = 0$, it takes longer to reach the stationary fraction f_{on}^* the larger f_{on}^*. This implies that, for low C, where f_{on}^* is small, the time to reach f_{on}^* is negligible. At the same time, f_{on}^* is reached faster the higher the switching rate. However, for bactericidal antibiotics, f_{on}^* increases so sharply with the antibiotic concentration C that the time to reach f_{on}^* increases for intermediate to high C (Fig 4.4, left).

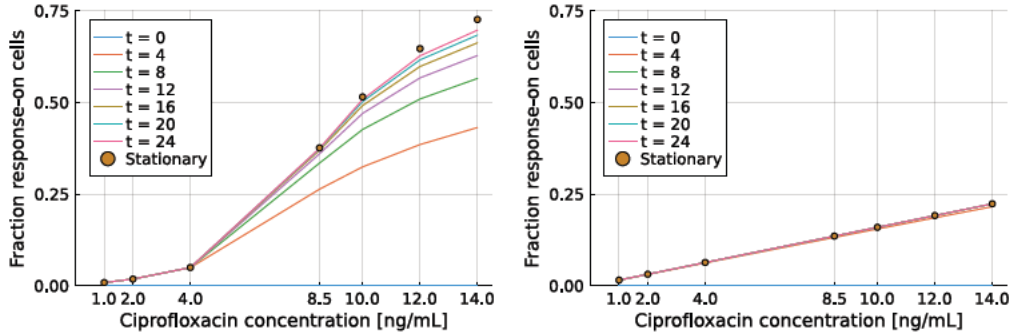

Figure 4.4: Fraction of the response-*on* subpopulation f_{on} depending on the concentration of a bactericidal drug. Left: Concentration-independent death rate of response-*on* cells, $\delta_{on} = 0.06\,h^{-1}$. Right: Response-*on* cells have the same death rate as response-*off* cells, $\delta_{on}(C) = \delta_{off}(C)$. Solid lines give the time-dependent variable, $f_{on}(t)$, and dots the stationary fraction f_{on}^*. Parameters as in Fig 4.3 ($r_{on} = 0$) with exception of δ_{on}.

On the other hand, if response-*on* cells have the same death rate as response-*off* cells (Eq 4.15), the stationary fraction of the response-*on* subpopulation simplifies to

$$f_{on}^* = \frac{sC}{1 - r_{on}}, \tag{4.20}$$

i.e. it increases linearly with the antibiotic concentration (Fig 4.4, right). For $\delta_{on}(C) \equiv \delta_{off}(C)$, the stationary fraction f_{on}^* is smaller than for a concentration-independent $\delta_{on} \equiv$ const., and, therefore, f_{on}^* is reached almost immediately.

Generally, I find that the fraction of the response-*on* subpopulation is slightly larger for a small non-zero relative division rate of response-*on* cells r_{on}, compared to $r_{on} = 0$. Still, the dependencies are unaffected qualitatively (Appendix Fig C.2, top).

4.3.2 Non-monotonic increase of the fraction of the response-*on* subpopulation for bacteriostatic antibiotics

For entirely bacteriostatic antibiotics, the switching rate depends non-monotonically on the antibiotic concentration C (Eq 4.17). For the stationary fraction of response-*on* cells, this implies

$$f_{on}^* = \begin{cases} \frac{sC\lambda(C)}{(1-r_{on})\lambda(C)+(1-sC)\delta_{on}}, & \text{if } \delta_{on} < \frac{r_{on}}{1-sC} - 1 \\ 1, & \text{else} \end{cases}. \tag{4.21}$$

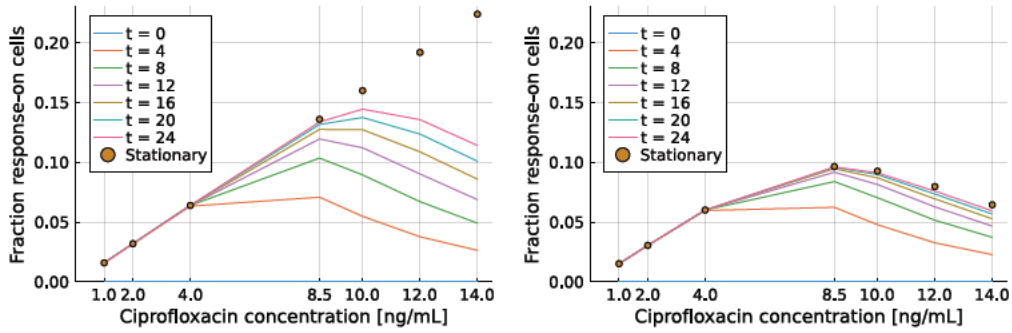

Figure 4.5: Fraction of the response-*on* subpopulation f_{on} depending on the concentration of a bacteriostatic drug. Death rate of response-*on* cells being zero, $\delta_{on} = 0$ (left) or non-zero, $\delta_{on} = 0.08\,h^{-1}$ (right). Solid lines give the time-dependent variable, $f_{on}(t)$, and dots the stationary fraction f_{on}^*. Parameters as in Fig 4.3 ($r_{on} = 0$) with exception of δ_{on}.

Interestingly, the relationship between the stationary fraction f_{on}^* and C depends again on the death rate of response-*on* cells. For $\delta_{on} \equiv 0$, the stationary fraction of the response-*on* subpopulation increases linearly with C as

$$f_{on}^* = \frac{sC}{1 - r_{on}}, \tag{4.22}$$

see Fig 4.5 (left). Notably, this is the same functional relationship as for a bactericidal drug with cell death in response-*on* cells equal to that in response-*off* cells (Eq 4.20). However, different than for bactericidal antibiotics, the time to reach the stationary fraction f_{on}^* is negligible only for low antibiotic concentrations C but increases for intermediate to higher C because the switching goes to zero. This implies that the fraction of the response-*on* subpopulation for finite times (on the order of a couple of hours/days) depends non-monotonically on the antibiotic concentration C (Fig 4.5, left).

Similarly, for $\delta_{on} \equiv \text{const.} > 0$, f_{on}^* increases for low C and decreases again for high C (Fig 4.5, right). The concentration at which f_{on}^* is maximal depends on the magnitude of δ_{on}: it is lower for higher δ_{on} (Appendix Fig C.1, right).

The same applies to the time-dependent fraction of the response-*on* subpopulation, $f_{on}(t)$; it depends non-monotonically on the antibiotic concentration C. The time to reach the stationary fraction f_{on}^* is negligible for low C. For intermediate to high C, f_{on}^* is reached more slowly, but the time to reach f_{on}^* remains roughly constant because both the magnitude of f_{on}^* and of α decrease.

Cell death	Bactericidal		Bacteriostatic	
	Time-dependent $\bar{M}_{t_f}(C)$	Stationary $\bar{M}(C)$	Time-dependent $\bar{M}_{t_f}(C)$	Stationary $\bar{M}(C)$
$\delta_{on} \equiv 0$	-	-	non-monotonic	linear
$\delta_{on} = \text{const.} > 0$	sigmoidal	sigmoidal	non-monotonic	non-monotonic
$\delta_{on}(C) = \delta_{off}(C)$	linear	linear	-	-

Table 4.1: Qualitative dependence of the increase in population-mean mutation rate on the concentration of a bacteriostatic/cidal antibiotic. For the death rate of response-*on* cells, I consider three cases overall: (i) Zero death rate, (ii) concentration-independent non-zero death rate, and (iii) death rate equal to the death rate of response-*off* cells. I evaluate the qualitative dependence of the increase in population-mean mutation rate as a time-dependent (calculated using $f_{on}(t)$) and as a stationary variable (calculated using f^*_{on}) on the concentration of bacteriostatic and -cidal antibiotics.

Again, I find that the fraction of the response-*on* subpopulation is slightly larger for a small non-zero r_{on} than for $r_{on} = 0$, but qualitatively unaffected (Appendix Fig C.2, bottom).

4.3.3 Mode of antibiotic action determines the increase in population-mean mutation rate qualitatively

Recalling that the increase in population-mean mutation rate $\bar{M}_{t_f}(C)$ is proportional to the fraction of the response-*on* subpopulation, these results imply that the dependence of $\bar{M}_{t_f}(C)$ on the antibiotic concentration qualitatively differs between bacteriostatic and bactericidal antibiotics, and depends on whether response-*on* cells have a non-zero or concentration-dependent death rate. For bacteriostatic antibiotics, $\bar{M}_{t_f}(C)$ is maximal for intermediate C, whereas for bactericidal ones, it monotonically increases with increasing C, see Table 4.1 for a summary. In any case, $\bar{M}_t(C)$ increases with time.

4.3.4 Comparison with experimental data

I want to compare my modelling results with the increase in mutation rate observed in experimental estimates by [62]. The authors treated *E. coli* MG1655 populations with ciprofloxacin concentrations ranging from $C = 1\,ng/mL$ to $C = 14\,ng/mL$ (MAC = $8.5\,ng/mL$, MIC = $12\,ng/mL$). Their experimental estimates (Fig 4.1) show a sharp increase of $\bar{M}_{t_f}(C)$ just below the MAC and a maximal value at the MAC. This rela-

tionship (sharp increase, non-monotonic) is qualitatively not consistent with a linear increase. Therefore, I only fit the models of bacteriostatic and -cidal antibiotics with a non-zero but concentration-independent death rate of response-*on* cells to the data. The parameters of the models are:

Informed by separate experimental estimates

- $\lambda_{\text{max}} = 1.66\,h^{-1}$: The (maximal) population growth rate in the absence of stress. Since I do not have an estimate from [62], I use the value estimated by [16], who used the same bacterial strain and LB as growth medium
- $h = 4$: The Hill coefficient of the dose-response curve of the population growth rate, fitted by [16]
- IC50 $= 4.9\,ng/mL$: Calculated from the MAC used in [62] via the dose-response curve (IC50 $= \frac{\text{MAC}}{9^{1/h}}$, see Eq 4.8)
- $s = 0.016 \pm 0.004$: The proportionality factor between the switching rate α and the division rate of response-*off* cells γ_{off} (which I fitted to data from [38] with Gaussian uncertainty; see Fig 4.2)
- $r_{on} \in \{0, 0.1\}$: The relative divsion rate of response-*on* cells compared to response-*off* cells. I consider the two cases that response-*on* cells do not divide at all or at a low relative rate based on estimates by [38]
- $n_{off}(0) = 10^4$: The initial population size of the response-*off* subpopulation; this corresponds to the inoculum size of cultures in the fluctuation assay by [62]
- $n_{on}(0) = 1$: The initial population size of the response-*on* subpopulation, which I assume to be small (consistent with results from [38])
- $t_f = 24\,h$: The duration of the growth phase used by [62]

Fitted to the observed data [62]

- δ_{on}: The concentration-independent death rate of response-*on* cells
- $\frac{\mu_{on}}{\mu_{off}}$: The specific increase in mutation rate associated with the induction of the stress response

I fitted the remaining two parameters, δ_{on} and $\frac{\mu_{on}}{\mu_{off}}$, to the estimated increase in population-wide mutation rate from [62] in the following way.

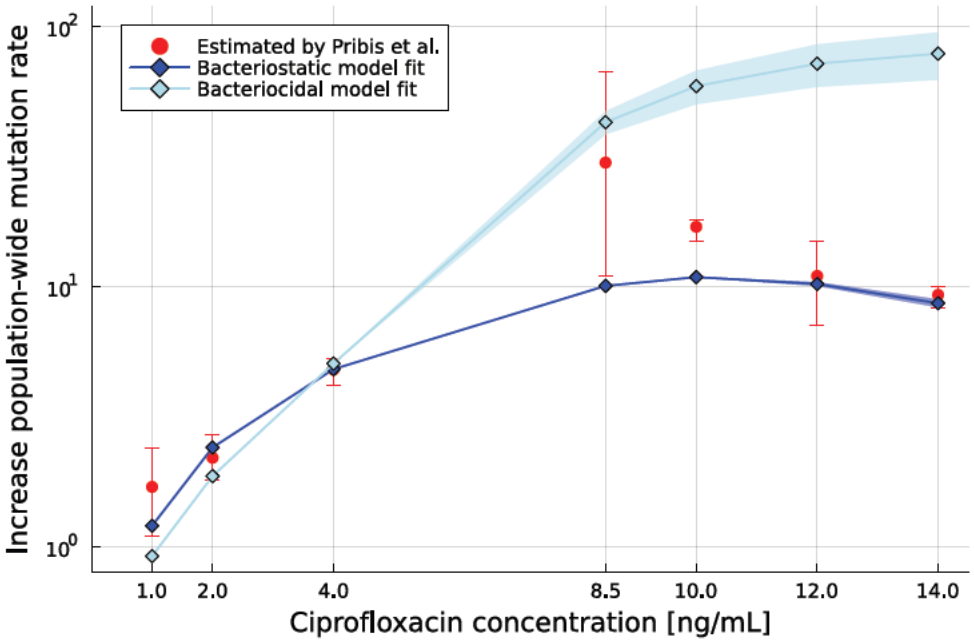

Figure 4.6: Increase in population-mean mutation rate in my bacteriostatic/cidal models fitted to estimates from [62]. The increase in population-mean mutation rate $\bar{M}_{t_f}(C)$ for a bacteriostatic/cidal antibiotic (blue/light blue diamonds), calculated using mostly parameters from the literature ($n_{off}(0) = 10^4$, $\lambda_{\max} = 1.66\,h^{-1}$, IC50 $= 4.9\,ng/mL$, $h = 4$, $s = 0.016 \pm 0.004$, $n_{on}(0) = 1$, $r_{on} = 0$, $t_f = 24\,h$, and $\delta_{off} = 0\,h^{-1}$ in the case of the bacteriostatic model); and fitting the remaining parameters, a concentration-independent death rate of response-*on* cells, $\delta_{on} \equiv 0.00\,h^{-1}$ for $s < 0.012$ and $\delta_{on} \equiv 0.07 \pm 0.05\,h^{-1}$ else (bactericidal) and $\delta_{on} \equiv 0.08 \pm 0.005\,h^{-1}$ (bacteriostatic), and the specific mutation-rate increase associated with the induction of the stress response $\frac{\mu_{on}}{\mu_{off}} = 103 \pm 38$ (bactericidal) and $\frac{\mu_{on}}{\mu_{off}} = 82 \pm 31$ (bacteriostatic), to the data from [62].

Bactericidal antibiotics: For the bactericidal model with concentration-independent cell death in response-*on* cells, I found that the increase in population-mean mutation rate at stationarity $\bar{M}$, increased sharply for intermediate antibiotic concentrations. In particular, the concentration of the inflection point depends on the magnitude of the death rate of response-*on* cells δ_{on} (Appendix Fig C.1, left). The increase in population-wide mutation rate estimated by [62] increased sharply just below the MAC. Therefore, I numerically calculated the value of δ_{on} such that $\bar{M}$ increases most steeply at the MAC.

Bacteriostatic antibiotics: For the bacteriostatic model with concentration-independent cell death in response-*on* cells, on the other hand, I found that $\bar{M}$ is maximal for an intermediate antibiotic concentration C. Thereby, the concentration of maximal $\bar{M}$ depends on the magnitude of the death rate of response-*on* cells δ_{on} (Appendix Fig C.1, right). In [62], the increase in population-wide mutation rate was estimated to depend on the antibiotic concentration non-monotonically with a maximal value at the MAC. Therefore, I numerically calculated δ_{on} such that the maximum $\bar{M}$ is reached at the MAC.

For both the bacteriostatic and -cidal model, I subsequently used a linear least squares approach to fit $\frac{\mu_{on}}{\mu_{off}}$ to the first three data points of $\bar{M}_{t_f}(C)$. The reason I used only the first three points is that, for low C, the fraction of response-*on* cells $f_{on}(t_f)$ increases approximately linearly with C independent of the model version (Figs 4.4 and 4.5). This allowed me to fit the proportionality factor using Eq 4.7 and obtain $\frac{\mu_{on}}{\mu_{off}}$. In contrast, the dependence of $\bar{M}_{t_f}(C)$ on C for higher C differs qualitatively between the model of bactericidal and bacteriostatic antibiotics.

For $r_{on} = 0$, this fitting procedure (using $s = 0.016 \pm 0.004$ with Gaussian uncertainty) resulted in the following parameter values. Bactericidal antibiotic model: $\delta_{on} \equiv 0.00\,h^{-1}$ for $s < 0.012$ (which has a cumulative probability of $\lessapprox 0.15$) and $\delta_{on} \equiv 0.07 \pm 0.05\,h^{-1}$ else, and $\frac{\mu_{on}}{\mu_{off}} = 104 \pm 38$. Bacteriostatic antibiotic model: $\delta_{on} \equiv 0.08 \pm 0.005\,h^{-1}$ and $\frac{\mu_{on}}{\mu_{off}} = 81 \pm 32$. Fig 4.6 shows the resulting increase in population-mean mutation rate.

I found very similar estimates for $r_{on} = 0.1$, but the mutation-rate increase $\frac{\mu_{on}}{\mu_{off}}$ was generally smaller than for $r_{on} = 0$ (Appendix Fig C.3). This agreed with my expectations, as $r_{on} > 0$ results in a larger fraction of the response-*on* subpopulation (Appendix Fig C.2). Therefore, a smaller value for $\frac{\mu_{on}}{\mu_{off}}$ is required to cause the same increase in population-mean mutation rate, see Eq 4.7.

The complete annotated documentation of this computational analysis can be found in the notebook **dose-dependence.ipynb** within the branch **dose-dependence** at `https://github.com/LucyL-J/estimu`.

4.4 Discussion

In this chapter, I modelled the dependence of the increase in population-mean mutation rate, $\bar{M}_{t_f}(C)$, on the antibiotic dose C. As previously shown [50], $\bar{M}_{t_f}(C)$ approximately matches the population-wide mutation rate as it would be estimated from a fluctuation assay (with a growth phase of duration t_f) using a standard inference method. My model consisted of two versions based on a purely bactericidal or purely bacteriostatic antibiotic.

Interestingly, I found that the resulting dependence of $\bar{M}_{t_f}(C)$ on the antibiotic concentration C differs qualitatively: For a purely bactericidal antibiotic, the increase in population-mean mutation rate increases monotonically with C, whereas for a purely bacteriostatic one, it is maximal for an intermediate concentration. In reality, the mode of action of any antibiotic is likely to be concentration-dependent itself. Many antibiotics act bacteriostatically at low concentrations, and most will become bactericidal for high C. Future work could combine the models of bacteriostatic and -cidal antibiotics in a dose-dependent manner.

I compared my modelling results with the estimated mutation rates obtained by [62], who treated *E. coli* MG1655 populations with ciprofloxacin at concentrations ranging from $1\,ng/mL$ to $14\,ng/mL$ (MIC = $12\,ng/mL$). Qualitatively, the model of a purely bacteriostatic antibiotic fits the data better because it can capture the non-monotonic dependence of the increase in population-wide mutation rate on the ciprofloxacin concentration. However, this result crucially relies on the assumption that the switching rate to the response-*on* state is proportional to the division rate of a cell. This model assumption has been shown to hold when nutrient conditions alter the division rate [38], but it might not hold for reductions by antibiotic treatment. Moreover, ciprofloxacin

is a bactericidal drug at intermediate to high concentrations, i.e. acting by causing cell death instead of reducing the division rate. The authors of [62] also quantified cell death at the MAC, confirming that ciprofloxacin acts bactericidally. My bactericidal model cannot explain the decrease of $\bar{M}_{t_f}(C)$ at concentrations above the MAC though.

A potential explanation for this discrepancy could be that my models are limited to the exponential growth phase. In a fluctuation assay, cultures are typically grown overnight (also done by [62]), and cultures reach stationary phase (at around $16h$ for [62]). In fact, the authors quantified the fraction of response-*on* subpopulation f_{on} over time at the MAC [62]. They found that it reaches a maximum at the end of the exponential growth phase but declines afterwards. On the other hand, in my model, f_{on} increases monotonically with time. It would be interesting to model the dynamics during the stationary phase in more detail. However, this would make the model significantly more complex and potentially analytically intractable.

Besides limitations of my model, the estimates of the increase in population-wide mutation rate $\bar{M}_{t_f}$ by [62] might themselves be inaccurate or biased. For example, the authors confirmed the presence of cell death, but neglected it in the estimation of mutation rates, which has been shown to lead to an overestimation of mutation rates [25]. However, the extent of cell death increases with antibiotic concentrations C, so if anything, we would expect the true mutation rates at the highest C to be even lower. Therefore, I do not expect the observation of a non-monotonic dependence $\bar{M}_{t_f}(C)$ to be explainable by the resulting biases of neglecting cell death. Still, the estimates might be less accurate than reported. Moreover, the reported 95% confidence intervals in [62] might underestimate the uncertainty because the authors calculated confidence intervals using the standard deviation of few biological replicates (between two and nine replicates per concentration).

Overall, I showed that simple population dynamic models of response-*off* and response-*on* subpopulations can explain various dose-dependencies of the resulting increase in population-mean mutation rate $\bar{M}_{t_f}(C)$. Notably, in my models, $\bar{M}_{t_f}(C)$ reflects a change in the fraction of the response-*on* subpopulation, and not a change in the intrinsic mutation rates μ_{off} or μ_{on}.

Arguably, the assumption that the mutation rate of response-*on* cells μ_{on} is a (constant) inherent property of the stress response is a strong simplification. In our model, μ_{on} is both time- and concentration-independent. However, a higher antibiotic concentration could lead to not only an increased switching rate but also more DNA

damage in response-*on* cells and, therefore, a higher mutation rate μ_{on}. Moreover, the continued DNA replication in response-*on* cells implies an increasing number of chromosomes inside the cells [62]. The presence of multiple chromosomes allows for enhanced homologous recombination and could lead to an increased rate of insertions, deletions or copy number variations. Consequently, the mutation rate of response-*on* cells could increase with the number of chromosomes, which in turn, depends on how long a cell has been in the response-*on* state. The constant mutation rate μ_{on} in our model should, therefore, be seen as an effective per-cell rate. Future work could model the occurrence of mutations in response-*on* cells in more detail. In particular, models could consider different types of resistance mutations: insertions/deletions and copy number variations occurring in the process of homologous recombination, and point mutations introduced by error-prone polymerases. These mutations are likely to arise at different rates (also depending on the number of chromosomes inside a cell) and confer different resistance levels.

The authors of [62] argue that antibiotic treatment significantly increases mutagenesis below the MIC (Fig 4.1), supposedly driving antibiotic resistance evolution. However, the relevance of measuring the (population-mean) mutation rate is questionable in this context. As argued by [71], the mutation rate does not account for other important ecological factors such as population size. The authors demonstrate that even if antibiotic treatment increases mutation rates, the reduction in population size can cancel out this effect, resulting in no overall increase (or even a decrease) in genetic diversity. If the increase in mutation rate is due to a highly mutating but slowly dividing subpopulation, the resulting genetic diversity would be even lower because most mutant cells divide slowly and could even be outcompeted by faster-growing non-mutant cells. In [71], the authors suggest focusing on metrics such as the total number of mutants (compared to an untreated control condition) as an indicator of evolvability. Interpreting the experimental estimates by [62] and my modelling results using this metric, the observed increase in mutagenesis for sub-MIC concentrations might not actually increase the risk of resistance evolution, and less caution regarding antibiotic dosing as previously thought could be necessary.

Chapter 5

General Discussion

The discussion is considered the least important section of a scientific paper by academics [35]. While undergraduates still value it as important as the results figures and tables (only outdone by the abstract), the discussion loses importance as researchers advance in experience. The focus shifts from general understanding (through abstract and discussion) to a deeper engagement with the raw data (results and methods) [35, 49]. On the other hand, the 'General Discussion' of a PhD thesis differs from the discussion of a scientific paper because it allows for a very personal perspective. I want to take this chance, step back, and look at my PhD as an *interdisciplinary project.*

My PhD project encompasses several scientific fields, both within and outside biology: evolutionary biology, microbiology, cell biology, mathematics, and computer science. My scientific background is in physics and mathematics, where I briefly encountered theoretical evolutionary biology. However, my experience in microbiology and cell biology was virtually non-existent; for example, I had no idea even on which time scale bacteria divide. Hence, I came into these fields blind.

I was lucky to have three supervisors in the fields of theoretical and experimental evolutionary biology (principal supervisor), cell and microbiology (second supervisor), and mathematics (third supervisor). In particular, my first and second supervisors were very engaged in the project, and we met weekly/bi-weekly to discuss. The disparity in disciplines meant that I was expected to attend double the lab meetings, seminars, and workshops, leaving me with less time for my own research (or alternatively, an increased workload).

The interdisciplinarity of my project also led to isolation at times. Again, I was fortunate at least to have a PhD-sibling who started an interdisciplinary PhD in similar fields at the same time as me. There were also initiatives from other PhD students in mathematical biology, such as seminars and reading groups. However, within my institute,

I had few opportunities to engage with peers scientifically, and I experienced the PhD as a solitary endeavour. And it appears I am not alone in this experience generally: Interdisciplinary PhD projects come with a whole set of additional challenges, such as having to ask 'stupid questions' or constantly adjust to different audiences [17], and interdisciplinary PhD students face tensions within monodisciplinary structures due to blurry expectations or confined roles [53].

I was curious whether other interdisciplinary PhD students in my institute felt similarly. Therefore, I conducted a small survey among my peers at the Institute of Ecology and Evolution (IEE), University of Edinburgh. I asked my peers about the scientific fields of their projects, their backgrounds, the interdisciplinary and collaborative methods they applied and how they experienced the interdisciplinary aspect of their PhD.

Interdisciplinary PhD projects in IEE encompass a wide range of fields: botany, chemistry, cell biology, chronobiology, computer science, ecology, epidemiology, evolutionary biology, genetics, immunology, informatics, mathematics, microbiology, physics, sociology, taxonomy and zoology. As expected, I found that all projects included at least one of the fields of ecology or evolutionary biology. Five of the eleven participants in my surveys are doing projects in fields only within biology; the projects of the remaining six include at least one field outside biology (Fig 5.1**A**).

The majority (six) of interdisciplinary PhD students in IEE have a purely biological background, three have a background both within and outside biology, and the background of two is entirely outside biology (Fig 5.1**B**). Moreover, I calculated the overlap (fraction covered) of the scientific fields of the PhD project and the background of the respective PhD student. It appears that students with backgrounds outside biology tend to have a lower overlap (Fig 5.1**C**), but the total number of participants is too small to draw any quantitative conclusions, of course.

Generally, the projects are equally shaped by interdisciplinary questions (for example, measuring bacterial growth curves to find universal growth laws) and approaches (for example, using mathematical modelling to understand collective antibiotic tolerance), see Fig 5.2**A**. However, the projects varied in the types of interdisciplinary collaborations (Fig 5.2**B**). Most students reported exchanging knowledge and ideas with peers $(9/11)$ and discussing with their supervisors from different fields $(8/11)$. Around half participate in lab meetings $(6/11)$ and joint projects $(5/11)$ across different fields. However, in only two cases the PhD led to an interdisciplinary publication, and in one case, none of the interdisciplinary collaborations mentioned above were present. The PhD students in IEE were satisfied with the interdisciplinarity of their projects overall

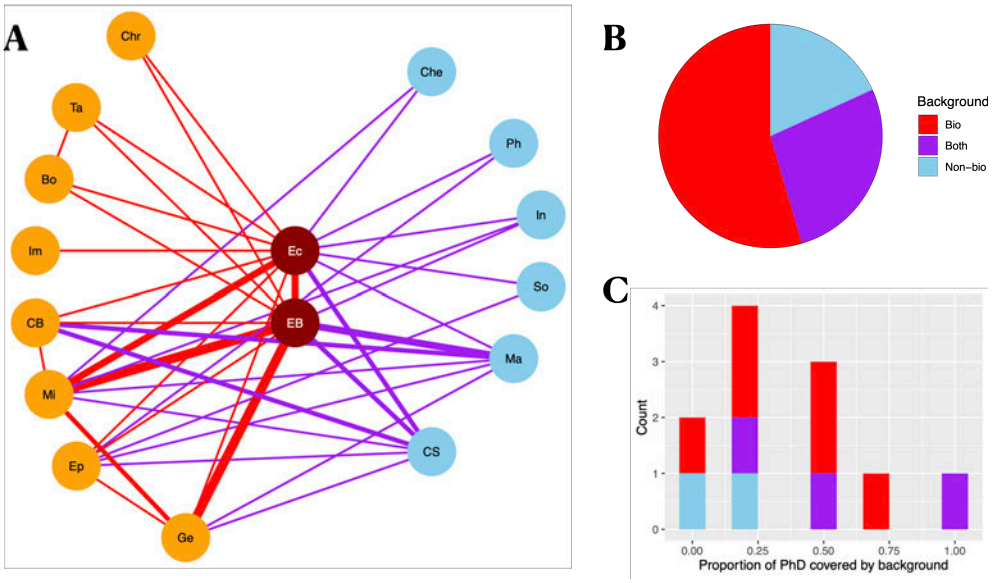

Figure 5.1: Scientific fields of interdisciplinary PhD projects in IEE, background of the respective PhD students and overlap between them. In total, eleven students replied to my survey, doing PhDs in the fields of botany (Bo), chemistry (Che), cell biology (CB), chronobiology (Chr), computer science (CS), ecology (Ec), epidemiology (Ep), evolutionary biology (EB), genetics (Ge), immunology (Im), informatics (In), mathematics (Ma), microbiology (Mi), physics (Ph), sociology (So), taxonomy (Ta) and zoology (Zo). **A** Interdisciplinarity network: The nodes give the scientific fields encompassed by projects, with edges connecting fields within the same project, weighted by how often the specific combination appears. The fields of Ecology and Evolutionary are shown in red in the centre. All remaining fields within biology are shown in orange on the left. Fields outside biology are shown in light blue on the right side of the network. **B** I classified the background of students as either purely biological (Bio, red), purely outside biology (Non-bio, light blue) or encompassing both (Both, purple). **C** I calculated the overlap of PhD project and background as the fraction of fields within the project covered by the student's background.

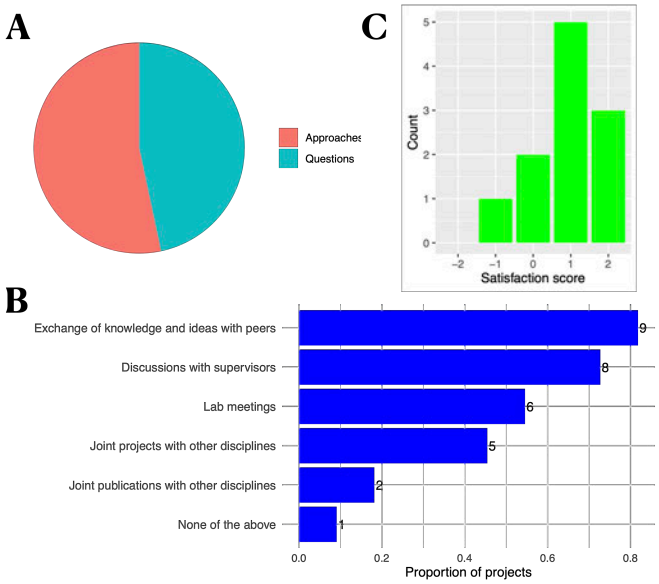

Figure 5.2: Methods, collaborations and satisfaction in interdisciplinary PhD projects in IEE. I asked the students whether they used interdisciplinary approaches and/or asked interdisciplinary questions (**A**), which form of interdisciplinary collaboration their project includes (**B**), and how satisfied they were with the interdisciplinarity (**C**).

(Fig 5.2**C**). My personal interpretation of these findings is that interdisciplinary PhD projects are experienced as enriching despite the additional challenges. However, most collaboration occurs among individuals (peers and supervisors), and structural support that would lead to joint projects and publications is lacking.

In conclusion, I want to reiterate the X-NET Recommendations Report [77] on obstacles faced by interdisciplinary researchers, especially those early in their careers. In particular, future work should address cohort building (recommendation 5), training of researchers on the advantages, challenges and values of interdisciplinary collaboration by their host institutions (recommendation 7) and recalibration of expectations due to the longer timescales needed for interdisciplinary research trajectories (recommendation 10).

In my PhD, I developed a computational tool to analyse fluctuation assay data, reanalysed published fluctuation assay data, advised on the experimental design of fluctuation assays, and made testable predictions of their outcomes. Interdisciplinary collaboration, i.e. directly working with experimentalists performing fluctuation assays, could have greatly enriched this work. For example, as pointed out in Chapter 2 and 3, it would be essential to perform separate experiments to quantify the fraction of cells

with an elevated expression of the stress response in addition to fluctuation assays under stress. This would allow us to estimate the specific increase in mutation rate associated with the stress response, which is relevant for understanding how stress impacts DNA damage, repair and mutagenesis at a molecular level. Sequencing resistant mutant colonies that arose in a fluctuation assay under stress to assess the number of mutations, or performing fluctuation assays under stress with selection for complex mutants on the plates (for example, two or more antibiotics) would be another interesting direction to study whether heterogeneity in mutation rates increases the risk of multidrug resistance evolution, as theoretical work suggests [1]. Moreover, as I pointed out in Chapter 4, there is no raw data available for the only study systematically assessing the increase in mutation rate depending on the antibiotic dose that we know of [62], and it would be desirable to repeat the experiments. Here, another interesting direction could be to consider varying antibiotic concentrations on the selective plates to assess whether there are mutations with different resistance levels occurring at different rates.

Appendix A

Supplementary information: Estimating mutation rates under heterogeneous stress responses

Supplementary information: Estimating mutation rates under heterogeneous stress responses

Lucy Lansch-Justen[1,*], Meriem El Karoui[2,3,4], and Helen K. Alexander[1,3,*]

May 17, 2024

[1]Institute of Ecology and Evolution, School of Biological Sciences, University of Edinburgh, Edinburgh, Scotland, United Kingdom
[2]Institute of Cell Biology, School of Biological Sciences, University of Edinburgh, Edinburgh, Scotland, United Kingdom
[3]Centre for Engineering Biology, University of Edinburgh, Edinburgh, Scotland, United Kingdom
[4]Bacterial Systems Biology and Anti Microbial Resistance, Laboratoire de Biologie et Pharmacologie Appliquée, École Normale Supérieure Paris-Saclay, Gif-sur-Yvette, France

*Corresponding authors
Email: (LLJ), (HKA)

A Deterministic treatment of response-*on* non-mutants

In Model and Methods, we derive the population sizes of the response-*off* and response-*on* non-mutants as

$$n_{off}(t) = n_{off}(0)\mathrm{e}^{(\gamma^s_{off}-\delta^s_{off}-\alpha)t} \tag{1}$$

$$n_{on}(t) = \frac{\alpha n_{off}(0)}{\gamma^s_{off}-\delta^s_{off}-\alpha-(\gamma_{on}-\delta_{on})}\left(\mathrm{e}^{(\gamma^s_{off}-\delta^s_{off}-\alpha)t}-\mathrm{e}^{(\gamma_{on}-\delta_{on})t}\right)+n_{on}(0)\mathrm{e}^{(\gamma_{on}-\delta_{on})t} \tag{2}$$

which assumes that the response-*on* subpopulation can be treated deterministically. However, for small initial population sizes $n_{on}(0)$, this assumption might not hold. Therefore, we test its validity using stochastic simulations; we simulate switching *on* of the response

as a time-inhomogeneous Poisson process with rate $\alpha n_{\mathit{off}}(t)$, the growth dynamics of the response-*on* subpopulation as a continuous-time linear birth-death process with rates

$$\begin{cases} N_{on} \to N_{on}N_{on}, & \text{rate } \gamma_{on} \\ N_{on} \to \varnothing, & \text{rate } \delta_{on} \end{cases} \tag{3}$$

until it reaches a size of $N = 10^4$, and according to Eq 2 afterwards. Then, we compare the resulting population size with Eq 2 at early and late time points: t_1, the expected time of the first mutation (which follows an exponentially-distributed waiting time) in the response-*off* subpopulation, given by

$$t_1 = \frac{\Gamma\left(0,\ \frac{\mu_{\mathit{off}} n_{\mathit{off}}(0)}{\gamma^s_{\mathit{off}} - \delta^s_{\mathit{off}} - \alpha}\right)}{\gamma^s_{\mathit{off}} - \delta^s_{\mathit{off}} - \alpha}, \tag{4}$$

and t_N, the time when the response-*off* subpopulation reaches a size of $N = 10^9$, given by

$$t_N = \frac{\log\left(\frac{10^9}{n_{\mathit{off}}(0)}\right)}{\gamma^s_{\mathit{off}} - \delta_{\mathit{off}} - \alpha}. \tag{5}$$

For two initial population sizes of the response-*on* subpopulation, (a) $n_{on}(0) = 0$ and (b) $n_{on}(0) = \frac{\alpha}{\gamma^s_{\mathit{off}} - \delta^s_{\mathit{off}}} \cdot n_{\mathit{off}}(0)$, which is a lower bound for the equilibrium fraction of the response-*on* subpopulation, we calculate the error relative to the median of $R = 100$ simulations and the coefficient of variation across the simulations (Fig A). We find that both relative error and coefficient of variation are larger at the earlier than the later time point and that they increase with decreasing relative switching rate $\tilde{\alpha} = \frac{\alpha}{\gamma^s_{\mathit{off}}}$ and increasing relative fitness of response-*on* cells $r_{on} = \frac{\gamma_{on} - \delta_{on}}{\gamma^s_{\mathit{off}} - \delta^s_{\mathit{off}}}$. In general, Eq 2 tends to slightly overestimate the size of the response-*on* subpopulation (indicated in red), but the error is with $< 1\,\%$ sufficiently small to justify our approximation.

B Example mutant count distributions

In the model selection in the main Results, we select between the homogeneous-response and the heterogeneous-response models and find that, in many cases, both models fit the simulated mutant count data similarly well. Here, to gain insight into why this is the case, we show example mutant count distributions using the same parameters as in respective main Results section. This includes distributions under permissive conditions using the standard model (Fig BI) and under stressful conditions for both homogeneous-response (Fig BII) and heterogeneous-response (Fig BIII) models. We consider parameter settings such that the increase in population mean mutation rate is comparable in both the homogeneous and heterogeneous cases ($\frac{\mu^s}{\mu^p} = \bar{M} = 5$).

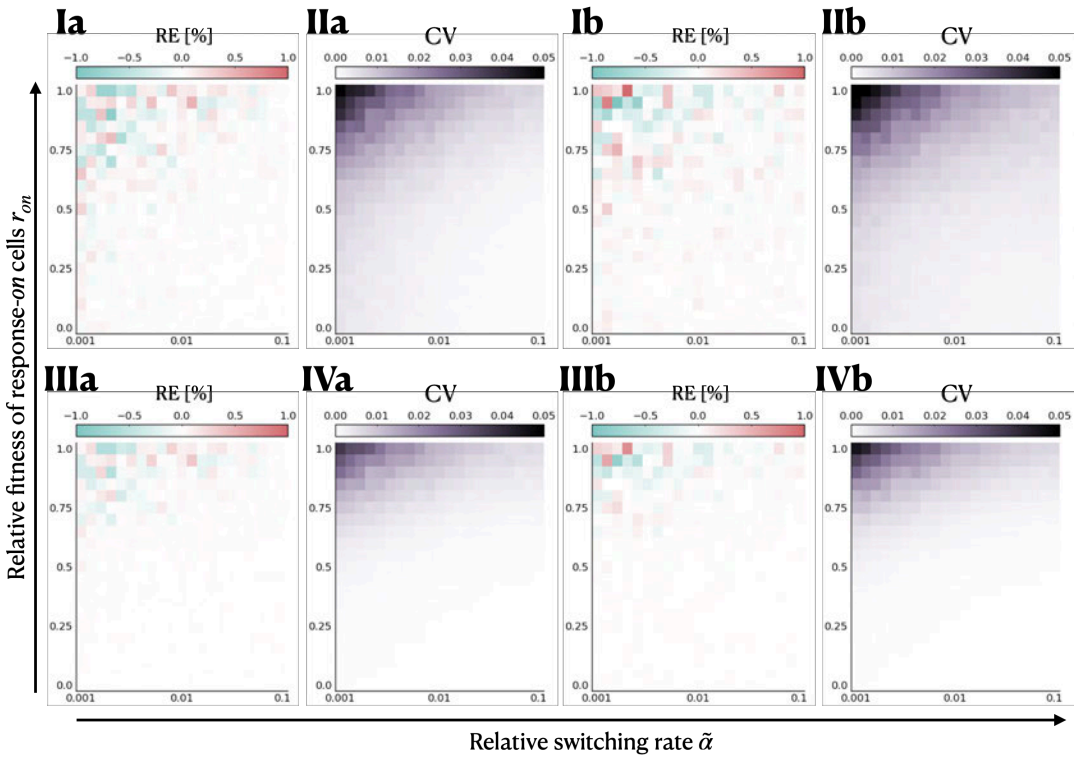

Figure A: **Response-*on* non-mutants can be treated deterministically.** Deterministic compared to stochastic dynamics of response-*on* non-mutants for initial population sizes of the response-*on* subpopulation of (**a**) $n_{on}(0) = 0$ and (**b**) $n_{on}(0) = \frac{\alpha}{\gamma^s_{off} - \delta^s_{off}} \cdot n_{off}(0)$. We simulate switching *on* of the response as a time-inhomogeneous Poisson process and the dynamics of response-*on* non-mutants as birth-death processes ($R = 100$ simulation runs). Then, we compare the resulting population sizes with Eq 2 at early and late time points. **I** Relative error of the median in % at t_1, **II** coefficient of variation across the simulations at t_1, **III** relative error of the median in % at t_N and **IV** coefficient of variation across the simulations at t_N. The parameters used in the simulations are $\gamma^s_{off} = 1\, h^{-1}$ $\delta^s_{off} = \delta_{on} = 0\, h^{-1}$, $\alpha \in [0.001,\ 0.1]\ h^{-1}$, $\gamma_{on} \in [0.0,\ 1.0]\ h^{-1}$.

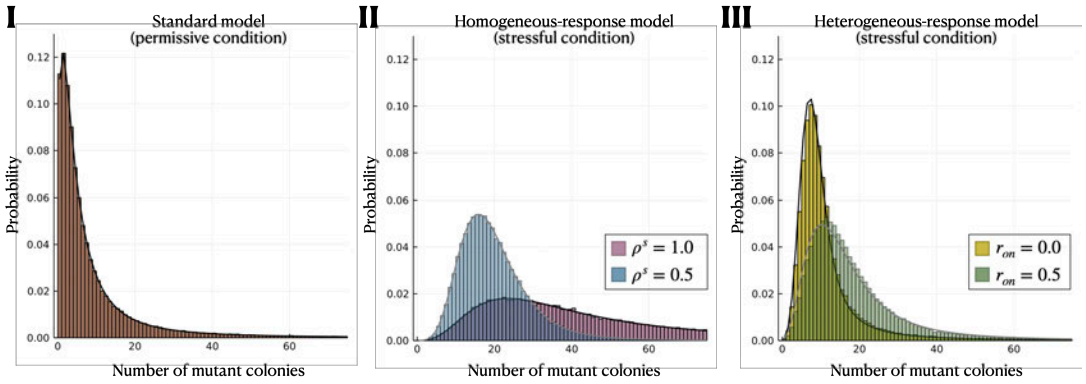

Figure B: **Example mutant count distributions.** We simulate $c = 10^5$ parallel cultures under **I** permissive conditions using the standard model, and under stressful conditions using **II** the homogeneous-response model with an increase in mutation rate of $\frac{\mu^s}{\mu^p} = 5$ and with either no mutant fitness cost ($\rho^s = 1$, purple) or halved fitness ($\rho^s = 0.5$, blue), or **III** the exact heterogeneous-response model with a zero ($r_{on} = 0$, yellow) or intermediate ($r_{on} = 0.5$, dark green) relative fitness of response-*on* cells. For the heterogeneous-response model, we simulate with a mutation-rate increase such that the increase in population mean mutation rate is $\bar{M} = 5$. The lines give the analytically derived distributions (approximate in the case of the heterogeneous-response model).

When there is no mutant fitness cost in the homogeneous-response model ($\rho^s = 1$; Fig BII, purple) and response-*on* cells are non-dividing in the heterogeneous-response model ($r_{on} = 0$; Fig BIII, yellow), the mutant count distributions are clearly different. However, when increasing the severity of the mutant fitness cost ($\rho^s = 0.5$; Fig BII, blue) or the division rate of response-*on* cells ($r_{on} = 0.5$; Fig BIII, dark green), the mutant count distributions have a similar shape. At the same time, the analytical mutant count distribution under the approximate heterogeneous-response model (lines in Fig BIII) deviates from the simulated exact distribution (bars), with a greater deviation for larger division rates of response-*on* cells.

C Calculation of the duration of the growth phase

In all simulations to test our inference method, we set the duration t_f of the growth phase such that the expected number of *mutations*, m (not *mutants*) equals one, by numerically

solving the following equations:

$$\text{Permissive conditions: } \mathbb{E}[m] = \int_0^{t_f} \nu_{off}^p n_{off}^p(t)\,\mathrm{d}t \stackrel{!}{=} 1 \tag{6}$$

$$\text{Stressful conditions: } \mathbb{E}[m] = \int_0^{t_f} \nu_{off}^s n_{off}^s(t) + \nu_{on} n_{on}(t)\,\mathrm{d}t \stackrel{!}{=} 1 \tag{7}$$

This way, the resulting number of resistant mutant colonies on each selective plate is similar across the considered parameter ranges and usually within an experimentally countable range of zero to a couple hundred. For example, the duration of simulated fluctuation assays under permissive conditions with the default parameter settings (main text Table 2) is set to $t_f \approx 9.21\,h$.

D Sensitivity of the estimation to the number of parallel cultures

In the first main Results section, we show that the estimation of the mutation-rate increase $\frac{\mu_{on}}{\mu_{off}}$ in the heterogeneous-response model is accurate and precise for sufficiently large mutation-supply ratio, $\mathcal{S} \sim \mathcal{O}(1)$. Here, we analyse how this result depends on the number of parallel cultures used to estimate $\frac{\mu_{on}}{\mu_{off}}$. We use the same simulation parameters as in the respective main Results section (with relative switching rate $\tilde{\alpha} = 0.05$) but smaller numbers of parallel cultures ($c = 25$, 12, 6, 3). We find that, as expected, our estimation method performs worse for smaller c (Fig CI). Nonetheless, the median relative error approaches zero for increasing simulated mutation-rate increase (Fig CII), implying that our method remains accurate (i.e. unbiased) independent of the number of parallel cultures used. However, the coefficient of variation across the estimates is consistently larger for smaller c (Fig CIII) and, therefore, precision is lost.

E Width of 95% confidence intervals on parameter estimates

In the first main Results section, we consider maximum likelihood point estimates of the mutation-rate increase $\frac{\mu_{on}}{\mu_{off}}$ from $R = 100$ simulated data sets under the heterogeneous-response model. There, we use the median relative error and the coefficient of variation across these 100 point estimates to measure the accuracy and precision, respectively, of our new inference method. Here, we evaluate our method's performance using 95% confidence intervals on each estimate, from the same simulated data as in the respective main Results section. To summarise the confidence intervals across $R = 100$ estimates, we calculate the median of their normalised width, i.e. the difference between the upper and lower bounds of the confidence interval divided by the maximum likelihood estimate (example in Fig DI). Generally, presenting boxplots of $R = 100$ maximum likelihood point estimates

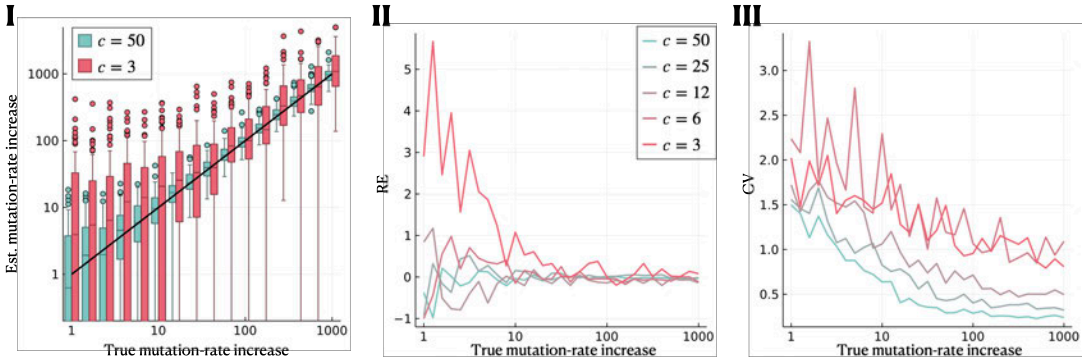

Figure C: **Sensitivity of the estimation to the number of parallel cultures.** Here, we use the same simulation parameters as in Results Fig 2 (where $c = 50$), but consider smaller numbers of parallel cultures ($c = 25, 12, 6, 3$). **I** Estimated compared to true mutation-rate increase using $c = 50$ (red) or $c = 3$ (light blue) parallel cultures. The black line gives the true value of $\frac{\mu_{on}}{\mu_{off}}$. **II** Median relative error and **III** coefficient of variation across the estimates for different numbers of parallel cultures.

(as done throughout the main Results) gives the same qualitative picture as presenting the median normalised width of $R = 100$ confidence intervals (compare Fig DI to Results Fig 2A). At the same time, the median normalised width of the confidence intervals shows a qualitatively similar relationship with $\frac{\mu_{on}}{\mu_{off}}$ and $\tilde{\alpha}$ (Fig DIII) as the coefficient of variation across $R = 100$ point estimates (Results Fig 2C): for a sufficiently large mutation-supply ratio $\mathcal{S} \approx \frac{\mu_{on}}{\mu_{off}}\tilde{\alpha} \sim \mathcal{O}(1)$, confidence intervals are narrow, with a normalised width < 2 (i.e. extending less than 2-fold around the maximum likelihood estimate). Moreover, we confirm that the number of cases in which the true value of $\frac{\mu_{on}}{\mu_{off}}$ lies outside the calculated 95% confidence interval is $< 5\%$ overall, with overestimation being slightly more frequent than underestimation (Fig DII).

F The impact of cell death on parameter estimation for a smaller switching rate

In the second main Results section, we show that the impact of cell death on the estimation of the mutation-rate increase depends on which subpopulation is affected by death. However, estimates remain largely unbiased when all cells are affected equally, although the variation of these estimates increases. This result is not an artefact of the specific parameters used in the respective main Results section: it also holds for different values of the relative switching rate, here shown with $\tilde{\alpha} = 0.01$ (Fig E) instead of $\tilde{\alpha} = 0.05$ (Results Fig 3).

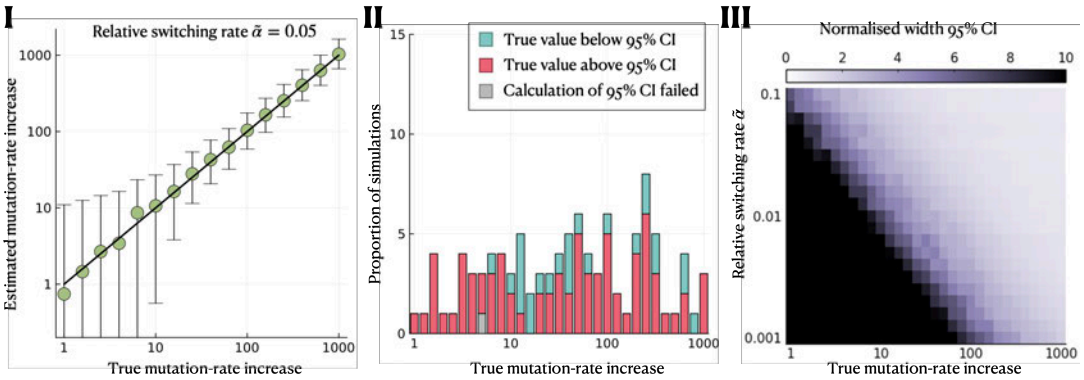

Figure D: 95% **confidence intervals on parameter estimates.** Here, we use the same simulated data as in Results Fig 2 but, additionally, calculate 95% profile likelihood confidence intervals around the maximum likelihood estimates of the mutation-rate increase $\frac{\mu_{on}}{\mu_{off}}$. **I** Median estimated $\frac{\mu_{on}}{\mu_{off}}$ with whiskers extending to the median lower and upper bound of the 95% confidence intervals. **II** Proportion of simulations for which the true value lies outside the 95% confidence interval. **III** Normalised width of 95% confidence intervals.

This result can be explained as follows. Generally, the estimation of μ_{off} is not noticeably impacted by cell death because it is jointly inferred under stressful and permissive conditions, and for the latter, there is no cell death. Therefore, any biases in the estimation of $\frac{\mu_{on}}{\mu_{off}}$ stem from biases in estimating μ_{on}. Now, death in response-*off* cells causes an underestimation of the number of cell divisions to reach the final population sizes, as pointed out in [1]. This, in turn, results in an overestimation of the mutation rate of response-*on* cells because this is calculated as mutations per response-*on* cell, per division in response-*off* cells ($\mu_{on} := \frac{\nu_{on}}{\gamma^s_{on}}$). At the same time, death in response-*on* cells can lead to the extinction of response-*on* mutant lineages, causing an underestimation of $\mathcal{S}$ and, with it, underestimation of μ_{on}. These two effects counteract each other, leading to an unbiased estimate overall.

G The impact of differential mutant fitness on parameter estimation

We next test the robustness of our method to differential mutant fitness, which is neglected in the inference under the heterogeneous-response model. For this purpose, we simulate fluctuation assays under an extended model of heterogeneous stress responses (Results Fig 1C) with differential mutant fitness using a parameter range of $\rho_{off} := \rho^p_{off} = \rho^s_{off} \in [0.0,\ 1.5]$. Note that we consider a differential mutant fitness only in response-*off* cells as

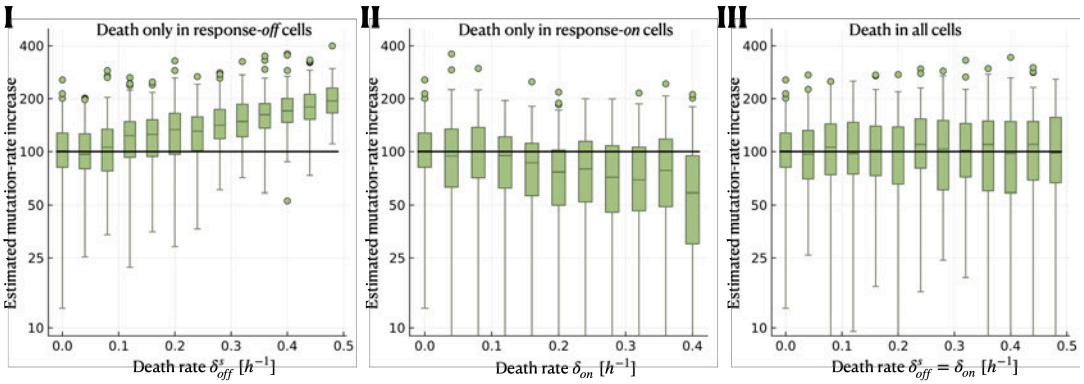

Figure E: **Cell death has limited impact on the estimation of the mutation-rate increase.** Here, we repeat the analysis in Results Fig 3 but with a lower switching rate, α. We simulate using the heterogeneous-response model extended by cell death but neglect cell death in the model used to estimate $\frac{\mu_{on}}{\mu_{off}}$. The black solid lines indicate the true mutation-rate increase used in the simulations. **I** Estimated mutation-rate increase when only response-*off* cells are affected by cell death, **II** when only response-*on* cells are affected by cell death and **III** when all cells are affected by cell death equally. The parameter range used in the simulations is $\alpha = 0.01\ h^{-1}$, $\delta^s_{off} \in [0.0,\ 0.5]\ h^{-1}$, $\delta_{on} \in [0.0,\ 0.5]\ h^{-1}$.

the response-*on* cells have a zero division rate in this set of simulations and are, therefore, unaffected by a differential mutant fitness.

From the resulting mutant count data, we estimate the mutation-rate increase $\frac{\mu_{on}}{\mu_{off}}$ and compare it with the true value to determine any biases caused by neglecting the differential mutant fitness in the inference (Fig F). We find that neglecting this effect in the inference leads to a slight underestimation of the mutation-rate increase when mutations bring a fitness advantage ($\rho_{off} > 1$). Fitness advantages could arise, for example, because the same antibiotic is used as a stressor and on the selective plates or because two different antibiotics are used, but mutants are cross-resistant [2]. However, the bias remains small (relative error of the median $< 17\,\%$) across the tested parameter range. If mutants have a fitness cost ($\rho_{off} < 1$), the mutation-rate increase is estimated accurately.

H Estimation when response-*on* cells have a known non-zero division rate

In the third main Results section, we evaluate the performance of our method in estimating the mutation-rate increase when response-*on* cells have a non-zero division rate for the

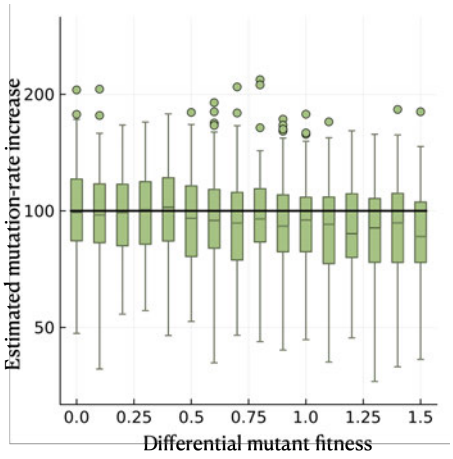

Figure F: **Differential mutant fitness has minimal impact on the estimation of the mutation-rate increase under the heterogeneous-response model.** We simulate using the heterogeneous-response model with mutants having a different division rate than non-mutants but neglect this effect in the model used to estimate $\frac{\mu_{on}}{\mu_{off}}$. The black solid line indicates the true mutation-rate increase. The parameter range used in the simulations is $\rho^p_{off} = \rho^s_{off} \in [0.0,\ 1.5]$.

cases that (i) the non-zero division rate is neglected in the inference (setting $r_{on} = 0$) and (ii) $r_{on} > 0$ is inferred additionally. Here, we consider a third case: r_{on} is set to the true value, which could, for example, be measured in microfluidics experiments using time-lapse microscopy and image analysis to estimate the division rate of cells identified as response-*on*. Interestingly, we find that setting r_{on} to the true value hardly improves the estimation of the mutation-rate increase (Fig G). The reason for this lies in the approximation of the size of the non-mutant response-*on* subpopulation (main text, Eq 13) which assumes that $\gamma_{on} - \delta_{on} \ll \gamma^s_{off} - \delta^s_{off} - \alpha$ and is no longer valid for large $r_{on} = \frac{\gamma_{on}-\delta_{on}}{\gamma^s_{off}-\delta^s_{off}} \to 1$. Therefore, setting r_{on} to the true value still results in a biased estimate. This suggests that, given the available inference method, obtaining a precise estimate of r_{on} from a separate experiment is not worthwhile besides validating that it is small.

I Estimates of the mutant fitness cost in the homogeneous-response model

In the model selection in the main Results, we select between homogeneous and heterogeneous-response models using a two-step selection procedure. Here, we show which version of the homogeneous-response model is chosen by the likelihood-ratio test in the first selection step and what mutant fitness costs are estimated by the chosen model. We find that, when

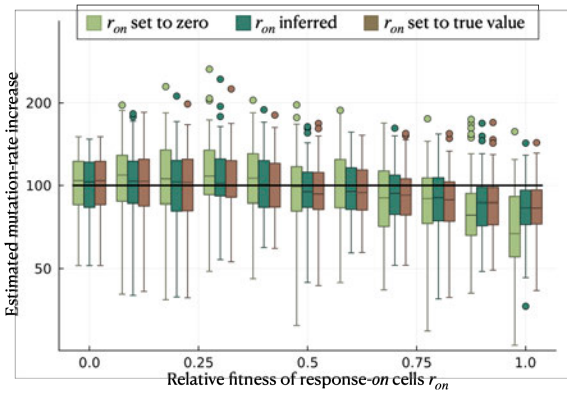

Figure G: **Setting the relative fitness of response-*on* cells to the true value only marginally improves the estimation of the mutation-rate increase.** We simulate using the heterogeneous-response model with $r_{on} \geq 0$ being the relative fitness of response-*on* cells compared to response-*off* cells. We consider three cases for the inference: (i) setting r_{on} to zero and only inferring μ_{off} and $\mathcal{S}$, (ii) inferring r_{on} additionally, and (iii) setting r_{on} to its true value and only inferring μ_{off} and $\mathcal{S}$. From the estimates of μ_{off} and $\mathcal{S}$ we calculate $\frac{\mu_{on}}{\mu_{off}}$. The solid black line indicates the true value of $\frac{\mu_{on}}{\mu_{off}}$. The parameter range used in the simulations is $\gamma_{on} \in [0.0,\ 1.0]\ h^{-1}$.

simulating with small relative fitness of response-*on* cells r_{on}, the homogeneous-response model with unconstrained mutant fitness (ρ^p and ρ^s inferred) is selected in most cases, whereas for large r_{on} the homogeneous-response model without differential mutant fitness ($\rho^p = \rho^s = 1$) is selected in most cases (Fig HI). The homogeneous-response model with constrained mutant fitness ($\rho^p = \rho^s$ inferred) is selected for only a small number of simulations.

For the homogeneous-response model with ρ^p and ρ^s inferred, the mutant fitness under permissive conditions (ρ^p) is correctly estimated as $\approx 0.98 \pm 0.17$. For the mutant fitness under stressful conditions (ρ^s), on the other hand, an increasingly severe mutant fitness cost is inferred the smaller the relative fitness of response-*on* cells (Fig HII, blue). The homogeneous-response model with constrained mutant fitness (Fig HII, purple) also infers a more severe mutant fitness cost for smaller r_{on} (under both permissive and stressful conditions, since $\rho^p = \rho^s$), but less severe than the unconstrained model version.

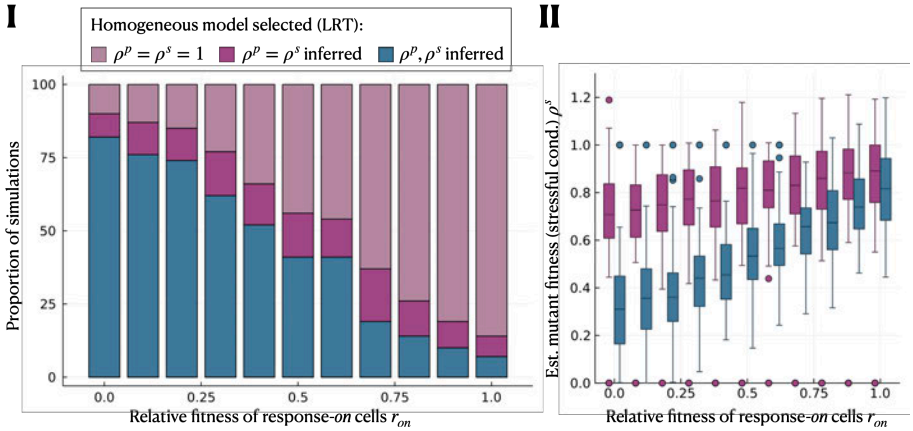

Figure H: **Estimation of mutant fitness cost by the best homogeneous-response model.** Here, we show additional estimation outputs to Results Fig 5. **I** Best homogeneous-response model, as chosen by a likelihood-ratio test in our first step in the model selection procedure. **II** Mutant fitness under stressful conditions as estimated by the homogeneous-response models with constrained (dark purple) or unconstrained (blue) mutant fitness.

J Parameter estimation and model selection for smaller mutation-rate increase

In the model selection in the main Results, we select between heterogeneous and homogeneous responses using simulated data where we set the true mutation-rate increase to $\frac{\mu_{on}}{\mu_{off}} = 100$. Here, we repeat this analysis for a mutation-rate ratio of $\frac{\mu_{on}}{\mu_{off}} = 10$. We find that the number of simulations in which the heterogeneous-response model is selected drops, reaching at most $\sim 25\%$ for small r_{on} (Fig II). In most of the remaining cases, either no model is preferred (more commonly for small r_{on}), or the homogeneous-response model without differential mutant fitness is selected (more commonly for large r_{on}). The homogeneous-response models with inferred mutant fitness are selected in only a few cases. Both heterogeneous and homogeneous-response models remain able to infer the mutation-supply ratio or increase in population mean mutation rate, respectively, reasonably accurately, with only a slight underestimation in both cases (Fig III and IIII).

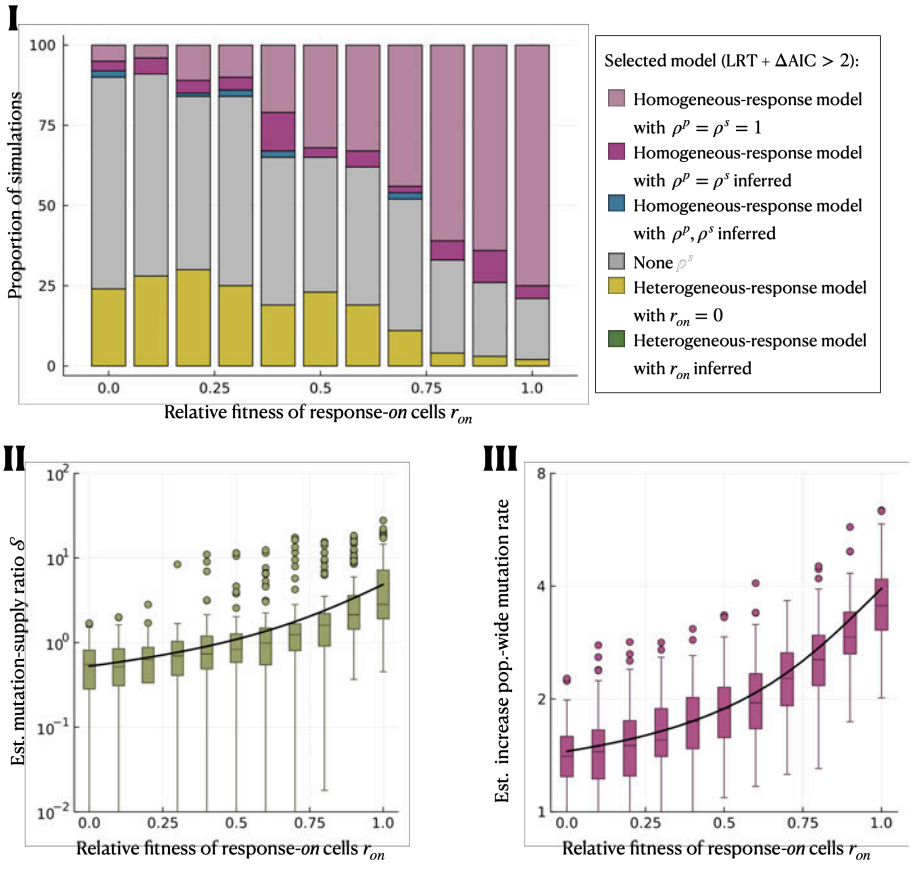

Figure I: **Model selection is more often inconclusive when the mutation-rate increase is smaller.** We simulate using the heterogeneous-response model for a range of relative fitness of response-*on* cells, r_{on}, and with a true mutation-rate ratio of $\frac{\mu_{on}}{\mu_{off}} = 10$; and infer using the same models as considered in the model selection in the main Results. **I** Model selection using LRT and AIC. **II** Estimated mutation-supply ratio, $\mathcal{S}$, by the best heterogeneous-response model. **III** Estimated increase in mutation rate, $\frac{\mu^s}{\mu^p}$, by the best homogeneous-response model. The black lines in **II** and **III** indicate the true values of $\mathcal{S}$ and the increase in population mean mutation rate, $\bar{M}$, respectively. The parameters used in the simulations are $\nu_{on} = 10^{-7}\ h^{-1}$ and $\gamma_{on} \in [0,\ 1]\ h^{-1}$.

K Parameter estimation and model selection when there is no increase in mutation rate

In all results so far, we used simulated data with a true increase in mutation rate under stress ($\mathcal{S} > 0$ for heterogeneous and $\frac{\mu^s}{\mu^p} > 1$ for homogeneous stress responses). Here, we test the parameter estimation and model selection when there is actually no increase in mutation rate under stress. For this purpose, we simulate a homogeneous stress response which does not impact the mutation rate ($\mu^s = \mu^p$), but results in a mutant fitness cost of varying severity ($\rho^p = 1$ and $\rho^s \in [0, 1]$). We then apply our LRT plus AIC two-step model selection procedure (as in the model selection in the main Results). We find that when mutants have a low fitness under stress (small ρ^s), the unconstrained homogeneous-response model is selected in the majority of cases (Fig JI). As the mutant fitness increases, no model is selected for an increasing proportion of simulations, suggesting that both heterogeneous- and homogeneous-response models can explain the data similarly well. Regardless of which model is selected, both perform fairly well in inferring little or no increase in mutation rate. In the heterogeneous-response model (Fig JII), a mutation-supply ratio of $\mathcal{S} = 0$ corresponds to no contribution from response-*on* cells, and the estimated $\mathcal{S}$ tends towards zero as mutant fitness cost decreases. For small mutant fitness, $\mathcal{S}$ is slightly over-estimated (median estimate $\mathcal{S} \approx 0.5$ for $\rho^s < 0.5$). This result again reflects the similarity in mutant count distributions produced by either the heterogeneous-response model with non-dividing response-*on* cells ($r_{on} = 0$) or the homogeneous-response model with severe mutant fitness cost (small ρ^s), cf. Fig B. Under the homogeneous-response model (Fig JIII), the estimated mutation-rate increase $\frac{\mu^s}{\mu^p}$ is unbiased, centred around the true value of 1, regardless of mutant fitness cost.

L Parameter estimation and model selection for different switching rates

In the model selection in the main Results, we perform model selection on simulated mutant count data from the heterogeneous-response model with varying relative fitness of response-*on* cells. Here, we carry out a similar analysis on simulations with varying relative switching rates $\tilde{\alpha}$ (i.e. rate of switching the response *on* under stress). Specifically, we simulate under the heterogeneous-response model without cell death and with non-dividing response-*on* cells ($r_{on} = 0$), and perform model selection between heterogeneous and homogeneous-response models using LRT plus AIC.

When the relative switching rate is small ($\tilde{\alpha} < 0.01$), the mutation-supply ratio $\mathcal{S} \ll 1$, which implies very little increase in population mean mutation rate under stressful conditions. In this case, we find that no model is selected in the majority of simulations (Fig KI), which is in accordance with the results when there is actually no increase in mutation rate

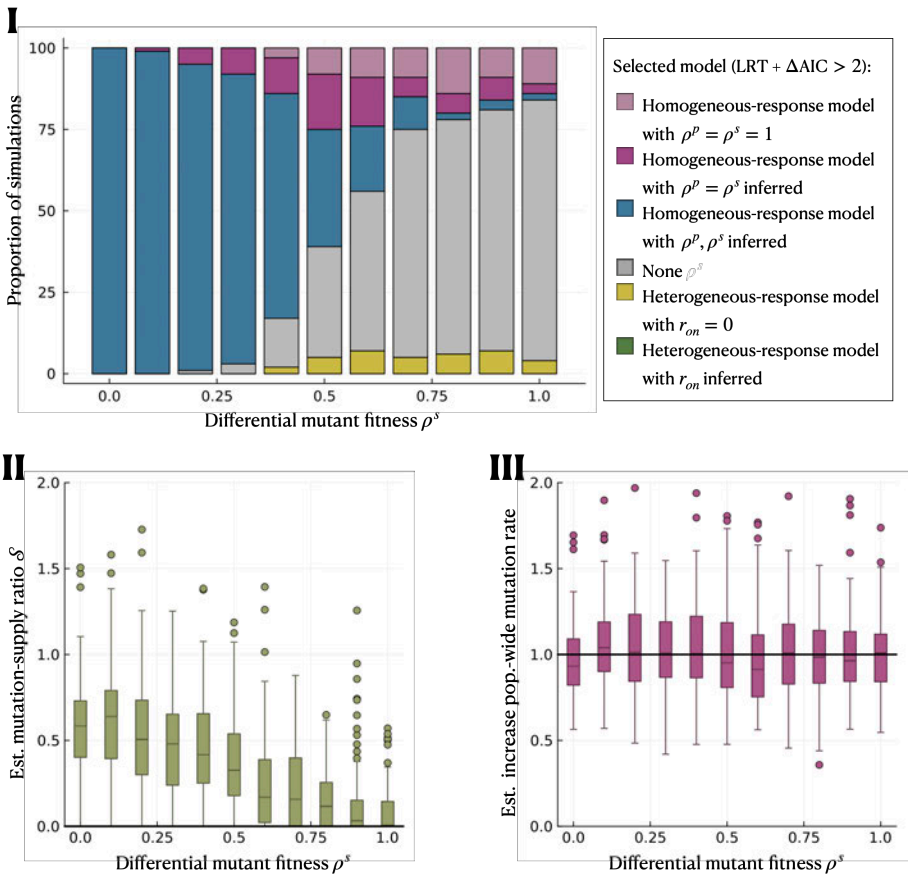

Figure J: **Model selection when there is no increase in mutation rate under stress.** We simulate under the unconstrained homogeneous-response model without an increase in mutation rate ($\mu^s = \mu^p$). **I** Model selection using the LRT and AIC. **II** Estimated mutation-supply ratio, $\mathcal{S}$, by the best heterogeneous-response model. **III** Estimated increase in mutation rate, $\frac{\mu^s}{\mu^p}$, by the best homogeneous-response model. The black lines in **II** and **III** indicate the true values ($\mathcal{S} = 0$ and $\frac{\mu^s}{\mu^p} = 1$, respectively). The parameters used in the simulations are $\rho^p = 1$ and $\rho^s \in [0,\ 1]$.

(previous section). For a relative switching rate of $\tilde{\alpha} = 0.05$, the heterogeneous-response model is selected in slightly less than 75% of simulations, similarly to our results with $r_{on} = 0$ in Results Fig 5, where we simulated under identical parameters. Interestingly, however, the fraction of simulations in which the heterogeneous-response model is selected does not increase further for larger $\tilde{\alpha}$. This implies that even for large relative switching rates, heterogeneous stress responses or mutant fitness cost under stress represent alternative model explanations for similar patterns in mutant count distributions and cannot be distinguished from fluctuation assay data alone.

The estimation of the mutation-supply ratio $\mathcal{S}$ by the best heterogeneous-response model is accurate and precise for sufficiently large relative switching rate $\tilde{\alpha}$ (Fig KII), which implies large $\mathcal{S}$, in accordance with our results presented in Results Fig 2. Furthermore, the increase in mutation rate estimated by the best homogeneous-response model ($\frac{\mu^s}{\mu^p}$) is a fairly accurate and precise estimate of the true increase in population mean mutation rate ($\bar{M}$) in the heterogeneous-response simulations, with only a slight underestimation of $\bar{M}$ for intermediate $\tilde{\alpha}$ (Fig KIII).

M Model selection limited to constrained mutant fitness in the homogeneous-response case

In last main Results section, we simulate under the heterogeneous-response model for a range of relative fitness of response-*on* cells (r_{on}) and perform model selection between the homogeneous-response model (a) without differential mutant fitness (setting $\rho^p = \rho^s = 1$), (b) with constrained differential mutant fitness, i.e. one additional inference parameter $\rho^s = \rho^s$, or (c) with unconstrained differential mutant fitness, i.e. two additional inference parameters ρ^s and ρ^s; and the heterogeneous-response model (d) with zero fitness of response-*on* cells (setting $r_{on} = 0$), or (e) with r_{on} and f_{on} as two additional inference parameters. Moreover, we evaluate the homogeneous-response models' performance in estimating the true increase in population mean mutation rate ($\bar{M}$) and the heterogeneous models' performance in estimating the true mutation-supply ratio ($\mathcal{S}$). Here, we repeat this analysis, but we consider only the homogeneous-response models (a) and (b), in which the mutant fitness under stressful and permissive conditions is equal ($\rho^p = \rho^s$). This represents a reasonable starting assumption in the absence of any *a priori* reason to expect that mutant fitness costs should differ in these conditions.

Performing model selection using LRT plus AIC, we find that the heterogeneous-response model with $r_{on} = 0$ is selected in most cases when the true relative fitness of response-*on* cells (r_{on}) is small (Fig LI). For intermediate values of r_{on}, the heterogeneous-response model with r_{on} inferred is selected more often (up to $\sim 30\%$), but no model is selected even more often (up to $\sim 40\%$). For large values of r_{on}, the homogeneous-response model

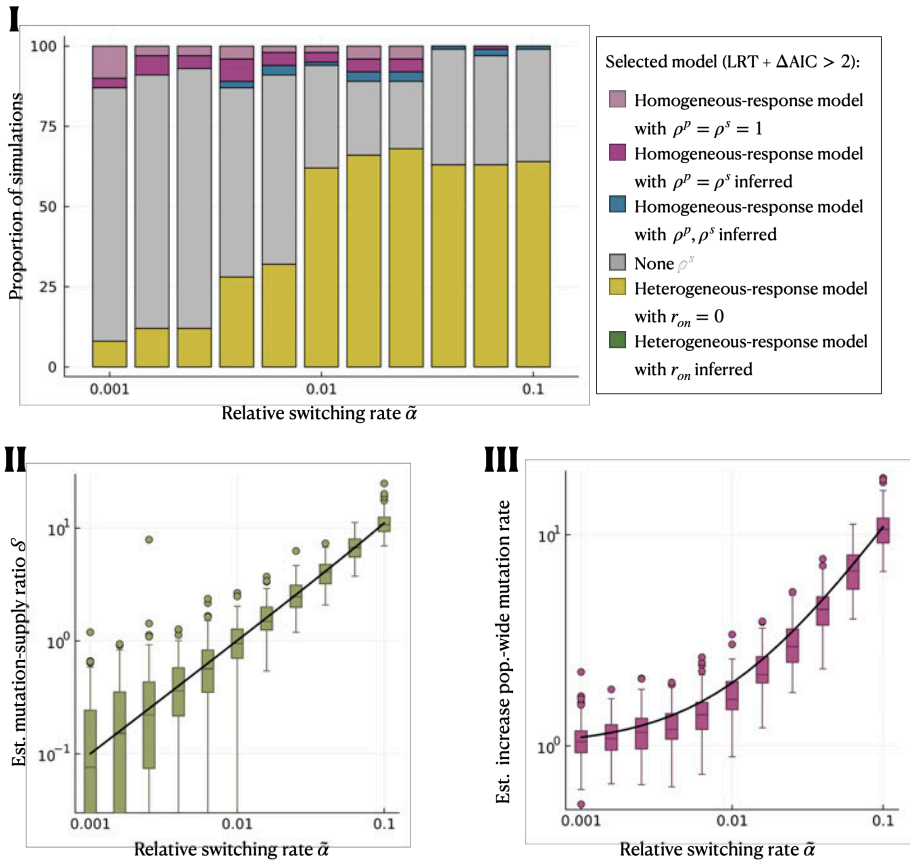

Figure K: **Model selection for varying relative switching rates.** We simulate under the heterogeneous-response model for a range of relative switching rates, $\tilde{\alpha}$. **I** Model selection between heterogeneous and homogeneous stress response models using LRT and AIC. **II** Estimated mutation-supply ratio, $\mathcal{S}$, by the best heterogeneous-response model. **III** Estimated increase in mutation rate, $\frac{\mu^s}{\mu^p}$, by the best homogeneous-response model. The black lines in **II** and **III** indicate the true values of $\mathcal{S}$ and the increase in population mean mutation rate, $\bar{M}$, respectively. The parameter range used in the simulations is $\alpha \in [0.001,\ 0.1]\ h^{-1}$.

without differential mutant fitness ($\rho^s = \rho^p = 1$) is selected in the majority of simulations. The homogeneous-response model with constrained differential mutant fitness is selected in only a few simulations, with the highest percentage of $\sim 10\%$ for intermediate r_{on}.

Overall, over the whole parameter range, the heterogeneous-response model is selected more often when we constrain mutant fitness to be equal under stressful and permissive conditions (Fig LI) compared to when it is also allowed to be unconstrained (Results Fig 5). The differential mutant fitness itself ($\rho^p = \rho^s$) is estimated to be around $\rho^s \approx 0.65$ over the whole range of r_{on} (Fig LII). Moreover, we find that constraining the mutant fitness results in a slight underestimation of the increase in population mean mutation rate $\bar{M}$, especially for small r_{on} (Fig LIII).

N Comparing model selection procedures

In the model selection in the main Results, we use a two-step procedure involving (i) a likelihood-ratio test (LRT) to choose the best homogeneous and the best heterogeneous model version, then (ii) the AIC to compare these two best models. There, we simulated under the heterogeneous-response model with $c = 50$ parallel cultures per fluctuation assay. Here, we analyse the performance of our model selection procedure for smaller numbers of parallel cultures ($c = 20$, 10). We also assess model selection when simulating under the homogeneous-response model. Moreover, in all cases, we show how results using the AIC in the second selection step compare to using the Bayesian information criterion (BIC). The BIC is defined as

$$\mathrm{BIC} = k \ln n - 2 \ln \mathcal{L} \tag{8}$$

with k being the number of inferred parameters and $n = 2c$ the number of data points, i.e. the total number of parallel cultures simulated under permissive plus stressful conditions. As for the AIC, we say that the BICs of two models are comparable if their difference is within ± 2. For an overview of the advantages and disadvantages of different model selection techniques, including AIC and BIC, see [3].

First, we evaluate the performance of the above-described model selection procedures when simulating under the heterogeneous-response model (Fig M) as done in Results Fig 5. When using $c = 50$ parallel cultures in the inference, the model selection procedure using BIC instead of AIC is more conclusive: BIC more often selects the heterogeneous-response model at small r_{on} and the homogeneous-response model with no differential mutant fitness as large r_{on}, whereas AIC selects no model in a larger fraction of cases. Interestingly, when fewer parallel cultures are used in the inference ($c = 20$, 10), the AIC selects the heterogeneous-response model less often when r_{on} is small but more often when r_{on} is large. Model selection using BIC, on the other hand, is more often inconclusive when using fewer parallel cultures, and performs similarly to model selection using AIC when $c = 10$.

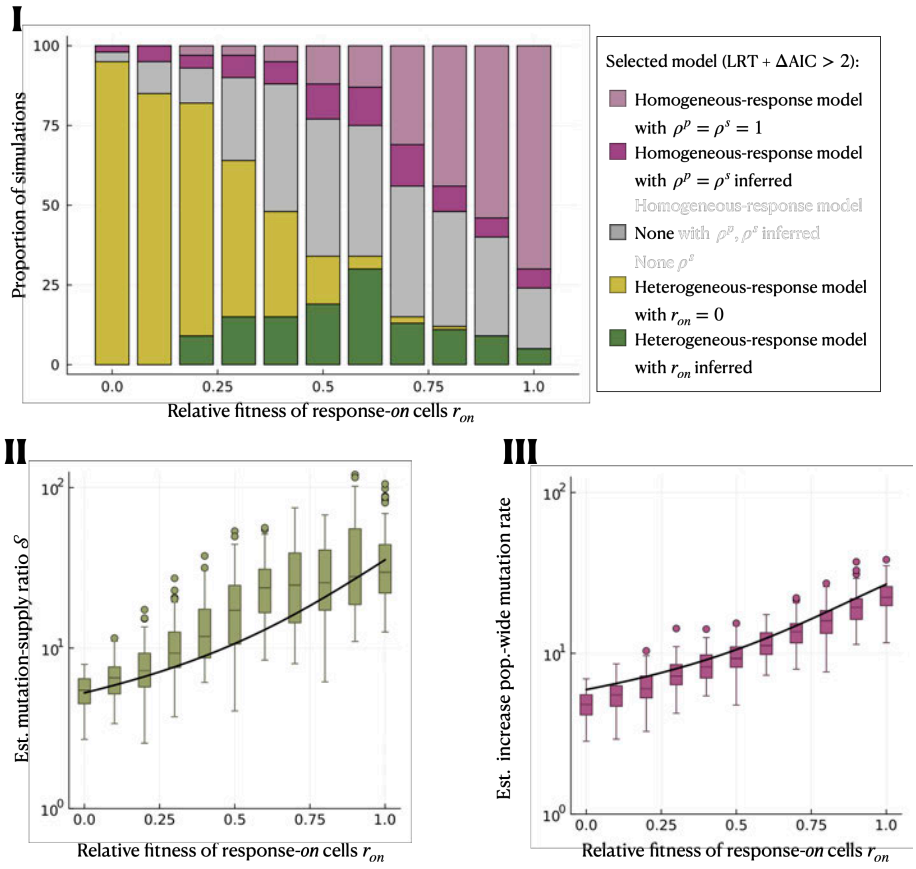

Figure L: **Model selection with constrained mutant fitness.** We use the same simulated data as in Results Fig 5, but for inference, we exclude the version of the homogeneous-response model with unconstrained mutant fitness. **I** Model selection amongst homogeneous response models with constrained mutant fitness (a-b) and heterogeneous-response models (d-e) using LRT and AIC. **II** Estimated mutation-supply ratio, $\mathcal{S}$, by the best heterogeneous-response model. **III** Estimated increase in mutation rate, $\frac{\mu^s}{\mu^p}$, by the best homogeneous-response model (a) or (b). The black lines in **II** and **III** indicate the true values of $\mathcal{S}$ and the increase in population mean mutation rate, $\bar{M}$, respectively. The parameter range used in the simulations is $\gamma_{on} \in [0, 1]\ h^{-1}$.

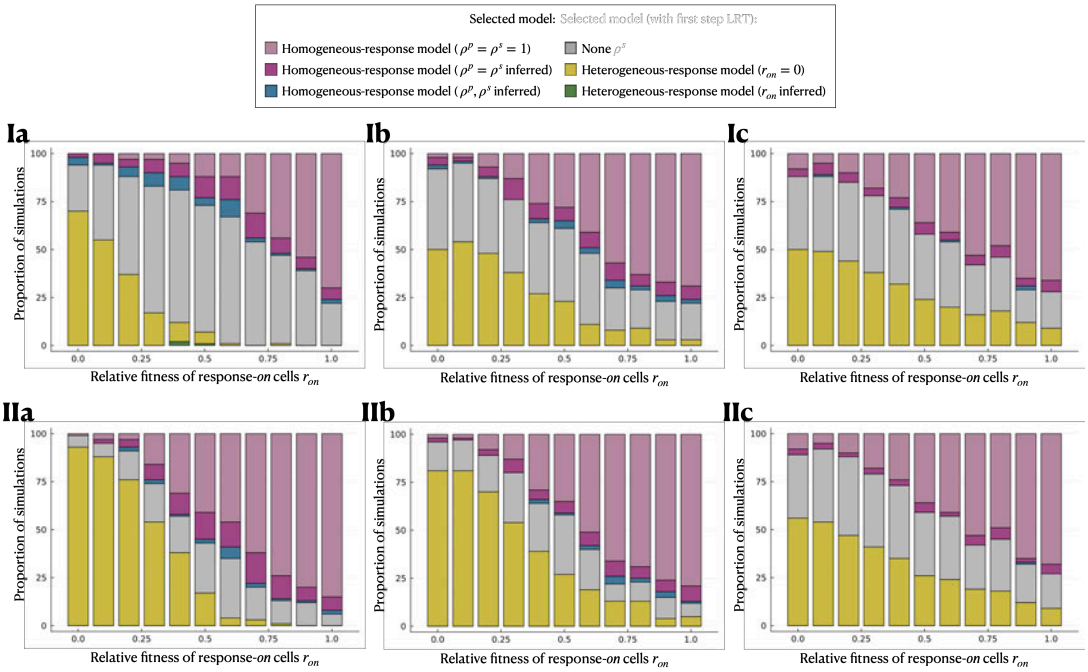

Figure M: **Model selection when simulating under the heterogeneous-response model.** We use the same simulation parameters as in Results Fig 5 and use a two-step model selection procedure with LRT as the first step and either AIC (**I**) or BIC (**II**) as the second selection step, and $c = 50$ (**a**), $c = 20$ (**b**) or $c = 10$ (**c**) parallel cultures in the inference.

The latter is expected as for $c = 10$ the penalising constant used in the BIC (Eq 8) equals $\ln 2c \approx 3$, close to the penalising constant ($= 2$) used in the AIC.

Next, we perform model selection when simulating under the homogeneous-response model with constrained mutant fitness cost ($\rho^p = \rho^s \in [0, 1]$), for various increases in population-wide mutation rate (Fig N). Again, we compare the performance of model selection procedures using AIC (**I**) or BIC (**II**). In all cases, the rate of false positives, i.e. selecting the heterogeneous-response model, is low; up to maximally $\approx 10\%$ for mutant fitness costs around $\rho^p = \rho^s = 0.8$.

Finally, we perform model selection when simulating under the homogeneous-response model with differential mutant fitness only under stressful conditions ($\rho^p = 1$ and $\rho^s \in [0, 1]$) and various increases population-wide in mutation rate (Fig O), using the AIC (**I**) or BIC (**II**) for model selection. For less severe mutant fitness costs ($\rho^s \to 1$), AIC tends to select the homogeneous-response model without differential mutant fitness regardless of

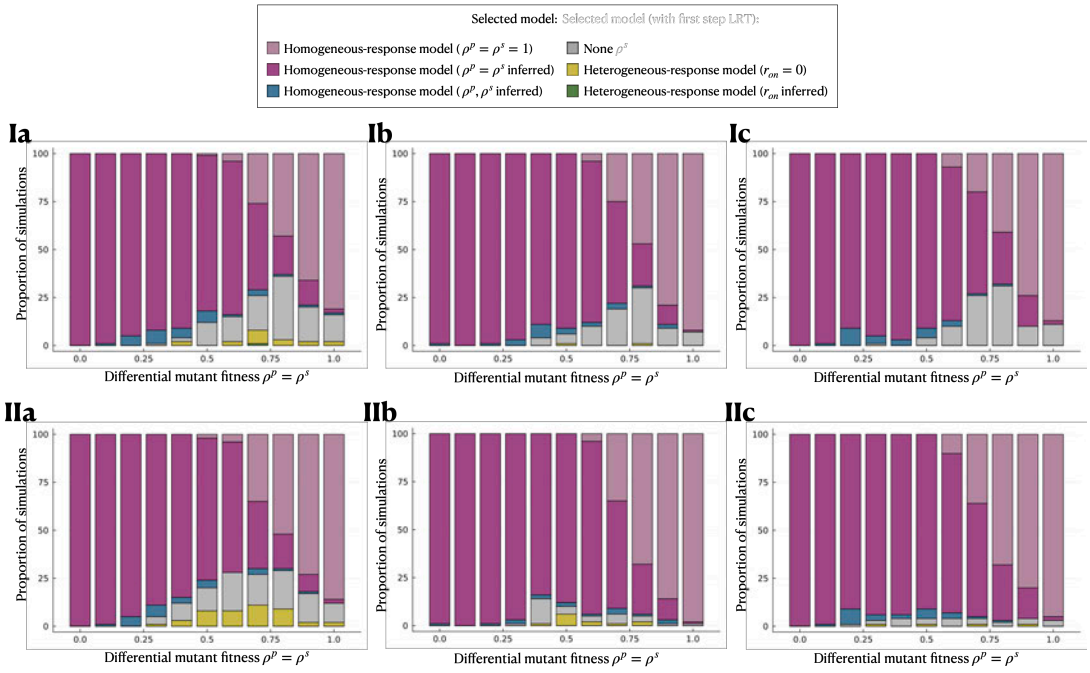

Figure N: **Model selection when simulating under the homogeneous-response model with constrained mutant fitness.** We use a two-step model selection procedure with LRT as the first step and either AIC (**I**) or BIC (**II**) as the second selection step, and a simulated increase in mutation rate of $\frac{\mu^s}{\mu^p} = 3.2$ (**a**), $\frac{\mu^s}{\mu^p} = 10$ (**b**) or $\frac{\mu^s}{\mu^p} = 32$ (**c**). The parameter range used in the simulations is $\rho^p = \rho^s \in [0,\ 1]$.

the true mutation-rate increase. For a severe mutant fitness cost (small ρ^s), the model selected by AIC depends on the true increase in mutation rate. When the mutation-rate increase is small ($\frac{\mu^s}{\mu^p} = 3.2$, left column), the AIC usually correctly selects the unconstrained homogeneous-response model. As the mutation-rate increase becomes larger, the model selection first becomes frequently inconclusive (for $\frac{\mu^s}{\mu^p} = 10$, middle column) and then tends to select the heterogeneous-response model with $r_{on} = 0$ (for $\frac{\mu^s}{\mu^p} = 32$, right column). The reason for this behaviour is that the underlying mutant count distributions are similar for both the homogeneous-response model with a large mutant fitness cost and the heterogeneous-response model with non-dividing response-*on* cells (recall Fig B), and the latter model has fewer inferred parameters.

In contrast, model selection using the BIC (Fig O, bottom) has a high rate of false positives, i.e. selecting the heterogeneous-response model (with $r_{on} = 0$) even though we simulated under the homogeneous-response model. For smaller mutation-rate increases ($\frac{\mu^s}{\mu^p} = 3.2$ and $\frac{\mu^s}{\mu^p} = 10$), the false-positive rate is highest when the mutant fitness cost is small, whereas for larger mutation-rate increase ($\frac{\mu^s}{\mu^p} = 32$), the false-positive rate is highest at intermediate ρ^s. For sufficiently small mutant fitness cost ($\rho^s \to 1$), BIC usually selects the homogeneous-response model with no mutant fitness cost ($\rho^s = \rho^p = 1$) regardless of the true mutation-rate increase.

To summarise, model selection using the BIC is more conclusive, with a higher rate of true positives (i.e. correctly selecting the heterogeneous-response model when it was used for simulations) than model selection using the AIC (Fig M). Both AIC and BIC show a low rate of false positives (i.e. incorrectly selecting the heterogeneous-response model) when simulating under the homogeneous-response model with equal mutant fitness costs under permissive and stressful conditions (Fig N) or a sufficiently small mutant fitness cost under stressful conditions only (Fig O). However, using the BIC results in a higher rate of false positives when simulating under the homogeneous-response model where mutants have a sufficiently large fitness cost only under stressful conditions (Fig O). For this reason, we decided to use AIC as our model selection procedure when presenting the main results. However, in the file called **inference.jl** at `https://github.com/LucyL-J/Quantifying-SIM`, we provide code to use either AIC or BIC in model selection.

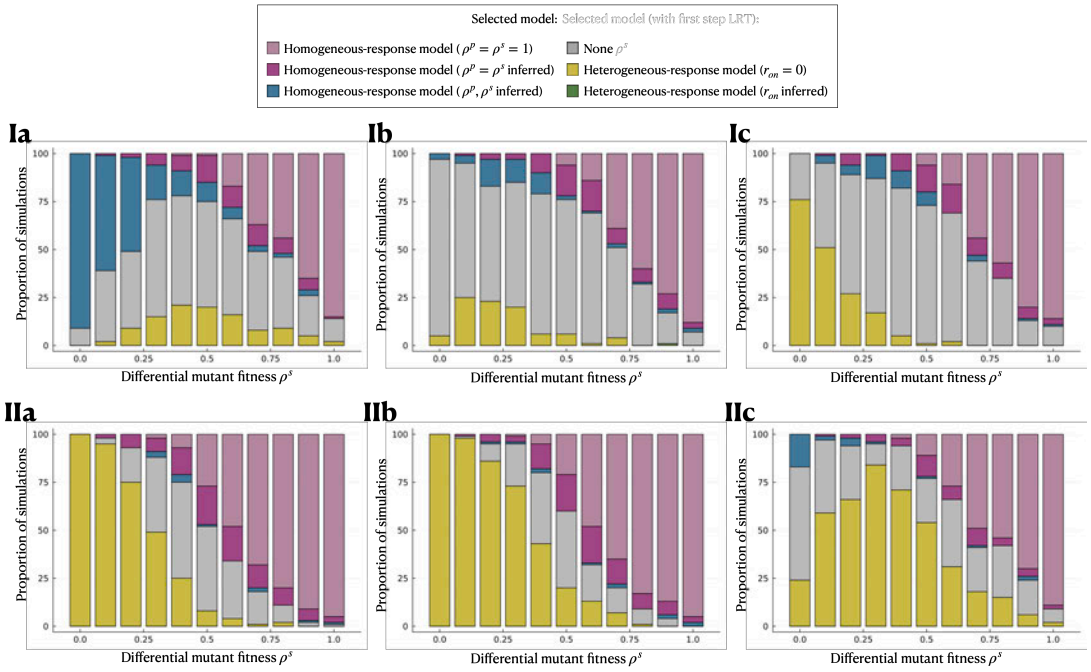

Figure O: **Model selection when simulating under the homogeneous-response model with mutant cost only under stressful conditions.** We use a two-step model selection procedure with LRT as the first step and either AIC (**I**) or BIC (**II**) as the second selection step, and a simulated increase in mutation rate of $\frac{\mu^s}{\mu^p} = 3.2$ (**a**), $\frac{\mu^s}{\mu^p} = 10$ (**b**) or $\frac{\mu^s}{\mu^p} = 32$ (**c**). The parameter range used in the simulations is $\rho^p = 1$ and $\rho^s \in [0,\ 1]$.

References

[1] Frenoy A, Bonhoeffer S. Death and population dynamics affect mutation rate estimates and evolvability under stress in bacteria. PLOS Biology. 2018 may;16(5):e2005056. Available from: https://dx.plos.org/10.1371/journal.pbio.2005056.

[2] Zheng Q. Estimation of Rates of Non-neutral Mutations When Bacteria are Exposed to Subinhibitory Levels of Antibiotics. Bulletin of Mathematical Biology. 2022 nov;84(11):131. Available from: https://doi.org/10.1007/s11538-022-01085-5https://link.springer.com/10.1007/s11538-022-01085-5.

[3] Ding J, Tarokh V, Yang Y. Model Selection Techniques: An Overview. IEEE Signal Processing Magazine. 2018;35(6):16-34.

Appendix B

MIC and experimental design

B.1 Antimicrobial concentrations relative to their respective MICs

We re-analysed experiments using antimicrobial concentrations below the MIC. In the studies [3, 10, 14, 15, 25, 30, 34, 60, 65, 68, 71], these concentrations were referred to as *subinhibitory*, *sublethal* or simply *sub-MIC*. In general, giving the antimicrobial concentration relative to the MIC, for example, in units of the MIC, could allow us to compare experiments with different bacterial strains or antimicrobials. However, how the MIC was determined (if at all) differed in the re-analysed studies. The majority (7 out of 11) did not explain how the MIC was determined. Two of these studies ([25] and [71]) did not report the value of the MIC, yet referred to the antimicrobial concentrations used in their experiments as *sub-MIC*. The approaches in the four studies, which explain how they determined the MIC, range from the lowest concentration leading to 'no visible growth in an overnight liquid culture' [65] and 'no visible colour change in an overnight liquid culture with supplemented resazurin' [60], to more quantitative measures such as '15% reduction in the area under the growth curve of an overnight culture' [10] and 'growth reduced to $\mathrm{OD}_{600} < 0.1$ in an overnight culture' [68].

The reason for choosing the specific sub-MIC concentration also varied between the re-analysed studies. [25] and [71], who did not report a value for the MIC, used antimicrobial concentrations to replicate previous studies [45, 64]. Some studies used a (seemingly) arbitrary fixed percentage of the MIC in their experiments, ranging from 1% to 75% [3, 14, 30, 60, 68], see Table B.1; others a sub-MIC concentration they

Study	Species strain (mutant)	Antimicrobial		
		Abbr.	([$\frac{\mu g}{mL}$])	[MIC]
Baharoglu et al. [3]	*E. coli* MG1655	Amp, Cip, Rif, Trim	0.05	1%
		Neo, Tob	0.1	
		Cm, Tet	0.15	
		Kan, Spec	0.2	
		MMC	missing	
Bulssico et al. [10]	*E. coli* TD2158	Cip	0.01	50%
Cortes et al. [14]	*S. pneumoniae* D39	Pen	0.024	75%
		Ery	0.09	
		Cm	3.0	
Dapa et al. [15]	*E. coli* MG1655 (ΔSulA)	MMC	1.0	(75%)
Frenoy et al. [25]	*E. coli* MG1655	H_2O_2	0.034	-
		Nor	0.05	
		Kan	3.0	
Giroux et al. [30]	*E. coli* MG1655	Trim	0.04	6.25%
Hocquet et al. [34]	*P. aeruginosa* PA14	Met	50.0	1.25%
Mo et al. [60]	*E. coli* MG1655 (ΔSulA)	Cip	0.01	35.7% (62.5%)
		Trim	0.032	25% (25%)
		MMC	0.5	12.5% (12.5%)
		Amp, Nitro	2.0	25% (33.3%)
		Strep	2.0	40% (33.3%)
		Novo	16.0	25% (12.5%)
Schmidt et al. [65]	*A. baylyi* ADP1	CHX	0.002	2%
		DDAC	0.02	
		Cip	0.036	
		BAC	0.24	
		Cu	1.0	
		Trim	16.0	
	B. subtilis 3610	DDAC	0.0002	0.4%
		BAC	0.0012	0.04%
		Cu	0.004	0.2%
		Trim	0.004	0.08%
		Cip	0.008	0.4%
		CHX	0.012	0.2%
	E. coli MG1655	Cip	0.0006	1%
		DDAC	0.01	
		Cu	0.025	
		BAC	0.03	
		Trim	0.2	
		CHX	0.012	0.2%
Torres-Barcelo et al. [68]	*P. aeruginosa* PA01 (LexAd)	Cip	0.048	24% (24%)
Vasse et al. [71]	*E. coli* MG1655	Cip	0.005	-
		Nor, Trim	0.005, 0.05	
		Tet	0.15	
		Cm	0.15, 1.5	
		MMC, Nal	1.0	
		Amp	1.0, 3.2	
		Kan	1.6	
		Strep	5.0	

Table B.1: Antimicrobial concentrations used in the re-analysed studies relative to their respective MICs. Concentrations are given in $\frac{\mu g}{mL}$ and in units of the MIC. If a study used a mutant strain, the concentration in units of the MIC is shown in brackets. A dash indicates studies that did not determine the MIC [25, 71].

argued would not significantly perturb growth [10, 15] or cause initial killing [65]. The latter study also compared the concentrations used with those found in the environment. One study used an antimicrobial concentration found in patients' plasma after treatment [34].

B.2 Experimental design impacts estimation uncertainty and chance of detecting SIM

In section 3.3.1, we noticed that experiments with large confidence intervals tended to use a small number of parallel cultures and partial plating, i.e. only a fraction (plating efficiency $E < 100\%$) of each parallel culture is plated onto the selective plates. 52 out of all 77 experiments that we analysed had a plating efficiency < 1, with plated fractions ranging from $E = 40\%$ down to $E = 0.0002\%$, highlighting the importance of our computational extension to consider partial plating in our model estimates. The number of parallel cultures also greatly varied between experiments, from $c_s = 2$ cultures treated with an antimicrobial and $c_0 = 3$ untreated cultures, up to $c_s = 240$ and $c_0 = 236$ (Table 3.2).

To make our observations more precise, we statistically analysed how these experimental design factors associate with the normalised width of the 95% confidence intervals of $\bar{M}$, that is $(\bar{M}_{\text{upper}} - \bar{M}_{\text{lower}})/\bar{M}_{\text{MLE}}$. We fitted the following linear model

$$\log_{10}[\bar{M}] \sim \log_{10}[E] + \log_{10}[c_s], \tag{B.1}$$

using the logarithm because the normalised CI width as well as plating efficiencies and numbers of parallel cultures in the treatment condition span several orders of magnitude (Fig B.1, left). We found that the log plating efficiency, but not the log number of cultures, significantly impacts the log normalised CI width, with a plating efficiency of $E = 10\%$ leading to a $(4.4 \pm 0.6)-$fold increase in the normalised CI width compared to $E = 100\%$ ($p < 2 \cdot 10^{-16}$, Fig B.1, right). At the same time, the plating efficiency and number of parallel cultures were positively correlated (Kendall's rank correlation coefficient $R = 0.45$, $p = 3.7 \cdot 10^{-7}$), implying that experimentalists using a higher number of parallel cultures also tend to plate larger fractions onto the selective plates.

B.2. Experimental design impacts estimation uncertainty and chance of detecting SIM120

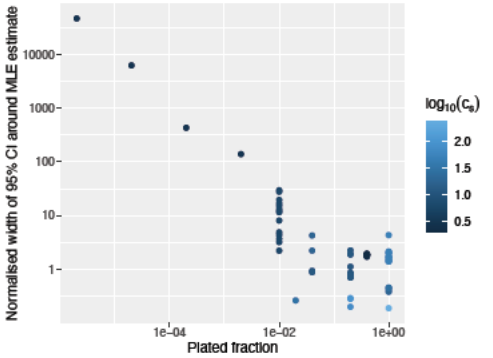


```
Call:
lm(formula = log10(width_CI) ~ log10(plated_fraction) + log10(n_cultures),
    data = df)

Residuals:
     Min       1Q   Median       3Q      Max
-1.43497 -0.34674  0.08344  0.40033  1.14495

Coefficients:
                      Estimate Std. Error t value Pr(>|t|)
(Intercept)           -0.04208    0.16701  -0.252    0.802
log10(plated_fraction) -0.63604    0.05603 -11.352   <2e-16 ***
log10(n_cultures)      -0.12240    0.11576  -1.057    0.294
---
Signif. codes:  0 '***' 0.001 '**' 0.01 '*' 0.05 '.' 0.1 ' ' 1

Residual standard error: 0.4703 on 74 degrees of freedom
Multiple R-squared:  0.7118,    Adjusted R-squared:  0.704
F-statistic: 91.37 on 2 and 74 DF,  p-value: < 2.2e-16
```

Figure B.1: Precision of the estimated increase in mutation rate is impacted by experimental design. Left: Normalised width of the 95% confidence intervals around the MLE of $\bar{M}$ plotted against the plated fraction E used in the re-analysed experiments. The colour indicates the respective number of parallel cultures c_s in the treatment condition. Right: Summary of the fitted linear model $\log_{10}[\bar{M}] \sim \log_{10}[E] + \log_{10}[c_s]$.

Next, we statistically analysed which factors impact whether SIM was detected by our model selection procedure. For this, we fitted a generalised linear mixed model using a binary response variable (whether SIM is detected or not), the antimicrobial concentration C in units of the MIC, the log plated fraction $\log_{10}[E]$ and the log number of parallel cultures $\log_{10}[c_s]$ in the treatment condition as continuous fixed effects, the target group (targeting DNA/DNA gyrase, ribosome-targeting and 'others') as a three-level fixed effect, and the respective control condition (the experiment used to estimate the baseline mutation rate) as a random effect:

$$\text{SIM} \sim C + \log_{10}[E] + \log_{10}[c_s] + \text{target group} + (1|\text{control condition}) \tag{B.2}$$

We found that the odds of detecting SIM were $\left(94 \pm \binom{4}{14}\right)\%$ less in the group of ribosome-targeting antimicrobials compared to antimicrobials targeting DNA/DNA gyrase ($p = 0.0163$), confirming our expectation we built in section 3.3.2. However, antimicrobials other then ribosome-targeting ones were not significantly less likely to induce detectable SIM than antimicrobials targeting DNA/DNA gyrase ($\approx 2\%$ lower, $p = 0.98$). Experimental design also impacted whether SIM was detected. Interestingly, the odds to detect SIM increased by $\left(86 \pm \binom{64}{49}\right)\%$ for experiments that used half the number of parallel cultures in the treatment condition ($p = 0.0417$). This could imply that the rate of false positives is higher for fewer parallel cultures. The plating efficiency did not significantly impact the detection of SIM ($\approx 11\%$ increase per order of magnitude in E, $p = 0.80$). Moreover, the higher the antimicrobial concentration (in units of

```
Random effects:
 Groups      Name        Variance Std.Dev.
 baseline_ID (Intercept) 0.5143   0.7171
Number of obs: 60, groups:  baseline_ID, 18

Fixed effects:
                       Estimate Std. Error z value Pr(>|z|)
(Intercept)              2.1206     1.5602   1.359   0.1741
of_MIC                   4.0468     1.8809   2.152   0.0314 *
groupOther              -0.0228     0.8030  -0.028   0.9774
groupRibosome           -2.8015     1.1657  -2.403   0.0163 *
log10(plated_fraction)   0.1011     0.3961   0.255   0.7986
log10(n_cultures)       -2.0474     1.0051  -2.037   0.0417 *
---
Signif. codes:  0 ‘***’ 0.001 ‘**’ 0.01 ‘*’ 0.05 ‘.’ 0.1 ‘ ’ 1
```

Figure B.2: Chance to detect SIM depends on antimicrobial target and concentration, and number of parallel cultures: Coefficients, standard errors and *p*-values estimated using a generalised linear mixed model of the form SIM $\sim C + \log_{10}[E] + \log_{10}[c_s] +$ target group $+ (1|$control condition$)$, which corresponds to SIM $\sim$ of_MIC $+ \log_{10}$[plated_fraction$] + \log_{10}$[n_cultures$] +$ group $+ (1|$baseline_ID$)$ in the R script used for analysis. The fixed effect ‘group’ has three levels: ‘DNA/DNA gyrase’, ‘Other’ and ‘Ribosome’. The intercept gives the log-odds of detecting SIM in the DNA/DNA gyrase group for an antimicrobial concentration of zero, and plating efficiency and number of parallel cultures equal to one.

the MIC), the higher the odds to detect SIM: per 1% increase in the antimicrobial concentration, the odds increased by $(4 \pm 2)\%$ ($p = 0.0314$), in accordance with our previous simulation study [50]. All estimates, standard errors and *p*-values are shown in Fig B.2.

Appendix C

Impact of death and division of response-*on* cells on stress-induced mutagenesis

C.1 Fraction of response-*on* cells depending on their death rate

In section 4.3.1, I showed that the fraction of the response-*on* subpopulation increases monotonically with the concentration of a bactericidal drug. In particular, for a concentration-independent death rate of response-*on* cells $\delta_{on} \equiv \text{const.} \geq 0$, the increase in $f_{on}(t)$ and f_{on}^* has a sigmoidal shape. Thereby, the inflection point depends on the magnitude of the death rate of response-*on* cells δ_{on}: the higher δ_{on}, the higher the concentration of the steepest increase (Fig C.1, left).

On the other hand, in section 4.3.2, I showed that for a bacteriostatic drug, the fraction of the response-*on* subpopulation f_{on} depends non-monotonically on the antibiotic concentration. In particular, the concentration for which the stationary fraction f_{on}^* is maximal depends on the (concentration-independent) death rate of response-*on* cells $\delta_{on} \equiv$ const.: the higher δ_{on}, the lower the concentration of maximal f_{on}^* (Fig C.1, right).

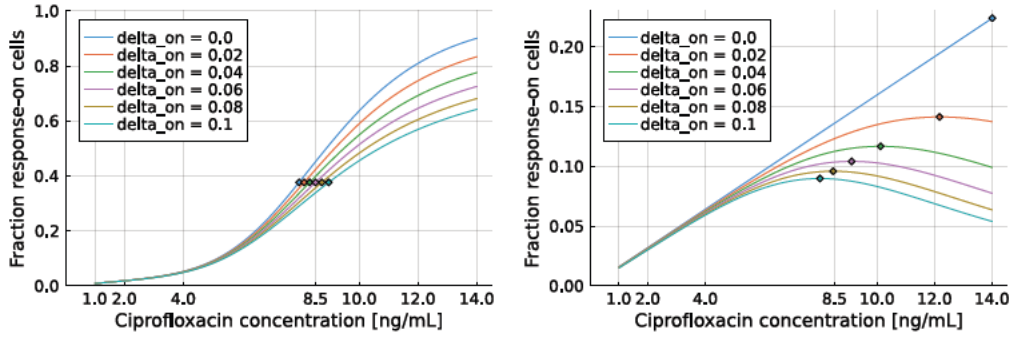

Figure C.1: Impact of a concentration-independent death rate of response-*on* cells $\delta \equiv$ const.$_{on} \geq 0$. Stationary fraction of the response-*on* subpopulation depending on the concentration of a bactericidal (left) and bacteriostatic (right) antibiotic for different magnitudes of death rates of response-*on* cells δ_{on}. The points of steepest increase in f^*_{on} (bactericidal antibiotic, left) and maximal value of f^*_{on} (bacteriostatic antibiotic, right) are shown as diamonds. Parameters as in Fig 4.3 with exception of δ_{on}.

C.2 Fraction of response-*on* cells when their relative division rate is non-zero

Here, I repeat the analyses shown in Figs 4.4, 4.5 and 4.6 with $r_{on} = 0$ for a small non-zero relative division rate of response-*on* cells, $r_{on} = 0.1$. The fraction of the response-*on* subpopulation (both the stationary and time-dependent variable) is comparably larger, but the dependence on the antibiotic concentration is not affected qualitatively (Fig C.2).

Fitting the models with $r_{on} = 0.1$ to the data obtained by [62] as described in section 4.3.4 resulted in the following parameter values. Bactericidal antibiotic model: $\delta_{on} \equiv 0.00\,h^{-1}$ for $s < 0.024$ (which has a cumulative probability of ≈ 0.94) and $\delta_{on} = 0.14 \pm 0.11\,h^{-1}$ else, and $\frac{\mu_{on}}{\mu_{off}} = 95 \pm 34$. Bacteriostatic antibiotic model: $\delta_{on} \equiv 0.07 \pm 0.004\,h^{-1}$ and $\frac{\mu_{on}}{\mu_{off}} = 73 \pm 27$. Fig C.3 shows the resulting increase in population-mean mutation rate.

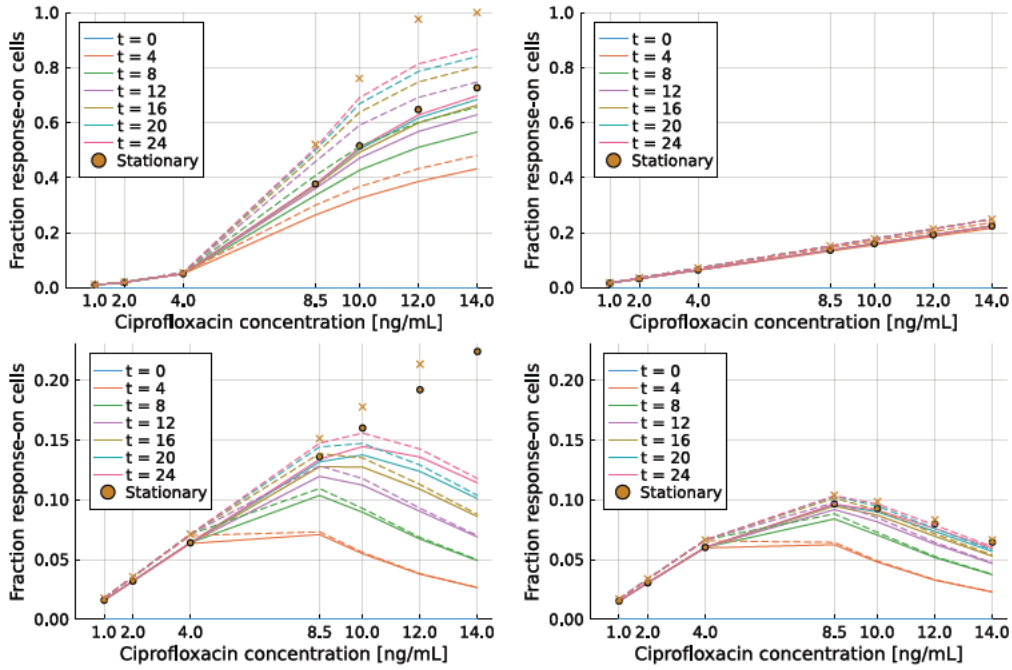

Figure C.2: Fraction of response-*on* subpopulation for non-zero relative division rate. Fraction of the response-*on* subpopulation f_{on} depending on the antibiotic concentration. Top: Bactericidal antibiotic with concentration-independent death of response-*on* cells, $\delta_{on} \equiv 0.06\,h^{-1}$ (left) and with death of response-*on* cells equal to response-*off* cells (right). Bottom: Bacteriostatic antibiotic with zero (left) and non-zero, $\delta_{on} \equiv 0.08\,h^{-1}$ (right) death rate of response-*on* cells. The solid lines show values for a zero relative division rate of response-*on* cells $r_{on} = 0$ and the respective dashed lines for $r_{on} = 0.1$. Dots give the stationary fraction for $r_{on} = 0$ and the respective crosses for $r_{on} = 0.1$. Parameters as in Figs 4.4 and 4.5 with exception of $r_{on} = 0.1$.

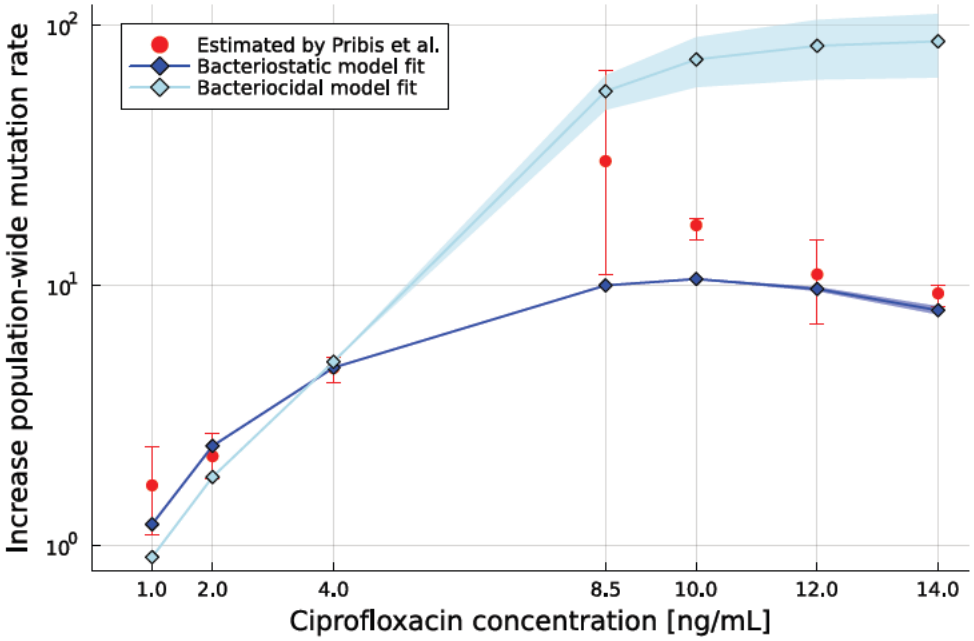

Figure C.3: Increase in population-mean mutation rate for non-zero relative division rate of response-*on* cells fitted to estimates from [62]. The increase in population-mean mutation rate $\bar{M}_{t_f}(C)$ for a bacteriostatic/cidal antibiotic (blue/light blue diamonds), calculated using the same fixed parameters as in Fig 4.6 except $r_{on} = 0.1$; and fitting the remaining parameters to the data from [62]: a concentration-independent death rate of response-*on* cells, $\delta_{on} \equiv 0.00\,h^{-1}$ for $s < 0.024$ and $\delta_{on} \equiv 0.14 \pm 0.11\,h^{-1}$ else (bactericidal) and $\delta_{on} \equiv 0.07 \pm 0.04\,h^{-1}$ (bacteriostatic), and the specific mutation-rate increase associated with the induction of the stress response $\frac{\mu_{on}}{\mu_{off}} = 95 \pm 34$ (bactericidal) and $\frac{\mu_{on}}{\mu_{off}} = 73 \pm 27$ (bacteriostatic).

Bibliography

[1] Helen K. Alexander, Stephanie I. Mayer, and Sebastian Bonhoeffer. Population Heterogeneity in Mutation Rate Increases the Frequency of Higher-Order Mutants and Reduces Long-Term Mutational Load. *Molecular Biology and Evolution*, 34(2):244, nov 2016. doi:10.1093/molbev/msw244.

[2] Georgios Asteris and Sahotra Sarkar. Bayesian procedures for the estimation of mutation rates from fluctuation experiments. *Genetics*, 142(1):313–326, 1996. doi:10.1093/genetics/142.1.313.

[3] Zeynep Baharoglu and Didier Mazel. *Vibrio cholerae* Triggers SOS and Mutagenesis in Response to a Wide Range of Antibiotics: a Route towards Multiresistance. *Antimicrobial Agents and Chemotherapy*, 55(5):2438–2441, may 2011. doi:10.1128/AAC.01549-10.

[4] Zeynep Baharoglu and Didier Mazel. SOS, the formidable strategy of bacteria against aggressions. *FEMS Microbiology Reviews*, 38(6):1126–1145, nov 2014. doi:10.1111/1574-6976.12077.

[5] Nathalie Q. Balaban, Sophie Helaine, Kim Lewis, Martin Ackermann, Bree Aldridge, Dan I. Andersson, Mark P. Brynildsen, Dirk Bumann, Andrew Camilli, James J. Collins, Christoph Dehio, Sarah Fortune, Jean-Marc Ghigo, Wolf-Dietrich Hardt, Alexander Harms, Matthias Heinemann, Deborah T. Hung, Urs Jenal, Bruce R. Levin, Jan Michiels, Gisela Storz, Man-Wah Tan, Tanel Tenson, Laurence Van Melderen, and Annelies Zinkernagel. Definitions and guidelines for research on antibiotic persistence. *Nature Reviews Microbiology*, 17(7):441–448, jul 2019. doi:10.1038/s41579-019-0196-3.

[6] María Rosario Baquero, Annika I. Nilsson, María Del Carmen Turrientes, Dorthe Sandvang, Juan Carlos Galán, Jose Luís Martínez, Niels Frimodt-Møller, Fernando Baquero, and Dan I. Andersson. Polymorphic mutation frequencies in *Escherichia coli*: Emergence of weak mutators in clinical isolates. *Journal of Bacteriology*, 186(16):5538–5542, 2004. doi:10.1128/JB.186.16.5538-5542.2004.

[7] M. S. Bartlett. *An Introduction to Stochastic Processes with Special Reference to Methods and Applications*. sep 1955. ISBN 0521215854.

[8] Mark A. Beaumont. Approximate Bayesian Computation in Evolution and Ecology. *Annual Review of Ecology, Evolution, and Systematics*, 41(1):379–406, dec 2010. doi:10.1146/annurev-ecolsys-102209-144621.

[9] Ivana Bjedov, Olivier Tenaillon, Bénédicte Gérard, Valeria Souza, Erick Denamur, Miroslav Radman, François Taddei, and Ivan Matic. Stress-Induced Mutagenesis in Bacteria. *Science*, 300(5624):1404–1409, may 2003. doi:10.1126/science.1082240.

[10] Julián Bulssico, Irina PapukashvilI, Leon Espinosa, Sylvain Gandon, and Mireille Ansaldi. Phage-antibiotic synergy: Cell filamentation is a key driver of successful phage predation. *PLoS Pathogens*, 19(9):1–29, 2023. doi:10.1371/journal.ppat.1011602.

[11] Adrian Campey, Urszula Łapińska, Remy Chait, Krasimira Tsaneva-Atanasova, and Stefano Pagliara. Antibiotic resistant bacteria survive treatment by doubling while shrinking. *mBio*, 15(12):2024.06.27.601114, dec 2024. doi:10.1128/mbio.02375-24.

[12] Martín Carballo-Pacheco, Michael D. Nicholson, Elin E. Lilja, Rosalind J. Allen, and Bartlomiej Waclaw. Phenotypic delay in the evolution of bacterial antibiotic resistance: Mechanistic models and their implications. *PLoS Computational Biology*, 16(5):1–24, 2020. doi:10.1371/journal.pcbi.1007930.

[13] Divya Choudhary, Valentine Lagage, Kevin R. Foster, and Stephan Uphoff. Phenotypic heterogeneity in the bacterial oxidative stress response is driven by cell-cell interactions. *Cell Reports*, 42(3):112168, mar 2023. doi:10.1016/j.celrep.2023.112168.

[14] Paulo R. Cortes, Germán E. Piñas, Andrea G. Albarracin Orio, and José R. Echenique. Subinhibitory concentrations of penicillin increase the mutation rate to optochin resistance in *Streptococcus pneumoniae*. *Journal of Antimicrobial Chemotherapy*, 62(5):973–977, 2008. doi:10.1093/jac/dkn322.

[15] Tanja Dapa, Sébastien Fleurier, Marie-Florence Bredeche, and Ivan Matic. The SOS and RpoS Regulons Contribute to Bacterial Cell Robustness to Genotoxic Stress by Synergistically Regulating DNA Polymerase Pol II. *Genetics*, 206(3): 1349–1360, jul 2017. doi:10.1534/genetics.116.199471.

[16] Suman G. Das, Susana O.L. Direito, Bartlomiej Waclaw, Rosalind J. Allen, and Joachim Krug. Predictable properties of fitness landscapes induced by adaptational tradeoffs. *eLife*, 9:1–24, may 2020. doi:10.7554/eLife.55155.

[17] Samuel Demharter, Nicholas Pearce, Kylie Beattie, Isabel Frost, Jinwoo Leem, Alistair Martin, Robert Oppenheimer, Cristian Regep, Tammo Rukat, Alexander Skates, Nicola Trendel, David J. Gavaghan, Charlotte M. Deane, and Bernhard Knapp. Ten simple rules for surviving an interdisciplinary PhD. *PLoS Computational Biology*, 13(5):3–9, 2017. doi:10.1371/journal.pcbi.1005512.

[18] Erick Denamur and Ivan Matic. Evolution of mutation rates in bacteria. *Molecular Microbiology*, 60(4):820–827, 2006. doi:10.1111/j.1365-2958.2006.05150.x.

[19] Erick Denamur, Stéphane Bonacorsi, Antoine Giraud, Patrick Duriez, Farida Hilali, Christine Amorin, Edouard Bingen, Antoine Andremont, Bertrand Picard, François Taddei, and Ivan Matic. High frequency of mutator strains among human uropathogenic *Escherichia coli* isolates. *Journal of Bacteriology*, 184 (2):605–609, jan 2002. doi:10.1128/JB.184.2.605-609.2002.

[20] Guillem A. Devin and Alejandro Couce. Trends in the Use of Proper Methods for Estimating Mutation Rates in Fluctuation Experiments. *Axioms*, 12(12):1100, 2023. doi:10.3390/axioms12121100.

[21] Marina Elez, Andrew W. Murray, Li-Jun Bi, Xian-En Zhang, Ivan Matic, and Miroslav Radman. Seeing Mutations in Living Cells. *Current Biology*, 20(16): 1432–1437, aug 2010. doi:10.1016/j.cub.2010.06.071.

[22] Aaron M. Ellison. Bayesian inference in ecology. *Ecology Letters*, 7(6):509–520, jun 2004. doi:10.1111/j.1461-0248.2004.00603.x.

[23] Patricia L Foster. Methods for determining spontaneous mutation rates. *Methods in enzymology*, 409:195–213, 2006. doi:10.1016/S0076-6879(05)09012-9.

[24] Patricia L. Foster. Stress-Induced Mutagenesis in Bacteria. *Critical Reviews in Biochemistry and Molecular Biology*, 42(5):373–397, jan 2007. doi:10.1080/10409230701648494.

[25] Antoine Frenoy and Sebastian Bonhoeffer. Death and population dynamics affect mutation rate estimates and evolvability under stress in bacteria. *PLOS Biology*, 16(5):e2005056, may 2018. doi:10.1371/journal.pbio.2005056.

[26] Errol C. Friedberg, Graham C. Walker, Wolfram Siede, Richard D. Wood, Roger A. Schultz, and Tom Ellenberger. The SOS Responses of Prokaryotes to DNA Damage. In *DNA Repair and Mutagenesis*, pages 463–508. ASM Press, Washington, DC, USA, apr 2014. doi:10.1128/9781555816704.ch14.

[27] Harshad Ghodke, Han Ho, and Antoine M. Van Oijen. Single-molecule live-cell imaging of bacterial DNA repair and damage tolerance. *Biochemical Society Transactions*, 46(1):23–35, 2018. doi:10.1042/BST20170055.

[28] Stephen H. Gillespie, Shreya Basu, Anne L. Dickens, Denise M. O'Sullivan, and Timothy D. McHugh. Effect of subinhibitory concentrations of ciprofloxacin on *Mycobacterium fortuitum* mutation rates. *Journal of Antimicrobial Chemotherapy*, 56(2):344–348, aug 2005. doi:10.1093/jac/dki191.

[29] Alexandre Gillet-Markowska, Guillaume Louvel, and Gilles Fischer. bz-rates: A web tool to estimate mutation rates from fluctuation analysis. *G3: Genes, Genomes, Genetics*, 5(11):2323–2327, 2015. doi:10.1534/g3.115.019836.

[30] Xavier Giroux, Wei-Lin Su, Marie-Florence Bredeche, and Ivan Matic. Maladaptive DNA repair is the ultimate contributor to the death of trimethoprim-treated cells under aerobic and anaerobic conditions. *Proceedings of the National Academy of Sciences*, 114(43):11512–11517, oct 2017. doi:10.1073/pnas.1706236114.

[31] A. Gutierrez, L. Laureti, S. Crussard, H. Abida, A. Rodríguez-Rojas, J. Blázquez, Z. Baharoglu, D. Mazel, F. Darfeuille, J. Vogel, and I. Matic. β-lactam antibiotics promote bacterial mutagenesis via an RpoS-mediated reduction in replication fidelity. *Nature Communications*, 4, 2013. doi:10.1038/ncomms2607.

[32] Brandon M. Hall, Chang Xing Ma, Ping Liang, and Keshav K. Singh. Fluctuation anaLysis calculator: A web tool for the determination of mutation rate using Luria-Delbück fluctuation analysis. *Bioinformatics*, 25(12):1564–1565, 2009. doi:10.1093/bioinformatics/btp253.

[33] Stephanie K. Henderson-Begg, David M. Livermore, and Lucinda M. C. Hall. Effect of subinhibitory concentrations of antibiotics on mutation frequency in *Streptococcus pneumoniae*. *Journal of Antimicrobial Chemotherapy*, 57(5):849–854, may 2006. doi:10.1093/jac/dkl064.

[34] Didier Hocquet and Xavier Bertrand. Metronidazole increases the emergence of ciprofloxacin- and amikacin-resistant *Pseudomonas aeruginosa* by inducing the SOS response. *Journal of Antimicrobial Chemotherapy*, 69(3):852–854, mar 2014. doi:10.1093/jac/dkt435.

[35] Katharine E. Hubbard and Sonja D. Dunbar. Perceptions of scientific research literature and strategies for reading papers depend on academic career stage. *PLoS ONE*, 12(12), 2017. doi:10.1371/journal.pone.0189753.

[36] Katharine E. Hubbard, Sonja D. Dunbar, Emma L. Peasland, Jacquelyne Poon, and Jeremy E. Solly. How do readers at different career stages approach reading a scientific research paper? A case study in the biological sciences. *International Journal of Science Education, Part B: Communication and Public Engagement*, 12(4):328–344, 2022. doi:10.1080/21548455.2022.2078010.

[37] Luis M. Jara, Pilar Cortés, Germán Bou, Jordi Barbé, and Jesús Aranda. Differential Roles of Antimicrobials in the Acquisition of Drug Resistance through Activation of the SOS Response in *Acinetobacter baumannii*. *Antimicrobial Agents and Chemotherapy*, 59(7):4318–4320, jul 2015. doi:10.1128/AAC.04918-14.

[38] Sebastián Jaramillo-Riveri, James Broughton, Alexander McVey, Teuta Pilizota, Matthew Scott, and Meriem El Karoui. Growth-dependent heterogeneity in the DNA damage response in *Escherichia coli*. *Molecular Systems Biology*, 18(5): 1–14, may 2022. doi:10.15252/msb.202110441.

[39] Emma C. Jones and Stephan Uphoff. Single-molecule imaging of LexA degradation in Escherichia coli elucidates regulatory mechanisms and heterogeneity of the SOS response. *Nature Microbiology*, jun 2021. doi:10.1038/s41564-021-00930-y.

[40] Simona Kamenšek, Zdravko Podlesek, Osnat Gillor, and Darja Žgur-Bertok. Genes regulated by the Escherichia coli SOS repressor LexA exhibit heterogenous expression. *BMC Microbiology*, 10(1):283, dec 2010. doi:10.1186/1471-2180-10-283.

[41] Peter Keller and Tibor Antal. Mutant number distribution in an exponentially growing population. *Journal of Statistical Mechanics: Theory and Experiment*, 2015(1):P01011, jan 2015. doi:10.1088/1742-5468/2015/01/P01011.

[42] David G Kendall. Birth-and-Death Processes, and the Theory of Carcinogenesis. *Biometrika*, 47(1/2):13, jun 1960. doi:10.2307/2332953.

[43] Craig Knox, Mike Wilson, Christen M Klinger, Mark Franklin, Eponine Oler, Alex Wilson, Allison Pon, Jordan Cox, Na Eun (Lucy) Chin, Seth A Strawbridge, Marysol Garcia-Patino, Ray Kruger, Aadhavya Sivakumaran, Selena Sanford, Rahil Doshi, Nitya Khetarpal, Omolola Fatokun, Daphnee Doucet, Ashley Zubkowski, Dorsa Yahya Rayat, Hayley Jackson, Karxena Harford, Afia Anjum, Mahi Zakir, Fei Wang, Siyang Tian, Brian Lee, Jaanus Liigand, Harrison Peters, Ruo Qi (Rachel) Wang, Tue Nguyen, Denise So, Matthew Sharp, Rodolfo da Silva, Cyrella Gabriel, Joshua Scantlebury, Marissa Jasinski, David Ackerman, Timothy Jewison, Tanvir Sajed, Vasuk Gautam, and David S Wishart. DrugBank 6.0: the DrugBank Knowledgebase for 2024. *Nucleic Acids Research*, 52(D1):D1265–D1275, jan 2024. doi:10.1093/nar/gkad976.

[44] Arthur L. Koch. Mutation and growth rates from Luria-Delbrück fluctuation tests. *Mutation Research/Fundamental and Molecular Mechanisms of Mutagenesis*, 95(2-3):129–143, aug 1982. doi:10.1016/0027-5107(82)90252-4.

[45] Michael A. Kohanski, Mark A. DePristo, and James J. Collins. Sublethal Antibiotic Treatment Leads to Multidrug Resistance via Radical-Induced Mutagenesis. *Molecular Cell*, 37(3):311–320, feb 2010. doi:10.1016/j.molcel.2010.01.003.

[46] Rok Krašovec, Roman V. Belavkin, John A.D. Aston, Alastair Channon, Elizabeth Aston, Bharat M. Rash, Manikandan Kadirvel, Sarah Forbes, and Christopher G. Knight. Mutation rate plasticity in rifampicin resistance depends on *Escherichia coli* cell-cell interactions. *Nature Communications*, 5:1–8, 2014. doi:10.1038/ncomms4742.

[47] Rok Krašovec, Huw Richards, Guillaume Gomez, Danna R. Gifford, Adrien Mazoyer, and Christopher G. Knight. Measuring microbial mutation rates with the fluctuation assay. *Journal of Visualized Experiments*, 2019(153):1–9, 2019. doi:10.3791/60406.

[48] Valentine Lagage and Stephan Uphoff. Pulses and delays, anticipation and memory: seeing bacterial stress responses from a single-cell perspective. *FEMS microbiology reviews*, 44(5):565–571, 2020. doi:10.1093/femsre/fuaa022.

[49] Lucy Lansch-Justen. I can confirm from my own experience. *Progress of my PhD*, 2024.

[50] Lucy Lansch-Justen, Meriem El Karoui, and Helen K. Alexander. Estimating mutation rates under heterogeneous stress responses. *PLoS Computational Biology*, 20(5 May):1–27, 2024. doi:10.1371/journal.pcbi.1012146.

[51] Krystian Łazowski. Efficient, robust, and versatile fluctuation data analysis using MLE MUtation Rate calculator (mlemur). *Mutation Research - Fundamental and Molecular Mechanisms of Mutagenesis*, 826(April), 2023. doi:10.1016/j.mrfmmm.2023.111816.

[52] D. E. Lea and C. A. Coulson. The distribution of the numbers of mutants in bacterial populations. *Journal of Genetics*, 49:264–285, 1949. doi:10.1007/BF02986080.

[53] Katrine Lindvig. The implied PhD student of interdisciplinary research projects within monodisciplinary structures. *Higher Education Research and Development*, 37(6):1171–1185, 2018. doi:10.1080/07294360.2018.1474343.

[54] S. E. Luria and M. Delbruck. Mutations of bacteria from virus sensitivity to virus resistance. *Genetics*, 28(6):491–511, 1943. doi:10.1093/genetics/28.6.491.

[55] Katarzyna H. Maslowska, Karolina Makiela-Dzbenska, and Iwona J. Fijalkowska. The SOS system: A complex and tightly regulated response to DNA damage. *Environmental and Molecular Mutagenesis*, 60(4):368–384, 2019. doi:10.1002/em.22267.

[56] Ivan Matic, Miroslav Radman, François Taddei, Bertrand Picard, Catherine Doit, Edouard Bingen, Erick Denamur, and Jacques Elion. Highly variable mutation rates in commensal and pathogenic *Escherichia coli*. *Science*, 277(5333):1833–1834, 1997. doi:10.1126/science.277.5333.1833.

[57] Adrien Mazoyer. Fluctuation analysis on mutation models with birth-date dependence. *Mathematical Biosciences*, 303(June):83–100, sep 2018. doi:10.1016/j.mbs.2018.06.006.

[58] Adrien Mazoyer, Rémy Drouilhet, Stéphane Despréaux, and Bernard Ycart. Flan: An R package for inference on mutation models. *R Journal*, 9(1):334–351, 2017. doi:10.32614/rj-2017-029.

[59] Jesse D. McCool, Edward Long, Joseph F. Petrosino, Hilary A. Sandler, Susan M. Rosenberg, and Steven J. Sandler. Measurement of SOS expression in individual *Escherichia coli* K-12 cells using fluorescence microscopy. *Molecular Microbiology*, 53(5):1343–1357, sep 2004. doi:10.1111/j.1365-2958.2004.04225.x.

[60] Charlie Y. Mo, Sara A. Manning, Manuela Roggiani, Matthew J. Culyba, Amanda N. Samuels, Paul D. Sniegowski, Mark Goulian, and Rahul M. Kohli. Systematically Altering Bacterial SOS Activity under Stress Reveals Therapeutic Strategies for Potentiating Antibiotics. *mSphere*, 1(4):1–15, 2016. doi:10.1128/msphere.00163-16.

[61] Peter Mrak, Zdravko Podlesek, Jos P. M. van Putten, and Darja Žgur-Bertok. Heterogeneity in expression of the *Escherichia coli* colicin K activity gene cka is controlled by the SOS system and stochastic factors. *Molecular Genetics and Genomics*, 277(4):391–401, apr 2007. doi:10.1007/s00438-006-0185-x.

[62] John P. Pribis, Libertad García-Villada, Yin Zhai, Ohad Lewin-Epstein, Anthony Z. Wang, Jingjing Liu, Jun Xia, Qian Mei, Devon M. Fitzgerald, Julia Bos, Robert H. Austin, Christophe Herman, David Bates, Lilach Hadany, P.J. Hastings, and Susan M. Rosenberg. Gamblers: An Antibiotic-Induced Evolvable Cell Subpopulation Differentiated by Reactive-Oxygen-Induced General Stress Response. *Molecular Cell*, 74(4):785–800.e7, may 2019. doi:10.1016/j.molcel.2019.02.037.

[63] Roland R. Regoes, Camilla Wiuff, Renata M. Zappala, Kim N. Garner, Fernando Baquero, and Bruce R. Levin. Pharmacodynamic Functions: a Multiparameter Approach to the Design of Antibiotic Treatment Regimens. *Antimicrobial Agents and Chemotherapy*, 48(10):3670–3676, oct 2004. doi:10.1128/AAC.48.10.3670-3676.2004.

[64] Alexandro Rodríguez-Rojas, Olga Makarova, and Jens Rolff. Antimicrobials, Stress and Mutagenesis. *PLoS Pathogens*, 10(10):e1004445, oct 2014. doi:10.1371/journal.ppat.1004445.

[65] Selina B.I. Schmidt, Alexandro Rodríguez-Rojas, Jens Rolff, and Frank Schreiber. Biocides used as material preservatives modify rates of de novo mutation and horizontal gene transfer in bacteria. *Journal of Hazardous Materials*, 437 (December 2021):129280, 2022. doi:10.1016/j.jhazmat.2022.129280.

[66] Paul D. Sniegowski, Philip J. Gerrish, and Richard E Lenski. Evolution of high mutation rates in experimental populations of *E. coli*. *Nature*, 387(6634):703–705, jun 1997. doi:10.1038/42701.

[67] Lei Sun, Helen K. Alexander, Balazs Bogos, Daniel J. Kiviet, Martin Ackermann, and Sebastian Bonhoeffer. Effective polyploidy causes phenotypic delay and influences bacterial evolvability. *PLOS Biology*, 16(2):e2004644, feb 2018. doi:10.1371/journal.pbio.2004644.

[68] Clara Torres-Barceló, Mila Kojadinovic, Richard Moxon, and R. Craig MacLean. The SOS response increases bacterial fitness, but not evolvability, under a sublethal dose of antibiotic. *Proceedings of the Royal Society B: Biological Sciences*, 282(1816):20150885, oct 2015. doi:10.1098/rspb.2015.0885.

[69] Stephan Uphoff. Real-time dynamics of mutagenesis reveal the chronology of DNA repair and damage tolerance responses in single cells. *Proceedings of the National Academy of Sciences*, 115(28):E6516–E6525, jul 2018. doi:10.1073/pnas.1801101115.

[70] Stephan Uphoff, Nathan D. Lord, Burak Okumus, Laurent Potvin-Trottier, David J. Sherratt, and Johan Paulsson. Stochastic activation of a DNA damage response causes cell-to-cell mutation rate variation. *Science*, 351(6277):1094–1097, mar 2016. doi:10.1126/science.aac9786.

[71] Marie Vasse, Sebastian Bonhoeffer, and Antoine Frenoy. Ecological effects of stress drive bacterial evolvability under sub-inhibitory antibiotic treatments. *ISME Communications*, 2(1), 2022. doi:10.1038/s43705-022-00157-w.

[72] Maxence S. Vincent and Stephan Uphoff. Bacterial phenotypic heterogeneity in DNA repair and mutagenesis. *Biochemical Society Transactions*, 48(2):451–462, apr 2020. doi:10.1042/BST20190364.

[73] Maxence S. Vincent and Stephan Uphoff. Cellular heterogeneity in DNA alkylation repair as a trade-off between cell survival and genetic plasticity. *bioRxiv*, 2021. doi:10.1101/2021.05.24.445533.

[74] Anthony C. Woo, Louis Faure, Tanja Dapa, and Ivan Matic. Heterogeneity of spontaneous DNA replication errors in single isogenic *Escherichia coli* cells. *Science Advances*, 4(6):2–10, jun 2018. doi:10.1126/sciadv.aat1608.

[75] Kun Wu, Danqi Qin, Yang Qian, and Haoxuan Liu. A new era of mutation rate analyses: Concepts and methods. *Zoological Research*, 45(4):767–780, 2024. doi:10.24272/j.issn.2095-8137.2024.058.

[76] Y. L. Wu, E. M. Scott, A. Li Wan Po, and V N. Tariq. Development of resistance and cross-resistance in *Pseudomonas aeruginosa* exposed to subinhibitory antibiotic concentrations. *APMIS*, 107(1-6):585–592, mar 1999. doi:10.1111/j.1699-0463.1999.tb01596.x.

[77] X-Net. Sweeping away barriers to interdisciplinary research: recommendations based on X-Net project outcomes - March 2024, 2024.

[78] Qi Zheng. On Bartlett's formulation of the Luria–Delbrück mutation model. *Mathematical Biosciences*, 215(1):48–54, sep 2008. doi:10.1016/j.mbs.2008.05.005.

[79] Qi Zheng. A Bayesian two-level model for fluctuation assay. *Genetica*, 139(11-12):1409–1416, dec 2011. doi:10.1007/s10709-012-9639-8.

[80] Qi Zheng. rSalvador: An R package for the fluctuation experiment. *G3: Genes, Genomes, Genetics*, 7(12):3849–3856, 2017. doi:10.1534/g3.117.300120.